Universität Hamburg
DER FORSCHUNG | DER LEHRE | DER BILDUNG

UKE
HAMBURG

Nanobody-Based Treatment Strategies in Glomerulonephritis

Dissertation for the attainment of the academic title
doctor rerum naturalium

presented by

Nastassia Liaukouskaya
From Skorodnoye, Belarus

Reviewed by Prof. Dr. med Friedrich Koch-Nolte,
Priv. -Doz. Dr. Gunther Zahner

Defense: 10.04.2025

Dissertation submitted to the University of Hamburg
Department of Biology
August 2024

“The universe is change;
our life is what our thoughts make it."
— Marcus Aurelius

The presented work was conducted from June 2020 until June 2024 in the III. Department of Medicine at the University Medical Center Hamburg-Eppendorf under the supervision of Dr. Nicola Wanner and Prof. Dr. med. Friedrich Koch-Nolte.

Eidesstattliche Versicherung:

Hiermit versichere ich an Eides statt, die vorliegende Dissertationsschrift selbst verfasst und keine anderen als die angegebenen Hilfsmittel und Quellen benutzt zu haben.

Sofern im Zuge der Erstellung der vorliegenden Dissertationsschrift generative Künstliche Intelligenz (gKI) basierte elektronische Hilfsmittel verwendet wurden, versichere ich, dass meine eigene Leistung im Vordergrund stand und dass eine vollständige Dokumentation aller verwendeten Hilfsmittel gemäß der Guten wissenschaftlichen Praxis vorliegt. Ich trage die Verantwortung für eventuell durch die gKI generierte fehlerhafte oder verzerrte Inhalte, fehlerhafte Referenzen, Verstöße gegen das Datenschutz- und Urheberrecht oder Plagiate.

Hamburg, 22.08.2024

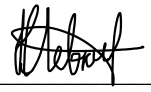

Nastassia Liaukouskaya

I hereby declare and affirm that this doctoral dissertation is my own work and that I have not used any aids and sources other than those indicated.

If electronic resources based on generative artificial intelligence (gAI) were used in the course of writing this dissertation, I confirm that my own work was the main and value-adding contribution and that complete documentation of all resources used is available in accordance with good scientific practice. I am responsible for any erroneous or distorted content, incorrect references, violations of data protection and copyright law or plagiarism that may have been generated by the gAI.

Hamburg, 22.08.2024

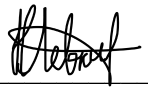

Nastassia Liaukouskaya

Ich versichere, dass dieses gebundene Exemplar der Dissertation und das in elektronischer Form eingereichte Dissertationsexemplar (über den Docata-Upload) und das bei der MIN Fakultät zur Archivierung eingereichte gedruckte gebundene Exemplar der Dissertationsschrift identisch sind.

Hamburg, 22.08.2024

Nastassia Liaukouskaya

I, the undersigned, declare that this bound copy of the dissertation and the dissertation submitted in electronic form (via the Docata upload) and the printed bound copy of the dissertation submitted to the faculty (responsible Academic Office or the Doctoral Office Physics) for archiving are identical.

Hamburg, 22.08.2024

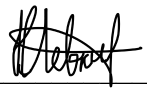

Nastassia Liaukouskaya

Table of Contents

Acknowledgements I

List of figures III

List of tables V

List of abbreviations VI

Summary IX

Zusammenfassung X

1. Introduction 1

1.1 Glomerulonephritis 1

1.2 Pathophysiological role of purinergic signalling 3

1.2.1 Structure and distribution of P2X7 receptor 3

1.2.2 P2X7 activation 5

1.3 Therapeutic potential of nanobodies 8

1.3.1 Nanobodies in Clinical Trials 11

1.4 P2X7 in glomerulonephritis 12

1.5 Aims of this work 13

2. Materials and Methods 15

2.1 Materials 15

2.1.1 Equipment 15

2.1.2 Consumables 15

2.1.3 Chemicals 16

2.1.4 Cell culture media 17

2.1.5 Buffers 18

2.1.6 Kits 19

2.1.7 Antibodies and nanobodies 19

2.1.8 Cell lines 21

2.1.9 Mouse strains 21

2.1.10 Software 21

2.2 Methods 22

2.2.1 Nanobody production 22
2.2.2 Histological techniques 24
2.2.3 Cell isolation and sorting 26
2.2.4 Molecular and genetic analysis 29
2.2.5 Biochemical and analytical assays 30
2.2.6 Animal handling 31
2.2.7 Statistical analysis 32
3. Results 33
3.1 Characterisation and visualization of P2X7 expression in kidney resident cells 33
3.1.1 Distribution of P2X7 expression by kidney-resident cells 33
3.1.2 Targeting of P2X7-expressing cells with alfa-tagged 13A7 nanobody 35
3.2 Impact of nanobody therapy on T cell dynamics in NTN progression 37
3.2.1 P2X7 blocking therapy does not alleviate proteinuria but shows a trend towards increased survival in severe NTN 38
3.2.2 Blocking of P2X7 does not reduce immune cell infiltration and immune-mediated renal damage 39
3.2.3 Nanobodies are not depleted with high proteinuria 45
3.2.4 Blocking of P2X7 in T cells mediates their survival and proliferation 45
3.3 Inflamed glomeruli express increased levels of P2X7 51
3.3.1 13A7 nanobody binding enhanced in inflamed glomeruli 53
3.3.2 The absence of P2X7 on glomerular endothelial cells does not affect NTN outcome 54
3.4 Blocking of P2X7 does not ameliorate acute autoimmune membranous nephropathy 56
3.4.1 13A7 nanobodies do not alleviate proteinuria and renal damage in acute MN 58
3.4.2 Depletion of P2X7 blocking nanobody in the blood is correlated with increased proteinuria in MN mice 59
3.5 Blocking of P2X7 in insidious membranous nephropathy might ameliorate disease progression 61
4. Discussion 65
4.1 Role of P2X7 blockade in treating glomerulonephritis 65
4.2 Insights into P2X7 function 69

4.3 Future research directions 71
4.3.1 The possible advantages of double blocking of P2X4 and P2X7 receptors 71
4.3.2 Enhanced P2X7 levels on GEC and increased nanobody binding open new avenues for targeted gene therapy in the kidney 72
4.3.3 P2X7 blockade in allergic reactions 73
Conclusion 74
Personal contributions 75
Publications 75
Conference attendance as presenter 76
List of references 77

Acknowledgements

First and foremost, I would like to express my deepest gratitude to Dr. N. Wanner for the opportunity to conduct my PhD thesis under her supervision. Thank you for being a remarkably supportive and trustworthy mentor despite your limited availability due to maternity leave. I greatly appreciated your readiness to discuss and assist, even at short notice. Your encouragement allowed me to explore and contribute to various exciting projects, significantly broadening my expertise beyond immunology and the nanobody field to include organoids, developmental nephrology, and genetics, resulting in six publications. Your unwavering support, both professionally and personally, was a source of strength during challenging times, and your belief in my abilities has profoundly impacted my growth as a researcher. I am truly grateful for your guidance and the opportunities you provided.

Special thanks to Professor F. Koch-Nolte, for his invaluable supervision, expertise, and innovative ideas, which greatly enriched my PhD experience. Your guidance and the opportunity to work with nanobodies have been pivotal to my research. I also deeply appreciate your outstanding team, Ms. Tode, Dr. Eden, Ms. Schaffrath, Mr. Schäfer, Dr. Stähler, and Dr. Espinoza. Their dedicated support, insightful suggestions, and collaborative efforts contributed significantly to the progress and achievements of this research and our goals.

I am very thankful to Professor T. B. Huber for the opportunity to conduct this PhD project in his lab, together with all the people who supported me and this project, especially Dr. Wu. You never refused to help, no matter which issue it was, even on weekends I could text you and know you were always in the lab and ready to help. Additionally, I am immensely thankful to our excellent technical assistants — Ms. Obser, Ms. Schaper, Ms. Edenhofer, Ms. Chilla, and Ms. Ziegert. Your invaluable help and support in teaching and refining the techniques were essential to the development of this project.

A heartfelt thank you to Dr. Zahner and Ms. Schnarre. I thoroughly enjoyed working with you on MN models and appreciated our long, yet incredibly stimulating meetings filled with ideas, explanations, and encouragement. Your support and enthusiasm helped me to persist through challenging times and understand the value of negative results, which are indeed important.

I would like to express my heartfelt gratitude to Professor H. J. Seitz for believing in me when I had doubts. Your invaluable and wise advice has been a guiding light throughout my journey. You

were one of the first people who helped me to develop my scientific career when I was living in Belarus. You helped to fix all issues during the COVID-19 pandemic and made it possible to start this project earlier than anybody thought when all borders, embassies and airports were closed and travelling was impossible.

My friends and family, спасибо что верили и поддерживали меня. Пашка, спасибо что верил в мою мечту с детства, без твоей поддержки мне было бы не с кем мечтать вслух. Мама и папа, спасибо что поддержали моим стремления и амбиции, верили в меня, хотя и хотели чтобы я осталась дома. Люблю вас и скучаю!

Der ganz besondere Dank gilt meinem Seelenverwandten Kolja. Du bist das größte Geschenk meines Lebens, mein größter Unterstützer. Selbst in den schwierigsten Zeiten meines Lebens glaubst du mehr an mich als ich es tue. Danke, dass du für mich da bist, ich liebe dich so sehr!

List of figures

Figure 1. Structure of glomerulus…… 1
Figure 2. Schematic structure of P2X7 monomer in physiological and prolonged stimulation…….. 4
Figure 3. Activation of P2X7 receptor……. 6
Figure 4. Structure and advantages of nanobodies…….. 9
Figure 5: Nanobody formats…… 10
Figure 6. Purification quality control of alfa-13A7dim-alb11 in SDS-PAGE gel…….... 23
Figure 7. Stages of glomerulosclerosis used for scoring……. 25
Figure 8. The principle of glomerular isolation……... 26
Figure 9. Flow cytometry gating strategy of isolated renal resident immune and glomerular cells……. 28
Figure 10. Gating strategy for FACS sorting of kidney resident T cells……. 29
Figure 11. Co-expression of P2X7 with T cells, macrophages, and glomerular cells in healthy mice kidney……. 34
Figure 12. 13A7 nanobody construction……. 35
Figure 13. Visualization of 13A7 nanobodies in the kidney……... 35
Figure 14. Functional test of alfa-tagged nanobodies…….…… 36
Figure 15. Experimental scheme of nanobody therapy in NTN model…….…….. 37
Figure 16. Proteinuria and survival in NTN mice…… 39
Figure 17. Macrophage infiltration is increased in NTN kidneys independent of therapy……..... 40
Figure 18. Increased $CD3^+$ T cell infiltration into NTN kidneys……. 41
Figure 19. NTN kidneys express the increased total number of T cells with an elevated expression of P2X7 ……... 43
Figure 20. 13A7 nanobody decreased glomerulosclerosis in mNTN despite severe renal damage……. 44
Figure 21. The common amount of nanobodies was not depleted in severely proteinuric mice…….. 45
Figure 22. RNA sequencing of kidney resident T cells …….. 47
Figure 23. Upregulated signalling pathways in renal T cells of NTN and control mice treated with 13A7 nanobodies……. 48

Figure 24. Signalling pathway within upregulated heparan sulfate proteoglycans in kidney T cells of mice treated with 13A7…… 49
Figure 25: Leading signalling pathways overactivated in kidney T cells in mice with P2X7 blockage……. 50
Figure 26. P2X7 expression is increased in NTN glomeruli……... 51
Figure 27. NTN kidneys express podocyte loss and increased P2X7 levels in GEC….. 52
Figure 28. Nanobody visualisation in NTN kidney……. 53
Figure 29. Cdh5.Cre induction scheme in NTN model……... 54
Figure 30. Characteristic of renal function in Cdh5.Cre mice with and without P2X7 expression on GEC…….. 56
Figure 31. Schematic of spontaneously developing MN in huPLA2R-positive mice…. 57
Figure 32. Experimental scheme of nanobody therapy in spontaneous MN model…… 58
Figure 33. P2X7 blockage with nanobodies did not affect spontaneous MN…….. 59
Figure 34. Nanobody identification in MN murine samples……... 60
Figure 35. Schematic of active MN mouse model…….……..… 61
Figure 36. 13A7 therapy partially ameliorated chronic MN…… 64

List of tables

Table 1. Classification of glomerulonephritis…….. 2
Table 2. List of equipment…….. 15
Table 3. List of consumables……... 15
Table 4. List of chemicals…… 16
Table 5. Eucaryotic cell culture media…… 17
Table 6. Buffer receipts…… 18
Table 7. List of kits…….. 19
Table 8. Antibodies used for histology…… 19
Table 9. Antibodies used for flow cytometry…….. 20
Table 10. Antibodies used in ELISA……... 20
Table 11. Nanobody constructs…… 20
Table 12. Peptide sequence of nanobodies domains…… 20
Table 13. List of cell lines…… 21
Table 14. List of mouse strains…… 21
Table 15. List of Software……... 21

List of abbreviations

AAV	Adeno-Associated Virus
Ab	Antibody
ACR	Albumin-Creatinine Ratio
Apc2	Adenomatous Polyposis Coli 2
Argef2	Rho/Rac guanine nucleotide exchange factor 2
ASC	Apoptosis-associated Speck-like protein containing a CARD
ATP	Adenosine Triphosphate
BBG	Brilliant Blue G
BCA	Bicinchoninic Acid
BCMA	B-cell Maturation Antigen
BSA	Bovine Serum Albumin
CAR T	Chimeric Antigen Receptor T-cell
Cdh	Cadherin
CDR	Complementary Determining Region
cGMP-PKG	Cyclic Guanosine Monophosphate – Protein Kinase G
CKD	Chronic Kidney Disease
CNS	Central Nervous System
CTL	Control
Cxcr	Chemokine Receptors
DAMP	Damage-Associated Molecular Pattern
DAPI	4',6-Diamidino-2-Phenylindole
eATP	Extracellular Adenosine Triphosphate
EGFP	Enhanced Green Fluorescent Protein
ELISA	Enzyme-Linked Immunosorbent Assay
ER	Endoplasmic Reticulim
ESRD	End-Stage Renal Disease
FACS	Fluorescence-Activated Cell Sorting
FCS	Fetal Calf Serum
Foxp3	Forkhead Box P3
FR	Framework Region
Gata3	GATA Binding Protein 3
GBM	Glomerular Basement Membrane

GEC	Glomerular Endothelial Cell
GFP	Green Fluorescent Protein
GN	Glomerulonephritis
GSI	Glomerulosclerosis Index
HBSS	Hank's Balanced Salt Solution
HcAb	Heavy chain Antibody
HEK cells	Human Embryonic Kidney cells
Herc2	Hect Domain and RLD 2
HRP	Horseradish Peroxidase
HS	Hidradenitis Suppurativa
IBA1	Ionized Calcium Binding Adapter Molecule 1
Ifng	Interferon g
IgG	Immunoglobulin G
IHC	Immunohistochemistry
IL	Interleukin
i.p.	Intraperitoneal
i.v.	Intravenous
KO	Knock-out
Ly6G	Lymphocyte Antigen 6 Complex, Locus G
MAPK	Mitogen-Activated Protein Kinase
MFI	Mean Fluorescence Intencity
MCP1	Monocyte Chemoattractant Protein-1
mIgG	Mouse Immunoglobulin G
MN	Membranous Nephropathy
mNTN	Milder Nephrotoxic Nephritis
Mtx1	Metaxin 1
Narf	Nuclear Atypical Rho GTPase-Associated Factor
nb	Nanobody
NFAT	Nuclear Factor of Activated T cells
Nhs	Nance-horan syndrome
NLR	Nod-Like Receptor
NLRP3	Nod-Like Receptor Pyrin Domain Containing 3
NTN	Nephrotoxic Nephritis

NTS	Nephrotoxic Serum
Olfr707	Olfactory Receptor 707
PAS	Periodic Acid-Schiff Stain
PBS	Phosphate-Buffered Saline
PEI	Polyethylenimine
PFA	Paraformaldehyde
PLA2R	Phospholipase A2 Receptor
RAS	Rat Sarcoma
RFU	Relative Fluorescence Units
Rorc	Retinoic Acid Receptor-Related Orphan Receptor C
RT	Room Temperature
s.c.	Subcutaneous
SDS PAGE	Sodium Dodecyl Sulfate Polyacrylamide Gel Electrophoresis
SERCA	Sarcoplasmic/Endoplasmic Reticulum Calcium ATPase
sNTN	Severe Nephrotoxic Nephritis
Spata2	Spermatogenesis-Associated 2
SR	Sarcoplasmic Reticulum
STIM	Stromal Interaction Molecule
Tbx21	T-box transcription factor 21
TCR	T Cell Receptor
Tg	Transgene
Th	T helper
TLR	Toll-Like Receptor
TMB	Tetramethylbenzidine
TNF	Tumor Necrosis Factor
TR-PCR	Reverse Transcription Polymerase Chain Reaction
Treg	Regulatory T cell
TUNEL	Terminal Nucleotidyl Transferase-Mediated dUTP-biotin Nick End-Labeling
VH	Variable Heavy
VHH	Variable domain of Heavy chain of Heavy-chain antibody
VL	Variable Light
WT	Wild Type

Summary

Glomerulonephritis is a diverse group of renal diseases characterized by immune-mediated damage of the glomerular structures. Without timely therapy, 10% to 15% of glomerulonephritis cases progress to end-stage renal disease, leading to dialysis or kidney failure. Due to the limited treatment options in nephrology, there is a huge need for novel therapies. Several studies have confirmed the involvement of immune cell membrane protein P2X7 in autoimmune and inflammatory diseases, including glomerulonephritis. Blocking of P2X7 or its genetic deletion in animal models has been shown to reduce glomerular damage. In this study, we investigate the therapeutic capacity of nanobodies, single-domain antibodies of camelids, for blocking the P2X7 ion channel in the treatment of glomerulonephritis. Using P2X7 GFP-transgenic mice, this study showed that the expression level of P2X7 is highly increased by kidney resident cells (T cells and glomerular cells) under inflammatory conditions (nephrotoxic nephritis). The application of immunohistochemistry, flow cytometry, ELISA, and biochemical analysis of blood serum and urine of mice with severe and acute glomerulonephritis models showed no effect of P2X7 blockade on disease parameters. In addition, bulk RNA sequencing of renal T cells isolated from P2X7-blocking nanobody-treated healthy and nephrotic mice showed the upregulation of genes associated with survival, proliferation, cell spreading and migration, indicating involvement in the inflammatory processes. However, P2X7-blocking nanobody therapy of a slowly developing form of membranous nephropathy resulted in the reduction of disease manifestations, including enhanced survival, decreased proteinuria, mitigation of immunisation-related allergic reactions and cases of remission. These contrasting results suggest that while P2X7 blockade may not be sufficient in severe forms of GN, it could offer therapeutic benefits in milder and slowly developing forms of the disease.

Zusammenfassung

Glomerulonephritis ist eine vielfältige Gruppe von Nierenerkrankungen, die durch immunvermittelte Schädigungen der glomerulären Strukturen gekennzeichnet ist. Ohne rechtzeitige Therapie schreiten 10 % bis 15 % der Glomerulonephritis-Fälle zur terminalen Niereninsuffizienz fort, was zu Dialyse oder Nierenversagen führt. Aufgrund der begrenzten Behandlungsmöglichkeiten in der Nephrologie besteht ein großer Bedarf an neuen Therapien. Mehrere Studien haben die Beteiligung des Immunzellmembranproteins P2X7 an Autoimmun- und Entzündungserkrankungen, einschließlich Glomerulonephritis, bestätigt. Die Blockade von P2X7 oder seine genetische Deletion in Tiermodellen hat gezeigt, dass die glomeruläre Schädigung reduziert wird. In der vorliegenden Arbeit untersuchen wir die therapeutische Kapazität von Nanobodies, Einzelketten-Antikörpern von Kamelen, zur Blockade des P2X7-Ionenkanals bei der Behandlung von Glomerulonephritis. Anhand von P2X7 GFP-transgenen Mäusen zeigte diese Studie, dass das Expressionsniveau von P2X7 durch nierenresidente Zellen (T-Zellen und glomeruläre Zellen) unter entzündlichen Bedingungen (nephrotoxische Nephritis) stark erhöht ist. Die Anwendung von Immunhistochemie, Durchflusszytometrie, ELISA und biochemischen Analysen von Blutserum und Urin bei Mäusen im schweren und akuten Glomerulonephritis-Modell zeigte keine Wirkung auf die Krankheitsparameter. Zusätzlich zeigte die Bulk-RNA-Sequenzierung von aus mit P2X7-blockierenden Nanobodies behandelten gesunden und nephrotischen Mäusen isolierten renalen T-Zellen eine Hochregulation von Genen, die mit Zellüberleben, Proliferation, Zellverbreitung und Migration assoziiert sind, was auf eine Beteiligung an den Entzündungsprozessen hinweist. Die P2X7-blockierende Nanobody-Therapie einer langsam entwickelnden Form der membranösen Nephropathie führte jedoch zu einer Verringerung der Krankheitsmanifestationen, einschließlich verbesserter Überlebensrate, verringerter Proteinurie, Minderung immunisierungsbedingter allergischer Reaktionen und Fällen von Remission. Diese widersprüchlichen Ergebnisse deuten darauf hin, dass die P2X7-Blockade bei schweren Formen der GN möglicherweise nicht ausreicht, aber bei milderen und langsam entwickelnden Formen der Erkrankung therapeutische Vorteile bieten könnte.

1. Introduction

1.1 Glomerulonephritis

Each adult human kidney contains approximately 1 million nephrons, which are its structural and functional units (Stahl/Hoxha 2016). Each nephron is comprised of a renal corpuscle and a renal tubule. The renal corpuscle includes the glomerulus, which features a highly specialized filtration barrier. This barrier is adept at filtering small to midsized molecules but excludes larger macromolecules. The effectiveness of this filtration is due to the unique architecture of the barrier, which consists of three key layers: the glomerular endothelial cells (GEC) lining the capillaries within the glomerulus; the glomerular basement membrane (GMB), a network of extracellular proteins; and the podocytes, which form filtration slits between their foot processes (Figure 1) (Menon et al. 2012).

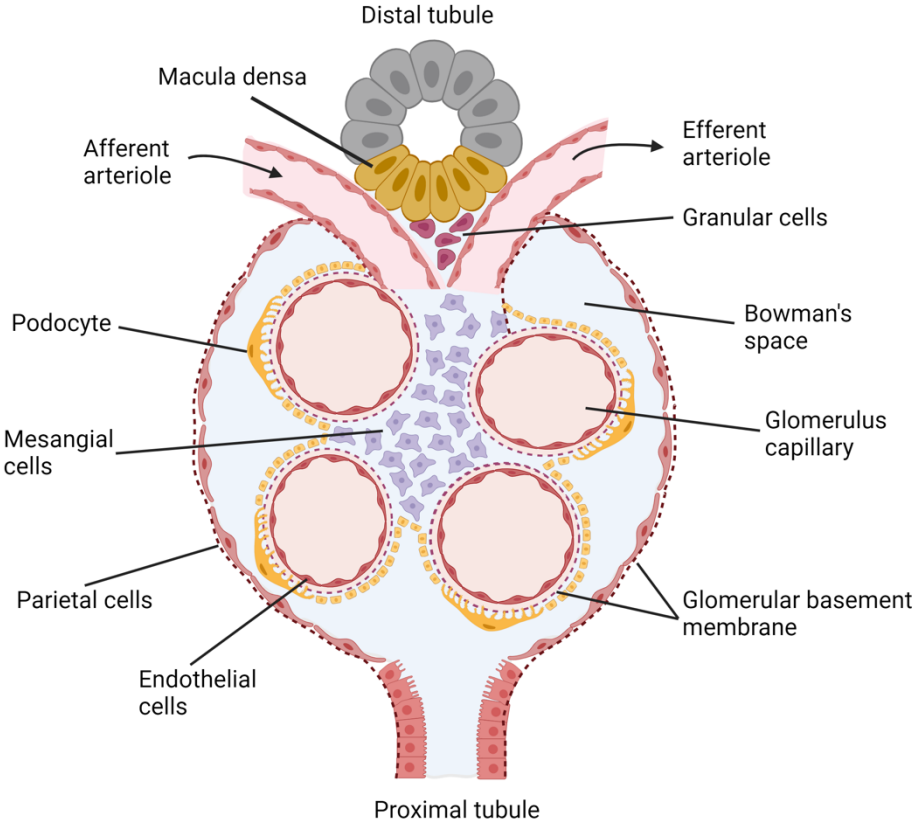

Figure 1. Structure of glomerulus. Blood enters the glomerulus through the afferent arteriole and is filtered through the renal filtration barrier, which is composed of glomerular endothelial cells, glomerular basement membrane and podocytes. The filtered blood leaves the glomerulus via the efferent arteriole, while water and filtration products enter the tubule for reabsorption of essential liquids and electrolytes. Non-reabsorbed molecules and toxins leave the kidney in the formed urine through the ureter (not shown). Created with BioRender.com

Since glomeruli act as high-flow filters generating significant ultrafiltrate, they are susceptible to inflammatory injury from numerous causes, leading to various forms of glomerular disorders (Anders et al. 2023).

Glomerulonephritis (GN) is a group of renal diseases characterised by immune-mediated damage of glomerular structures. Untreated GN can rapidly progress into acute kidney injury (AKI) or chronic GN with the progression to chronic kidney disease (CKD) and end-stage renal disease (ESRD). The progression to ESRD in most cases is relatively quick, developing within weeks or months of the beginning of acute nephrotic syndrome (Kazi/Hashmi 2023). These conditions lead to kidney function deterioration and the inability to filtrate blood properly, which requires renal replacement therapy, including dialysis and kidney transplantation.

GN includes a diversity of glomerular diseases and may occur primarily in the glomeruli due to autoimmunity, medications or idiopathic reasons, or present as renal involvement in the context of systemic diseases (vasculitis, bacterial infection). GN can be etiologically classified based on clinical presentation, which can range from severe proteinuria (>3.5 g albumin/day) and oedema indicative of nephrotic syndrome, to nephritic syndrome where hematuria and hypertension are more prominent, with less pronounced proteinuria (Table 1) (Kazi/Hashmi 2023).

Table 1. Classification of glomerulonephritis. (Kazi/Hashmi 2023).

Nephrotic Glomerulonephritis	Nephritic Glomerulonephritis
• Minimal change disease • Focal segmental glomerulosclerosis • Membranoproliferative glomerulonephritis • Membranous nephropathy • HIV associated nephropathy • Diabetic nephropathy • Amyloidosis	• IgA nephropathy • Henoch Schonlein purpura • Post streptococcal glomerulonephritis • Anti-GBM disease • Rapidly progressive glomerulonephritis • Granulomatosis with polyangiitis • Eosinophilic granulomatosis with polyangiitis • Polyarteritis nodosa • Idiopathic crescentic glomerulonephritis • Goodpasture syndrome • Lupus nephritis • Hepatitis C infection • Membranoproliferative glomerulonephritis

In some cases, symptomatic therapy is sufficient, however, in other patients, GN can present as a medical emergency requiring immediate and aggressive treatment to prevent the loss of renal function, however, those methods are often accompanied by side effects (Stahl/Hoxha 2016). In the absence of standard therapeutic strategies with limited options to treat GN, there is a huge need in nephrology for novel therapies.

Several studies have provided evidence suggesting the major role of immune cell membrane protein P2X7 gating by extracellular adenosine triphosphate (eATP), and the product of its activation

IL-1ß in the development and progression of many inflammatory diseases, including GN (Savio et al. 2018: 10 ff., Turner et al. 2007). These findings may provide a new basis for better disease understanding and the development of new therapeutic strategies in GN.

1.2 Pathophysiological role of purinergic signalling

ATP has long been known as a universal energy source for all biochemical processes, playing a major role in energy exchange in the cells of living organisms. Synthesized in mitochondria, ATP is stored in the cytosol in high concentration (5-10 mmol), where it is used for various cellular processes and energy-requiring activities (Giuliani et al. 2019: 17). A small amount of ATP (nanomolar range) is released into extracellular space via exocytosis, playing a vital role in several specialized physiological reactions in virtually every mammalian system through purinergic P2X receptors, P2X1-P2X6 (Di Virgilio et al. 2017: 15, Giuliani et al. 2019: 16 ff.). However, under pathological conditions, stressed, damaged or dying cells release a large amount of ATP (0.05 – 1 mM) through the injured cell membrane, serving as a danger signal that drives phagocyte migration to damaged sites and mediates clearance of cell debris, at the same time activating inflammatory mechanisms, all mediated by distinct P2X receptor family member P2X7 (Trautmann 2009, cited in Giuliani et al. 2019:17 ff., Burnstock/Kennedy 2011, cited in Oliveira-Giacomelli et al. 2021:2).

Overactivation and overexpression of P2X7 have been linked to the pathogenesis of several inflammatory diseases, including respiratory, gastrointestinal, central nervous and autoimmune disorders, diabetes and diabetes-related comorbidities, tumours and kidney diseases, highlighting its critical role in driving inflammatory responses (reviewed in Savio et al. 2018: 10 ff.).

1.2.1 Structure and distribution of P2X7 receptor

Human *P2rx7* is located on the long arm of chromosome 12, at 12q24.31, centromeric and close to *P2rx4* (12.q24.32). Mouse *P2rx7* is located on chromosome 5, 62.50 cM (Di Virgilio et al. 2017:16). Mammalian P2X7 subunits are typically 595 (or 594) amino acid residues in length and show 77 – 97 % identity to human P2X7 (Jiang et al. 2013: 2 ff., cited in Sluyter 2017: 20). Each P2X7 subunit consists of two transmembrane helices (about 24 aa each), short (26 aa) intracellular N- and long (239 aa) C- termini, and a large ectodomain with two ATP-binding sites (282 aa) (Surprenant et al. 1996, cited in Di Virgilio et al. 2017:16). In contrast to most P2XRs, where prolonged exposure to the agonist causes receptor inactivation, P2X7R (and possibly P2X2 and

P2X4) may promote a further increase in permeability and large pore formation that allows transmembrane fluxes of large hydrophilic molecules up to 900 kDa (Figure 2) (Karasawa et al. 2017; Falzoni et al. 1995, cited in Di Virgilio et al. 2017:18).

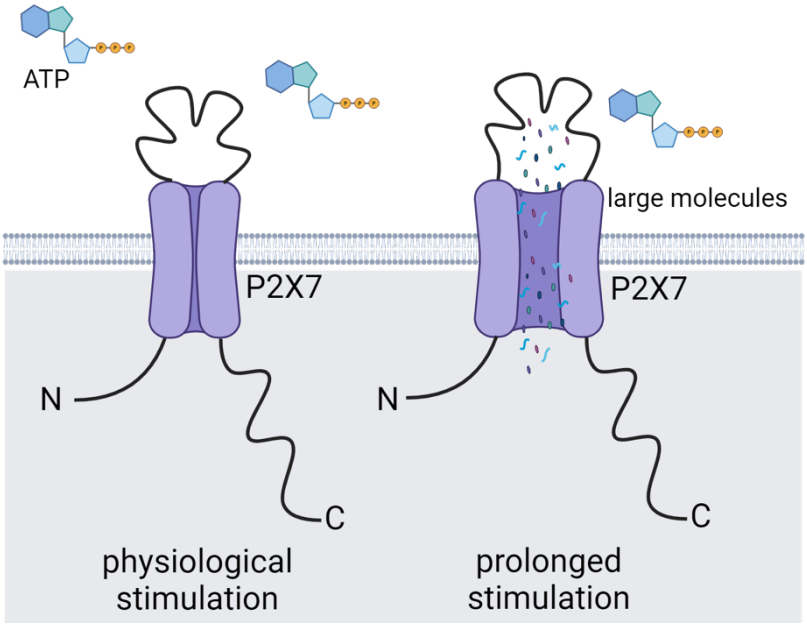

Figure 2. Schematic structure of P2X7 monomer in physiological and prolonged stimulation. Prolonged eATP stimulation causes pore formation and flux of large molecules. Created with BioRender.com

Sequence analysis and tertiary structure of the ATP-binding pocket entrance show a lack of positively charged amino acids and restricted access, suggesting a rather small volume of binding cavity and difficult entry for hydrophobic compounds. This might explain the typically low affinity for ATP in P2X7 (Di Virgilio et al. 2017:18).

P2X7 subunits predominantly assemble as homotrimeric receptors. However, in some cases, P2X7 subunits can coassemble with P2X4 subunits to form heterotrimeric receptors (Boumechache et al. 2009). In addition, P2X2 and P2X5 subunits can also form heterotrimeric receptors that exhibit P2X7-like properties, which makes it complicated to identify P2X7R in cells and tissues via functional studies (Compan et al. 2012).

The functional P2X7 receptor is expressed in a wide range of cell types, including hematopoietic and mesenchymal stem cells, leukocytes, erythrocytes, ocular cells, bone cells, dental pulp cells, endothelial cells, muscle cells, various malignant cell types, and neural cells (Sluyter 2017: 19). Despite its ubiquitous presence, the functions of P2X7 are most extensively characterized in immune cells, highlighting its pivotal role in the assembly of the NLRP3 inflammasome and modulating immune responses (Oliveira-Giacomelli et al. 2021, Swanson et al. 2019).

1.2.2 P2X7 activation

Following ATP stimulation at high concentration, the P2X7 ion channel promotes the influx of Ca^{2+} and Na^{+} ions while concurrently coordinating with the TWIK2 potassium channel, thereby facilitating the efflux of K^{+} ions. These coordinated events, particularly the pivotal K^{+} efflux, play crucial roles as upstream events in the initiation of NLRP3 inflammasome assembly (Swanson et al. 2019: 480). The NLRP3 inflammasome, comprising a sensor component (NLRP3), an adaptor molecule (ASC), and an effector protein (caspase-1), undergoes a highly regulated activation cascade after stimulation. Upon initiation, NLRP3 undergoes oligomerization, subsequently recruiting ASC and initiating the formation of helical ASC filaments. The aggregation of these filaments leads to the formation of a singular macromolecular focus, which in turn recruits caspase-1, facilitating its auto-proteolytic cleavage and activation (Swanson et al. 2019: 477). Caspase-1 is responsible for converting pro-IL-1ß into mature IL-1ß, cleaving the autoinhibitory domain of Gasdermin-D-C (free carboxy-terminal ending), and subsequently creating its Gasdermin-D-N (free amino terminal ending) active form (He et al. 2015, cited in Oliveira-Giacomelli et al. 2021:2). Gasdermin-D-N plays a key role in forming a membrane pore necessary for the efficient unconventional secretion of interleukin-1 (IL-1) family members, such as IL-1β and IL-18 (Figure 3) (Liu et al. 2016, cited in Oliveira-Giacomelli et al. 2021: 2).

IL-1ß, in turn, is a pro-inflammatory cytokine, a key mediator of the immune response and inflammation. It is involved in the activation, proliferation of T and B cells, their migration to the site of inflammation and memory formation (Ben-Sasson et al. 2013). Among all proinflammatory mediators, IL-1ß is recognized as one of the earliest and most potent inflammatory molecules, synthesized in response to infection and injuries (Gabay et al. 2010, cited in Giuliani et al. 2017: 1). In addition, IL-1ß is one of the cytokines that is responsible for fever induction during infection. Those mechanisms are essential for the host's defence and resistance to pathogens, but at the same time, they exacerbate damage during chronic disease and acute tissue injury (Horai et al. 1998, Lopez-Castejon/Brough 2011).

The importance of IL-1ß in GN was demonstrated in the rat model of nephrotoxic nephritis (NTN) by Tesch et al. The level of IL-1ß was increased in this renal model and has been shown to play a significant role in glomerular crescent formation and tubulointerstitial injury (Tesch et al. 1997, cited in Taylor et al. 2009: 1275). The treatment with an IL-1 receptor antagonist prevented the

progression of crescentic GN (Lan et al. 1995, cited in Taylor et al. 2009: 1275). In addition, crescentic GN is less severe in IL-1ß or IL-18 KO mice, and the treatment with caspase inhibitors reduced renal inflammation and apoptosis (Timoshanko et al. 2004, cited in Taylor et al. 2009: 1275). All these data indicate the crucial role of IL-1 in renal pathophysiology in the experimental model of GN.

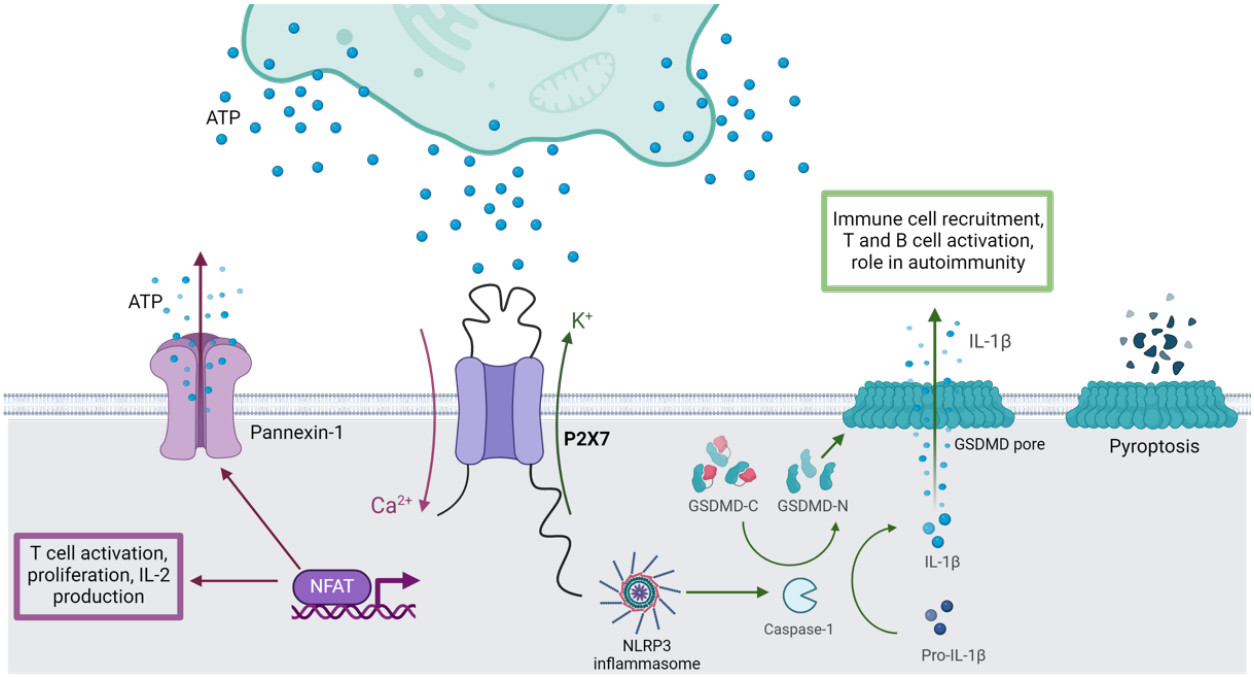

Figure 3. Activation of P2X7 receptor. High concentrations of ATP, released from injured, stressed, or dying cells, activate the P2X7 receptor, resulting in K^+ efflux and Ca^{2+} influx. Potassium ion release triggers the assembly of the NLRP3 inflammasome, which subsequently converts pro-IL-1ß into mature IL-1ß via caspase-1 and forms gasdermin pores necessary for IL-1ß release. $Ca2^+$ influx leads to the activation of NFAT, which promotes T cell activation, proliferation, and IL-2 production, as well as the activation of pannexin-1, facilitating further ATP release. This ATP acts as an autocrine positive feedback signal to sustain P2X7 receptor activation. Prolonged P2X7 receptor stimulation ultimately induces pyroptosis, a form of cell death mediated by gasdermin pores. Modified from Oliveira—Giacomelli et al. 2021, created with BioRender.com

The P2X7R is the most potent plasma membrane receptor triggering pro-IL-1ß processing and release and thus is a crucial initiator of inflammation (di Virgilio et al. 2017: 20, Mortaz et al. 2012). P2X7R KO mice are less prone to initiate inflammation in response to a variety of stimuli. Secretion of mature IL-1ß is severely reduced and the initiation of the inflammatory cytokines cascade is also impaired (Solle et al. 2001).

In addition to the IL-1ß release, the NLRP3/gasdermin-D pathway is also responsible for inducing membrane permeabilization and pyroptosis. This specialized and highly inflammatory mechanism of cell death is characterized by membrane pore formation, and rapid influx of water, which leads to cell swelling and membrane rupture, resulting in the release of the intracellular content outside

of the cell. Released extracellular content from dying cells acts as a damage-associated molecular pattern (DAMP), recruiting and activating more immune cells thereby exacerbating inflammatory status (Oliveira-Giacomelli et al. 2021: 2).

As mentioned above, the activation of P2X7R is followed by Ca^{2+} influx, which in turn is required for activation of the nuclear factor of activated T cells (NFAT), leading to T cell activation, IL-2 production, and T cell proliferation. Moreover, T cell receptor (TCR) stimulation triggers the rapid release of ATP, giving the autocrine positive feedback loop and promoting T cell activation, which was shown in the stimulated by CD3/CD28 ligation of Jurkat T cells (Yip et al. 2009). Pathologically increased ATP release and uncontrolled activation and stimulation of P2X7 act as a positive feedback loop, greatly contributing to the inflammatory process. Immune cells release more cytokines and chemokines, damaging the surrounding tissues, attracting more immune cells, exacerbating the inflammatory scenario, and activating pro-apoptotic cascades culminating in cell death (Oliveira-Giacomelli et al. 2021: 2).

P2X7 plays a major protective role in host defence against infections, stimulating microbicidal mechanisms and producing inflammatory mediators in phagocytic cells. However, its overactivation and overexpression have been linked to the pathogenesis of several diseases, including renal (glomerulonephritis, diabetic nephropathy, tubulointerstitial nephritis, hypertensive nephropathy, acute kidney injury, chronic kidney disease, polycystic kidney disease and renal cancer), respiratory (pulmonary hypertension, asthma, chronic obstructive pulmonary disease, acute lung injury and pulmonary fibrosis), Cron's disease, experimental bowel disease and chemically induced colitis, liver fibrosis, diabetes type 1 and 2 and diabetes-related comorbidities (cardiovascular alterations, diabetic retinopathy and kidney injury), CNS disorders (Traumatic Brain injury, Parkinson's disease, Alzheimer's disease, ischemia, epilepsy, Huntington's disease and Multiple Sclerosis), tumours (leukaemia, melanoma, neuroblastoma, pancreatic adenocarcinoma, breast cancer, prostate cancer, colorectal cancer) other pathological conditions (reviewed in Savio et al. 2018: 10 ff.).

Despite the established role of the P2X7 receptor in the development of a large number of inflammatory diseases, only a few selective small-molecule inhibitors of P2X7 have been developed for the treatment of inflammatory conditions by Janssen Pharmaceuticals (JNJ-47065567), Pfizer (CE-224,535) and other pharmaceutical companies (Guile et al. 2009, Duplantier et al. 2011). Most of the existing P2X7 inhibitors are non-selective antagonists, i.e. BBG, which has been widely used in several studies due to its low cost. However, non-selective antagonists also block other

members of the P2XR family, their usage might lead to divergent and unexpected results due to cross-binding and therefore should be critically analysed (Savio et al. 2018: 3).

1.3 Therapeutic potential of nanobodies

While small-molecule inhibitors of the P2X7 receptor have shown promise in the treatment of certain inflammatory conditions, their selectivity and efficacy can vary, leading to divergent results in clinical trials. In contrast, monoclonal antibodies offer a more targeted approach for a single protein, they have low toxicity, simple pharmacodynamic and potentially can provide greater specificity and efficacy in treating inflammatory diseases. Monoclonal antibodies, large tetrameric proteins of ca 150 kDa, possess an extended half-life of over 10 days due to their inability to pass the renal filtration barrier. Current anti-inflammatory antibodies predominantly target cytokines, cytokine receptors, growth factors and molecules involved in cell-cell interaction (Danquah et al. 2016: 1, Nolte et al. 2019). While ion channels hold potential as therapeutic targets on immune cells for inflammatory diseases, they have remained unexplored in the context of antibody therapeutics. Although conventional antibodies can diminish ion channel function by inducing endocytosis, they rarely directly interfere with ion channel function. Also, with a size of 150 kDa, conventional antibodies are rather large molecules when compared to the exposed surface of ion channels. Because of their unique property to bind functional crevices on proteins and due to their small size and the same specificity as antibodies, nanobodies may fulfil the need for highly specific therapeutics toward ion channels (Danquah et al. 2016: 1).

Nanobody (nb) is a single variable domain of heavy chain antibody originally occurring in camelids (camels, dromedaries, alpacas, llamas, vicunas, guanacos) and some sharks (Figure 4, A). Nb holds a diverse array of loop lengths and structures, showcasing full antigen-binding capacity with high specificity and affinity levels comparable to or even greater than conventional antibodies and have additional advantages (Figure 4, B) (Wanner et al. 2021, Liu et al. 2021).

Structurally, nanobody from camels HcAbs has a similar architecture to conventional antibodies' variable heavy (VH) domain. They both consist of four conserved framework regions (FR1-FR4) and three hypervariable antigen-binding loops (complementarity determining regions CDR1-CDR3) (Wang et al. 2016, cited in Liu 2021: 2). However, nanobody has a few distinct structural features, different from antibodies: nanobodies have enlarged CDR1 and CDR3 relative to the VH

domain of antibodies, which gives them greater structural flexibility and capacity to penetrate cavities on antigens and increases their binding affinity, facilitating the interaction with epitopes that conventional VH-VL pairs cannot access (Salvador et al. 2019: 1706, Liu et al. 2021: 2).

A)

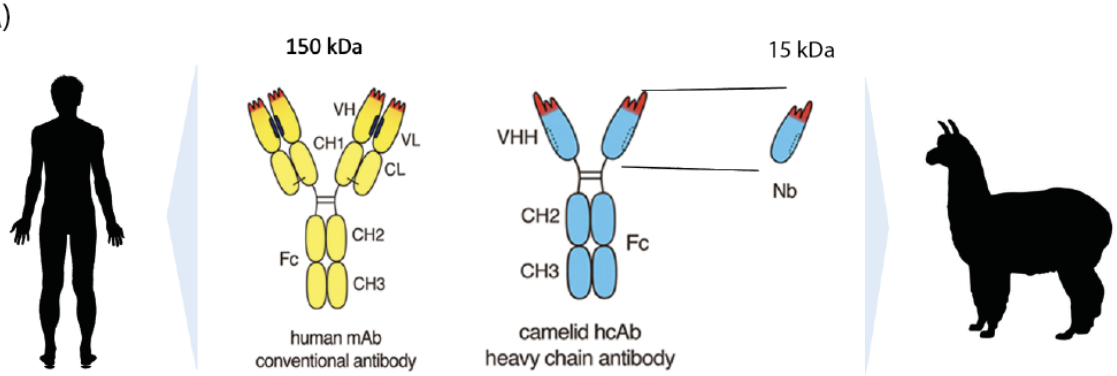

B)

Advantages over monoclonal antibodies:

- Better tissue penetration due to small size
- High stability
- High affinity and specificity to their target
- Reduced immunogenicity
- Wide range of applications
- Ease of production
- Low manufacturing costs

Figure 4. Structure and advantages of nanobodies. A) Nanobodies consist of a single variable domain derived from the heavy-chain antibodies found in camelids. B) Their small size and unique structural features confer numerous advantages over conventional antibodies, attracting significant attention for various biomedical and biotechnological applications. Modified from Bannas et al. 2017.

Another structural difference is that conventional antibodies have a large number of hydrophobic residues in the FR2 region where the variable heavy domain interacts with the variable light domain (VL). In the absence of a light chain, the hydrophobic residues on the surface of VH are exposed, making them prone to aggregation under in vitro conditions. The replacement of hydrophobic by hydrophilic residues in CDR3 reduces the aggregation ability and improves the water solubility of VHH (Sun et al. 2021: 2339).

Since the passive intercellular diffusion rate within a tissue depends on the molecular size, a 15 kDa nanobody has better penetrability compared to the performance of Abs (150 kDa). The relatively large size of conventional antibodies prevents their penetration into, for example, solid tumours and causes high systemic accumulation (Salvador et al. 2019: 1707). Because of their small size, nanobodies can be cleared rapidly through the kidney. For some specific applications, this feature may have advantages, avoiding the toxicity effect. However, several methods have been

established to prolong their half-life, such as genetic fusion to an albumin-specific nanobody domain, adding polyethylene glycol, or fusion to an FC fragment of a conventional antibody (Salvador et al. 2019: 1707).

In addition to their unique structural characteristics, the small size and monomeric nature of nanobodies make them adaptable to engineering and manipulation, opening possibilities for their application in various fields, such as biotechnology, biomedical research, diagnostics, and therapy. Nanobodies can be engineered into multivalent formats with increased avidity and strength of binding due to the targeting of multiple nanobodies to the same epitope. At the same time, nanobodies can be engineered into multiparatopic formats with different nanobody domains binding to distinct epitopes, enhancing their specificity (Tijink et al. 2008, cited in Wanner et al. 2021: 446.). For example, a single therapeutic nanobody might be attached to a tumour and immune cell, which could help the immune system to fight cancer (https://www.sanofi.com/en/magazine/our-science/nanobody-technology-platform). Additionally, nanobodies can be fused to various functional groups or proteins for different applications: to radioisotopes for use in molecular imaging and targeted radiotherapy; to fluorochromes and fluorescent proteins for in vivo imaging or fluorescence microscopy studies; to toxins for targeting delivery to cancer cells and other diseased tissues (Figure 5) (Wanner et al. 2021: 446).

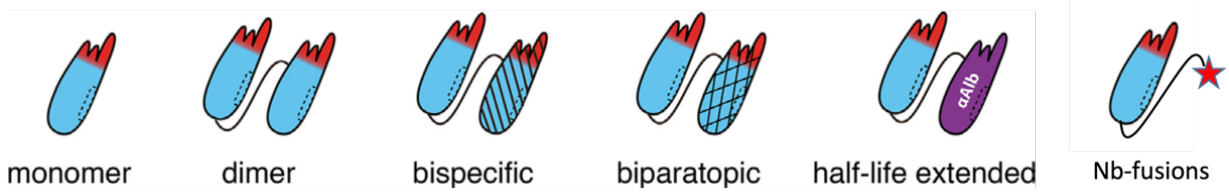

Figure 5: Nanobody formats. A nanobody consists of a single domain (monomer). To increase its specificity and avidity, it can be engineered to consist of two domains (dimer). Bispecific nanobodies recognize and bind to two different epitopes simultaneously, while biparatopic nanobodies are designed to bind to two distinct epitopes on the same antigen. The addition of an anti-albumin nanobody increases half-life by binding to albumin and preventing clearance through the renal filtration barrier. For scientific or diagnostic purposes, a nanobody can be linked to a toxin, fluorescent protein, radioisotope, etc. Adapted from Bannas et al. 2017.

Another valuable characteristic of nanobodies is high thermostability. Nanobody can maintain 80% activity at 37°C for one week, and after denaturation at 90°C, they can restore their natural active conformation (Arbabi Ghahroudi et al.1997, Perez et al. 2001, cited in Sun et al. 2021: 2340). Lui et al tested the stability of nanobodies by preincubating them along with the sample and found that all VHH assays kept their properties intact after 5 min at 50°C and some of them could even be used after 5 min at 100°C. In addition, the authors showed that nanobodies were

able to reach 60% of their activity after 75 min at 90°C (Liu et al. 2017, cited in Salvador et al. 2019: 1708). Similar behaviour has been found regarding the robustness of the nanobodies at different pH. Wang et al demonstrated great stability between pH 7.4 and 10, with stability in other pH ranges (Wang et al. 2014, cited in Salvador et al. 2019: 1708, De Vos et al. 2013, cited in Liu 2021: 3).

In contrast to large monoclonal antibodies, which usually undergo post-translational modifications, and require sophisticated machinery via eucaryotic system with long screening and purification steps, nanobodies can be easily expressed in the microbial system and rapidly selected from libraries. In addition, to achieve clinical efficacy in treatments, antibodies have to be administrated in large doses, leading to very expensive production costs, making their usage hampered by the availability due to the high costs, while nanobodies are manageable for large quantities of production and high-throughput screenings (Liu et al. 2018, cited in Sun et al. 2021: 2340, Salvador et al. 2019: 1707).

In addition to all valuable properties, camelid VHH domains present a high degree of homology with human VH domains, giving no unexpected immunogenicity reactions, making them a great tool for clinical applications (Muyldermans 2013).

1.3.1 Nanobodies in Clinical Trials

Nanobodies' valuable and unique features make them a great candidate for therapeutic, diagnostical and scientific applications. Some of them have entered clinical trials and were approved for therapeutic purposes.

The first therapeutic nanobody, caplacizumab (ALX-0081, Ablynx), was approved in the European Union in 2018 and in the USA in 2019 for the treatment of rare thrombotic microangiopathy, acquired thrombotic thrombocytopenic purpura in conjunction with plasma exchange and immunosuppression in adults. Caplacizumab is a humanised, bivalent anti-von Willebrand (vWF) factor nanobody, which inhibits the interaction of vWB with platelets, preventing thrombocytopenia, hemolytic anaemia and tissue ischemia (Scully et al. 2019).

Ozoralizumab (Nanozora®, Taisho Pharmaceutical Co. Ltd, license from Ablynx) is the next therapeutic nanobody, approved in 2022 in Japan. It is a trivalent anti-TNFa nanobody used for the treatment of RA in patients who have no adequate response to conventional therapies (Keam 2023).

Another promising nanobody therapeutic is Sonelokimab (M1095, Avillion LLP), a trivalent nanobody targeting human IL-17A, IL-17F and albumin. This nanobody showed rapid and significant clinical benefit in the phase IIb clinical trials in the treatment of severe plaque-type psoriasis compared to placebo and raises great hopes in the III phase (Papp et al. 2021, Iznardo/Puig 2021). Sonelokimab is also currently tested in phase II for the treatment of active psoriatic arthritis which affects one-third of psoriatic patients, especially those with moderate to severe form (Iznardo/Puig 2021, Alinaghi et al. 2019); and in phase II for the treatment of hidradenitis suppurativa (HS), an inflammatory skin disease with limited therapeutic options, having only one approved treatment, a TNF-a targeting monoclonal antibody adalimumab (Hunt et al. 2023). One more nanobody therapeutic for HS, SAR 442970 (Sanofi), targeting OX40L and TNF-a is being tested in phase II clinical trials. Besides nanobodies for the treatment of HS, Sanofi produced one more VHH tested in phase II (lunsekimig, SAR-443765) targeting IL-13 and TSLP for the treatment of asthma (https://www.sanofi.com/en/our-science/our-pipeline). Other promising nanobody therapeutics include Vobarizumab (ALX-0061, Ablynx), currently in phase II for the treatment of rheumatoid arthritis and systemic lupus erythematosus, targeting IL-6R (Van Roy et al. 2015); anti-ADAMT55 (M6495, Merck and Ablynx) potential therapeutic for the treatment of osteoarthritis showed safety and tolerance is ready to be tested in phase II (Bihlet et al. 2024).

Many studies have shown that CAR T cell therapy is a promising and potent curative option for cancers, although CAR nanobodies combine the benefits of traditional CAR T cell therapy with added advantages which were discussed above, making them a prospective achievement in the field of cancer immunotherapy. The first two nb-CARs are currently tested in phase I clinical trials for the treatment of refractory or relapsed multiple myeloma (BCMA nanobody CAR-T cells) and relapsed or refractory B cell lymphoma (CD19/20 bispecific nanobody), aiming to evaluate their safety, tolerability, and efficacy, potentially paving the way for more effective and targeted cancer treatments in the future (Zhang et al. 2023, De Munter et al. 2018).

1.4 P2X7 in glomerulonephritis

The evidence for the role of P2X7 in GN was demonstrated by Turner et al. in the mouse and rat model of accelerated nephrotoxic nephritis. In this model, authors showed an increase of glomerular P2X7R expression and glomerular apoptotic cells using RT-PCR, Immunohistochemistry and TUNEL assay. The renal biopsy tissue analysis of patients with lupus nephritis showed as well as an increased glomerular and tubular expression of P2X7R (Turner et al. 2007).

Considering the elevated expression of P2X7 in GN and various other inflammatory diseases, Taylor et al utilized P2X7 KO mice in the NTN model to investigate its role in disease development and progression. Their findings demonstrated a 60% reduction in glomerular thrombosis in P2X7 knockout (KO) mice by day 9 post-NTN induction. Additionally, these mice exhibited a 52% decrease in proteinuria and a 38% reduction in serum creatinine levels at the end of the experiment compared to control wild-type (WT) mice. Although the immune response to sheep IgG did not differ between the two experimental groups of mice, glomerular deposition of mouse IgG was reduced by 26% in P2X7 -/- mice. Moreover, the level of monocyte chemoattractant protein 1 (MCP-1), a chemokine crucial for glomerular recruitment of macrophages and crescent formation, as well as glomerular macrophage infiltration in NTN mice, was significantly reduced in the urine of P2X7-/- mice. In contrast, no difference was found in the number of interstitial macrophages in both groups of animals (Taylor 2009: 1276 ff.).

The first therapeutic approach with P2X7-blocking nanobodies in experimental anti-podocyte nephritis was conducted in 2016, demonstrating promising results in disease treatment (Danquah et al. 2016). Mice receiving P2X7 antagonistic nanobodies, developed little, if any renal inflammation, compared with the control group. The blocking of P2X7 prevented the development of nephrotic syndrome, maintaining normal levels of blood urea nitrogen, serum triglycerides, cholesterol, IL-6 and MCP-1 in urine. Albuminuria was significantly lower after 15 days of the experiment and the histopathological signs of kidney damage were reduced. Immunohistochemical analysis revealed significantly reduced immune cell infiltration ($Ly6G^+$ granulocytes and $CD3^+$ T cells). Conversely, the application of P2X7 activating nanobody 14D5 showed the opposite effect, enhancing the signs of disease progression (showed in proteinuria level and immune cell infiltration) compared to control nephritic mice. In addition, the application of 14D5 in P2X7 -/- mice in the model of anti-podocyte nephritis did not cause any significant effect on disease progression, confirming that the aggravating effect of this nanobody is mediated via the P2X7 receptor (Danquah et al. 2016: 4 ff.).

1.5 Aims of this work

The treatment of GN remains a significant healthcare challenge worldwide. The lack of effective therapeutic strategies, coupled with the adverse effects of existing medications, underscores the need for novel therapies to prevent the development of irreversible renal pathologies, such as ESRD, which requires renal replacement therapy and significantly reduces patients' quality of life. Previous studies have shown that blocking or deleting P2X7 significantly decreases inflammatory

renal damage in mouse models of GN (nephrotoxic nephritis and anti-podocyte nephritis), indicating this protein as a promising target for treating glomerular diseases. Therefore, the objectives of this thesis are:

1. To study P2X7 expression and localization in healthy and GN-affected kidneys;
2. To establish the therapeutic potential of P2X7-blocking nanobodies in mouse models of GN;
3. To determine the physiological outcome of P2X7 blocking on kidney resident immune cells.

The study of P2X7 blocking therapy is conducted on the most commonly used mouse model of GN, nephrotoxic nephritis, induced by high and low doses of nephrotoxic serum; and on membranous nephropathy, one of the autoimmune types of GN and the leading cause of nephrotic syndrome (Ronco et al. 2021, Alok/Yadav 2023).

2. Materials and Methods

2.1 Materials

2.1.1 Equipment

Table 2. List of equipment

Equipment	Model	Manufacturer
Centrifuges	5910 R 5424 R Rotanta 460 R SPROUT™	Eppendorf Eppendorf Hettich Biozym
CO2 Incubator	MCO-20AIC	Anyo Electric Co.
Dissociator	GentleMACS™	Miltenyi Biotec
ELISA readers	Victor3 1420 Sunrise™	Perkin-Elmer Tekan
FACS sorter	FACSAria™Fusion	BD Biosciences
Flow cytometer	FACSSymphony™A3	BD Biosciences
Laminar Flow Hood	Gelaire Typ BST6	Gelman
Light microscopes	Confocal, LSM 800 with airyscan THUNDER Imager 3D S6E Axio Scope. A1 Evos Scope A1	Carl Zeiss AG Leica Microsystems Leica Microsystems Carl Zeiss AG Thermo Fisher Scientific
Micropipette	Various sizes	Gilson
Multichannel Micropipette	Various sizes	Eppendorf
Pipette Controller	Pipetroy 2	Integra
Power supply for SDS PAGE	PowerPac 200	BioRad
Roller	Mixer SRT6	Staurt
Shaker with heat block	Thermomixer Comfort	Eppendorf
Steam cooker	FS 10	Braun
Sterile work bench	BSB4	GELAIR
Vertical electrophoresis system for SDS-PAGE	Xcell SureLock MiniCell	Thermo Fisher Scientific
Vortexer		Heidolph
Water installation with heating circulator	Corio c	Julabo
Weight scale	Quintix	Sartorius

2.1.2 Consumables

Table 3. List of consumables

Consumables	Type	Manufacturer
C-tube	gentleMACS(TM)	Miltenyi Biotec
Cell culture flask	T-75, T-225	Greiner bio one/Nunc™
Cell strainers	70 µm, 100 µm	Sigma-Aldrich
DANN LoBind tube	2 ml	Eppendorf

Disposable chromatography column	10 ml	BioRad
ELISA plate	High binding, F	Sarstedt AG
ELISA tubes	Matrix 1.4 ml Blank tubes	Thermo Fisher Scientific
Erlenmeyer flask	Various sizes	PP Corning Inc
FACS tubes	5 ml tube with 35 µm cell-Strainer cup	Corning
Falcon tubes	15 ml, 50 ml	Greiner
Gloves	Dermagrip	WRP
Magnetic particle concentrator	DynaMag™-2	Invitrogen
Microcentrifuge tubes	Various sizes	Eppendorf
Microtest plate	96 well, F	Sarstedt AG
Multistix® 10 SG	Urinalysis test strips	Siemens
Pipette tips	Various sizes	TipOne®, Sarstedt AG
PD-10 columns	G-25 M	Cytiva
Scissors, forceps, scalpels	Various sizes	FST, Braun
SDS-PAGE gels	10% and 12% NuPAGE	Invitrogen
Serological pipettes	Various sizes	BD Falcon
Sterile filtration	Steriflip, Stericup	Millipore
Surgical blade	No. 20	Feather
Syringes and needles	Various sizes	Braun

2.1.3 Chemicals

Table 4. List of chemicals

Chemicals	Manufacturer
4',6-Diamino-2Phenylidole, Dihydrochloride (DAPI)	Thermo Fisher Scientific
Aqua ad iniectabilia	Braun
ATP, sodium salt	Sigma-Aldrich/Merck
Blasticidin	Invivogen
Bovine serum albumin (BSA)	Sigma-Aldrich
Carbonate-Bicarbonat	Sigma
Collagenase II	Worthington Biochemical
Collagenase D	Merck
Collagenase V	Sigma-Aldrich
Dispase II	Sigma-Aldrich
DMEM medium	Gibco™ /Thermo Fisher Scientific
DNAse I	Roche
Dynabeads™ M-450 Tasylactivated	Invitrogen
Dynabeads™ M-450 Epoxy	Invitrogen
Ethanol	ChemSolute
Ethylenediaminetetraacetic acid (EDTA)	Sigma-Aldrich/Merck
Eukitt	Sigma-Aldrich
Fetal calf serum (FCS)	Gibco™ /Thermo Fisher Scientific
Haematoxylin	Roth
Hank's Balanced Salt Solution (HBSS)	Gibco™ /Thermo Fisher Scientific
Heparin	Braun
Hepes, 1M	Gibco™ /Thermo Fisher Scientific
Hydrochloric acid	Roth
IgG Elution butter pH 2.8	Thermo Fisher Scientific
Isoflurane	Sigma-Aldrich/Merck

L-Glutamine, 200mM	Gibco™ /Thermo Fisher Scientific
NEM, non-essential amino acid, 10 mM	Gibco™ /Thermo Fisher Scientific
NuPAGE™ LDS Sample Buffer, 4x	Invitrogen/Thermo Fisher Scientific
NuPAGE™ Sample Reducing Agent, 10x	Invitrogen/Thermo Fisher Scientific
Paraformaldehyde (PFA)	Sigma-Aldrich/Merck
Percoll™, 1,130 g/ml	GE Healthcare
Periodic acid	Roth
Phosphate buffered saline (PBS)	Gibco™ /Thermo Fisher Scientific
Polyethylenimine (PEI), MW 25000	Polysciences, Inc.
Prolong Gold Antifade	Thermo Fisher Scientific
Pronase E	Merck
Protein A Sepharose 4 Fast Flow	GE Healthcare
Red blood cell lysing buffer	Sigma
RPMI 1640	Gibco™/Thermo Fisher Scientific
Schiff's reagent	Roth
Sodium Chloride, 0.9%	Braun
Sodium pyruvate, 100 mM	Gibco™ /Thermo Fisher Scientific
Sterile rinse water	Braun
Sulfuric acid	Roth
Target Retrieval Solution	Dako
TiterMax® Gold Adjuvant	Merck
TMB One substrate	Kementec
Tris/BSA	Sigma
Tris-HCL Buffer pH9	G-Biosciences
Tris-Tween	Sigma
TruStain FcX	Biolegend
Trypsin, 10x	Invitrogen/Thermo Fisher Scientific
Tween 20	Sigma-Aldrich/Merck
Xylol	Roth

2.1.4 Cell culture media

Table 5. Eucaryotic cell culture media

Eukaryotic cell culture media	Composition
Complete DMEM	DMEM medium 2 mM L-Glutamine 1 mM Sodium pyruvate 10 mM HEPES 1x NEM (non-essential amino acids) 5 % FCS
F17 Feeding Medium	F17 Transfection medium 20 % (w/v) Tryptone N1
F17 Transfection medium	F17 Expression medium 4 mM L-Glutamine 0.1 % Pluronic
Trypsin solution	10 % Trypsin EDTA PBS -/-

2.1.5 Buffers

Table 6. Buffer receipts.

Buffers	Composition
Cell preparation	
Density gradient solution	4 ml Percoll 0.44 ml 10 x PBS 5.5 ml RPMI
Digestion solution immune cells	4.5 ml RPMI 10% (500 µl) FBS 0.25 mg/ml Collagenase D 10 U/ml DNAse I
Digestion solution glomeruli (Collagenase V solution)	5.5 ml HBSS 5.5 ml DMEM 27.5 mg BSA 11 mg Collagenase V
Digestion solution glomerular cells (Collagenase II solution)	300 U/ml Collagenase II (1:100) 87.5 U/ml Pronase E (1:16) 1.25 U/ml Dispase II (1:20) 100 U/ml DNAse I (1:100) Up to 2 ml HBSS +/+
Magnetic beads solution	37.5 µl Tosylbeads 37.5 µl Epoxybeads 4.5 ml HBSS
Cell transfection	
NaCl 300 mM	300 mM NaCl in deionized water
PEI (Polyethylenimine)	7.5 mM 25 kDa linear polyethylenimine 0.333 mg/ml in deionized water at 60°C
ELISA	
Coating buffer	100 ml H_2O 0.05 M Carbonate-Bicarbonate
Postcoat buffer	1 l H_2O 50 mM TBS, 1 % BSA
Sample diluent	Postcoat buffer 0.05 % Tween 20
Stop solution	179,6 ml ddH_2O 21.4 ml H_2SO4
Washing buffer	1 l H_2O 50 mM TBS, 0.05 % Tween 20
Flow cytometry	
FACS buffer	0.1 % BSA 0.02 % NaAzide

	PBS
Fixation	2% PFA PBS
IHC	
Blocking solution	5 % NDS 5 % NGS 0.3 % Tween 20 PBS
Antibody diluent	1 % BSA 1 % NGS 1 % NDS 0.3 % TWEEN 20 PBS
SDS-PAGE	
MES Running Buffer	50 mM MES 50 mM Tris Base 1% SDS 1 mM EDTA (pH 7.3)

2.1.6 Kits

Table 7. List of kits

Kits	Manufacturer
BCA™ Protein Assay kit	Pierce
Creatinine	Labor & Technik
SMART-Seq® mRNA	Takara Bio

2.1.7 Antibodies and nanobodies

Table 8. Antibodies used for histology

Antigen	Conjugate	Dilution	Manufacturer
Alfa	AF-647	1:500	NanoTag
CD3		1:100	Abcam
Endomucin		1:400	Santa Cruz Biotechnology
F4/80		1:2000	Ivitrogen
GFP		1:100	Santa Cruz Biotechnology
Nephrin		1:200	Progen
mPLA2R1		1:800	Sigma
huPLA2R1		1:400	Sigma
Laminin	Cy3	1:500	Sigma
mIgG	Cy2	1:100	Jackson ImmunoResearch

Table 9. Antibodies used for flow cytometry

Antigen	Conjugate	Dilution	Manufacturer
Alb (mAbH0077)		0.2 mg	Ablynx
CD105	PE	1:400	Biolegend
CD11b	PE Cy7	1:400	BioLegend
CD3	FITC	1:400	BioLegend
CD4	AF700	1:100	Miltenyi Biotec
CD45	PE-Vio770	1:100	Miltenyi Biotec
CD45	PE	1:20	BioLegend
CD45	BV785	1:500	BioLegend
CD69	PE	1:100	Miltenyi Biotec
CD8a	APC	1:100	Miltenyi Biotec
IgG1 a-ms	BV421	1:100	BioLegend
Podocalyxin	AF-647	1:400	R&D Systems

Table 10. Antibodies used in ELISA

Antigen	Conjugate	Dilution	Manufacturer
Albumin		1:100	Biomol
Albumin	HRP	1:40000	Bethyl
hCys-C8 (PLA2R)	Streptavidin	75 ng	Bethyl

All secondary antibodies were purchased from Thermo Fisher Scientific and diluted in 1:500.

Table 11. Nanobody constructs

Nanobody	Target	Purpose
13A7	P2X7	mP2X7-blocking
L-10	Clostridium difficile toxin	Control

Table 12. Peptide sequence of nanobodies domains

Domains	Peptide sequence
Alfa	PSRLEEELRRRLTEPH
13A7	EVQLVESGGGLVQPGESLRLSCTASRFMLDYYDIGWFRQAPGKEREGVSCRFT-NDGSTAYADSVKGRFTISRDIVKHTVYLQMNSLQPEDTAVYYCAAGPLTKRRQCVPG DFSMDFWGEGTLVTVSS
L-10	QVQLVESGGGLVQAGGSLRLSCVASGLTFSLYKMGWFRQGPGKAREFVATITTSG-GITHY-ADSVKGRFTIFRDNAKNMVYLQMNSLNAEDTAIYFCASGAPTTSGYKYWGQGTQVTV SS
Alb-11	EVQLVESGGGLVQPGNSLRLSCAASGFTFSSFGMSWVRQAPGKGLEWVSSISGSGSD-TLYADSVKGRFTISRDNAKTTLYLQMNSLRPEDTAVYYCTIGGSLSRSSQGTLVTVSS

2.1.8 Cell lines

Table 13. List of cell lines

Eukaryotic cell lines	
HEK293T, untransfected	Received from group of Prof. Nolte
HEK293_mP2X7	Stably transfected with murine P2X7 (group of Prof. Nolte)

2.1.9 Mouse strains

Table 14. List of mouse strains

Mouse strains	References
C57BL/6 WT, P2X7 Tg	Kaczmarek-Hajek et al. 2018
C57BL/6 CdH5.Cre P2X7 fl mTmG	Muzumdar et al. 2007 (mTmG) Sörensen et al. 2009 (Cdh5.cre) Kaczmarek-Hajek et al. 2018 (P2rx7 flox)
BALB/c huPLA2R1 PodoCre	Tomas et al. 2023a
BALB/c mhPLA2R PodoCre	Tomas et al. 2023b

The Nephrotoxic serum and recombinant PLA2R1 were kindly provided by the group of Prof. Ulf Panzer and PD Dr. Gunther Zahner.

2.1.10 Software

Table 15. List of Software

Software	
GraphPad Prism	GraphPad Software, Inc.
FIJI	ImageJ
Flowjo	BD Biosciences
Illustrator	Adobe

2.2 Methods

2.2.1 Nanobody production

DNA of P2X7-blocking nanobody alfa-13A7dim-alb11 and control nanobody alfa-L-10dim-alb11 were kindly provided by the group of Prof. Friedrich Koch-Nolte.

Cell culture was conducted under sterile conditions in a laminar flow hood. Sterile media were used, and all prepared solutions were sterilized by filtration through a 0.22 µM filter using either a Stericup or Steriflip vacuum filter. Adherent HEK293 cell lines were cultured in a complete DMEM medium with 5% FCS in T-75 culture flasks with filter caps. For sub-culturing or ***harvesting***, cells were washed with PBS and incubated for 5 min with 1 ml of trypsin solution. Trypsin was inactivated by adding a culture medium, and cells were routinely split at a 1:5 to 1:10 ratio every two to four days, depending on cell density. HEK293 cells stably transfected with mouse P2X7 were maintained with the addition of 10 µg/ml blasticidin once a week. All cells were cultured in a steam-saturated incubator at 37 °C with 5% CO2.

The HEK293-6E cells were ***transfected*** with DNA using the transfection reagent PEI. For transfecting cells in a 30 ml culture volume in a T-225 flask, a solution of 20 µg plasmid DNA and 80 µg PEI was prepared in 3 ml of 150 mM NaCl, mixed thoroughly by vortexing, and incubated at room temperature (RT) for 20 minutes. This mixture was then added dropwise to the cells, which were subsequently cultured at 37 °C with 5% CO2. Twenty-four hours post-transfection, the cells were supplemented with 500 µl of F17 feeding medium (20% w/v Tryptone). Six days later, the supernatants containing secreted proteins were collected by double centrifugation at 4000 rpm for 10 minutes and stored at 4 °C until subsequent control and purification.

The harvested supernatant was subjected to ***sterile purification*** using 2 ml of Protein A in a disposable chromatography column. The column was subsequently washed with 10 ml of PBS -/- and the harvested nanobodies were loaded onto the column, where they bound to the Protein A ligand. The column was then washed again with 10 ml of PBS -/- to remove unbound proteins.

Nanobody dissociation from Protein A was performed by adding the elution buffer to the column three times (1.2 ml for the first elution (E1) and 2.5 ml for the second and third elutions (E2, E3)). Subsequently, extracted nanobodies were neutralized using a 10-fold dilution of neutralization buffer: 120 µl for E1 and 250 µl for both E2 and E3.

For buffer exchange, a new 5 ml PD10 column was washed with 25 ml of PBS containing calcium and magnesium ions (PBS+/+) after draining the storage buffer. Subsequently, collected nanobodies with an additional 3.5 ml PBS +/+ were drained through the column and collected into a new 15 ml tube.

The Protein A column was regenerated by successive washing with 10 ml of elution buffer, followed by 20 ml of PBS -/-, and finally, 10 ml of PBS containing 20% ethanol. The column was then stored at 4 °C with 5 ml of ethanol solution until the next purification process.

Samples (20 µl) from all solutions passing through the columns were collected into 1.5 ml Eppendorf tubes for purification quality analysis via ***sodium dodecyl sulfate-polyacrylamide gel electrophoresis (SDS-PAGE)***, where 10 µl of analysed samples were denatured by boiling for 10 minutes at 70 °C in a 10 µl solution containing LDS sample buffer and a sample reducing agent. The samples were then loaded into the wells of a polyacrylamide gel and run in electrophoresis for 40 minutes at 200 V, where the proteins were separated based on size, with smaller proteins migrating faster through the gel. After electrophoresis, the proteins in the gel were stained with Coomassie brilliant blue for visualization and analysed for size determination and purity (Figure 6).

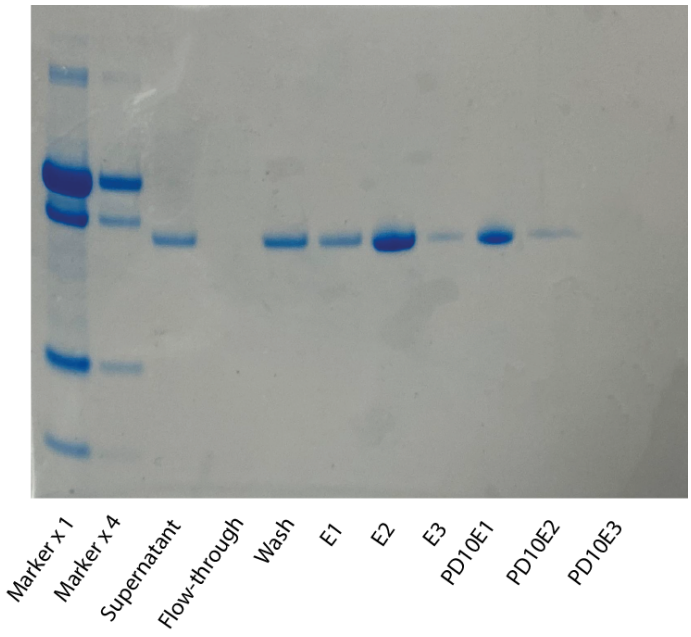

Figure 6. Purification quality control of alfa-13A7dim-alb11 in SDS-PAGE gel. Supernatant identifies the stock nanobody solution for purification. Flow-through shows no nanobodies were lost during purification, however, during washing, some quantity of nanobodies unbonded Protein A. E1-E3 shows eluted nanobodies, PD10E1 – PD10E2 show purified nanobodies with exchanged buffer.

The concentration of purified nanobodies was determined using a ***bicinchoninic acid (BCA) test***. 10 µl of nanobody samples and standards were mixed with a working reagent containing bicinchoninic acid and copper sulfate and incubated for 30 min at 37 °C. The concentration was measured using a spectrophotometer at a wavelength of 562 nm.

Concentration adjustments were made either by using Amicon 10K centrifugal filters (spinning at 4000 rpm for 5 minutes) or by diluting the nanobodies in PBS +/+. The nanobodies, at a concentration of 0.5 mg/ml, were collected into 1.5 ml tubes and stored at -80 °C.

The functionality of nanobodies was identified using the ***functional test***. Its principle is based on 13A7 nanobodies' ability to bind to P2X7 receptors and prevent pore formation, thereby inhibiting the entry of nuclear dye into the cell. Non-functional P2X7-blocking nanobodies or P2X7-activating nanobodies do not prevent this effect, resulting in increased dye uptake, which can be observed via flow cytometry.

For the assay, P2X7-expressing HEK cells were washed and resuspended in the RPMI medium. 100 µl of cells were incubated with 1 mg of nanobody for 10 minutes, followed by the addition of 2 µl DAPI. The cells were then incubated with 100 µl of ATP at both low and high concentrations for 5 minutes in a water bath at 37 °C. After washing, the cells were analysed for DAPI uptake using flow cytometry.

2.2.2 Histological techniques

For histological analysis, 0.3 cm thin pieces of PBS-perfused kidney tissues were fixed in PFA 4% overnight at 4 °C, afterwards washed 4 times for 20 minutes in PBS on the shaker at RT and stored by 4 °C in PBS until subsequent paraffin embedding.

For ***immunohistochemistry (IHC)***, 2 µm thin paraffin-embedded kidney sections were deparaffinised as follows: 2 x 10 minutes in xylol; 5 minutes each in 100 %, 75 %, and 50 % ethanol with subsequent rehydration in PBS for 10 minutes. Antigen retrieval was conducted in pre-heated DAKO buffer pH 6 or pH 9 in a water bath for 30 minutes and cooled down at RT for 20 minutes. After washing in PBS, the samples were blocked for 1 hour at RT in a blocking solution. After blocking, the samples were stained overnight at 4 °C with primary antibodies. On the next day, the tissues were washed 3 x 15 minutes in PBS and stained with fluorochrome-conjugated secondary antibodies for 1 hour at RT. After subsequent washing 3 x 15 minutes in PBS, the samples were mounted with antifade gold and analysed in a fluorescent microscope within one week.

The brightness and contrast of immunofluorescent figures were adjusted in ImageJ software. The counting of P2X7-expressing cells and co-localization with other markers (CD3, CD4, iba-1 and endomucin) was conducted manually using the plugin 'Cell Counter'. The expression level of dyes was evaluated using intensity analysis.

For ***periodic acid Schiff staining (PAS)***, deparaffinized and rehydrated 2 µm thin paraffin-embedded kidney sections were oxidized in 1 % Periodic acid for 15 minutes and washed for 3 minutes in flowing water with subsequent incubation for 1 hour in Schiff's reagent. After additional washing, the nuclei were stained with Haematoxylin for 1 - 3 minutes and rewashed for 2 minutes. The staining was differentiated in Hydrochloric acid alcohol and washed for 2 minutes. Staining quality was controlled under a microscope, repeating nuclei staining if needed. The samples were dehydrated in ascending alcohol series (70 %, 2 x 96 %, 4 x 100 %), xylol and mounted with Eukitt.

Glomerulosclerosis index (GSI) was determined on PAS staining of paraffin-embedded tissue on a light microscope. Each of 100 glomeruli per mouse was analysed for sclerotic damage level, where no sclerosis characterized 0 stage; 0 - 25 % sclerosis – 1 stage; 25 - 50 % sclerosis – 2 stage; 50 - 75 % sclerosis – 3 stage; and 75 - 100 % - 4 stage (Figure 7). GSI was calculated using a formula:

$$GSI = \frac{(1 * n1) + (2 * n2) + (3 * n3) + (4 * n4)}{n0 + n1 + n2 + n3 + n4}$$

Where n_x – is the sum of glomeruli at each grade of glomerulosclerosis.

Samples were analysed in a blinded fashion, with unbinding of mouse number and group occurring after the determination of GSI and the percentage of sclerotic glomeruli.

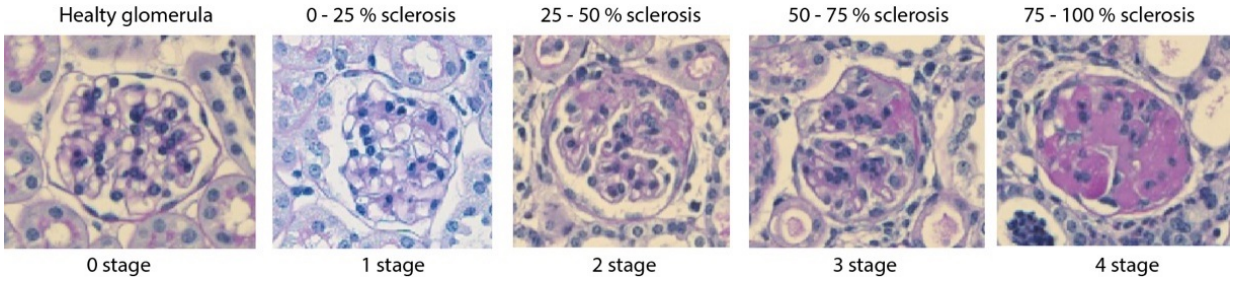

Figure 7. Stages of glomerulosclerosis used for scoring.

2.2.3 Cell isolation and sorting

To prevent ***immune cell*** death during isolation from the kidney, 50 µg of 13A7 nanobody was injected i.p. 20 minutes before euthanasia. To divide circulating immune cells from kidney resident immune cells for FACS sorting and RNA sequencing, a-CD45 antibody (5 µl in 100 µl PBS) was injected i.v. 3 minutes before sacrifice, kidneys were isolated without perfusion. For flow cytometry analysis, the kidneys were perfused with PBS via *arteria renalis* without CD45 i. v. injection.

Isolated kidneys were chopped into tiny pieces, transferred into a MACS/Miltenyi C-tube containing 5 ml of digestion solution, vortexed, and incubated in a water bath at 37 °C. After 10 and 20 minutes, the samples were mixed on a gentleMACS Dissociator using the programs Spleen 1_1 and Lung 2_1, respectively. The digested kidneys were passed through a 70 µm cell strainer into a 50 ml tube, gently mashed with a 1 ml syringe plunger base, and washed with additional PBS by centrifugation at 400 × g for 5 minutes at 4 °C.

The resulting cell pellet was resuspended in 5 ml of 40% Percoll solution and centrifuged at 400 x g without acceleration and deceleration for 20 minutes at RT. The cell pellet at the bottom of the tube was washed in 10 ml of FACS buffer. Erythrocytes were lysed with 3 ml of Red Blood Cell lysis buffer for 3 minutes. After an additional wash, the cells were resuspended in 100 µl of FACS buffer for staining.

The principle of ***glomerular cell isolation*** involves perfusing the kidney through the renal artery with magnetic beads that do not pass through the filtration barrier and instead accumulate in the glomeruli. Following gentle dissociation, the glomeruli containing the magnetic beads are separated from the remaining cell mass using a magnet. These isolated glomeruli are then subjected to a secondary dissociation to separate the glomerular cells and remove the beads (Figure 8) (Liu et al. 2023).

Figure 8. The principle of glomerular isolation. A) Kidneys were perfused through renal arteries under a microscope with magnetic beads. Created with BioRender.com. B) Glomeruli filled with magnetic beads are concentrated on the magnet. C) PAS staining of the perfused kidney shows magnetic beads entering the glomerulus.

Isolated kidneys were perfused with magnetic beads solution 2 ml per kidney via *arteria renalis*, subsequently minced and transferred into MACS/Miltenyi c-tube containing 5 ml collagenase V digestion solution. For digestion, minced kidneys were incubated for 5 min at 37 °C, mixed on gentleMacs dissociator on program m. spleen 01_01, digested in the water bath for 5 min and mixed on gentleMacs on program m. spleen 01_02.

Digested kidneys were transferred to a 100 µm cell strainer on a 50 ml falcon tube and smashed gently through the strainer with the plunger base of a 1 ml syringe. The falcon tube containing the digested kidneys was washed with HBSS and transferred again on the cell strainer with the subsequent addition of HBSS until a final volume of 45 ml. After centrifugation at 300 x g for 4 min at 4 °C, the cellular pellet was resuspended in 3.5 ml HBSS, transferred into 2 x 2 ml low bind tubes, and inserted into a magnetic particle concentrator. The supernatant was collected into new 2 x 2 ml low-bind Eppendorf tubes into a magnet for more glomerular cell concentration. The quality of glomeruli isolation was controlled on a microscope.

Isolated glomeruli were placed into 2 ml low-bind Eppendorf tubes, resuspended in 2 ml collagenase II solution, and incubated for 40 min at 37 °C on a thermomixer, shaking at 1400 rpm. Isolated glomeruli were mixed by pipetting twice at 5, 10, 20, 25 and 35 minutes of incubation and sheered with a 27G needle attached to a syringe at 15 minutes of incubation. Podocytes were loosened by vortexing once (level 5 out of 6) at 10, 20, and 30 minutes; and vortexed three times at 40 minutes of incubation. Digested glomeruli were pipetted up and down five times with a 200 µl pipette at 30 and 40 min. Separated glomerular cells were then sieved through the 35µl filter cup on the FACS tube and washed with FACS buffer. The result of digestion was controlled on a microscope.

To analyse isolated kidney cells in ***flow cytometry***, the cells were incubated with FC blocker for 10 minutes on ice and stained with fluorochrome-conjugated antibodies for 20 - 30 min. Cells were washed with 2 ml FACS buffer at 350 x g for 4 minutes at 4 °C. Isolated cells for flow cytometry analysis were fixed with 150 µl of 2 % PFA for 10 minutes at RT, washed with FACS buffer, and analysed within 2 days on flow cytometry. P2X7R was analysed using transgenic GFP expression of P2X7 Tg mice. Isolated $CD4^+$ and $CD8^+$ T cells for further RNA sequencing were analysed and sorted within a few hours on a FACS sorter. Gating strategies for flow cytometry analysis of renal T cells and glomerular cells are shown in Figure 9. The gating strategy for renal resident T cells sorting on FACS is shown in Figure 10.

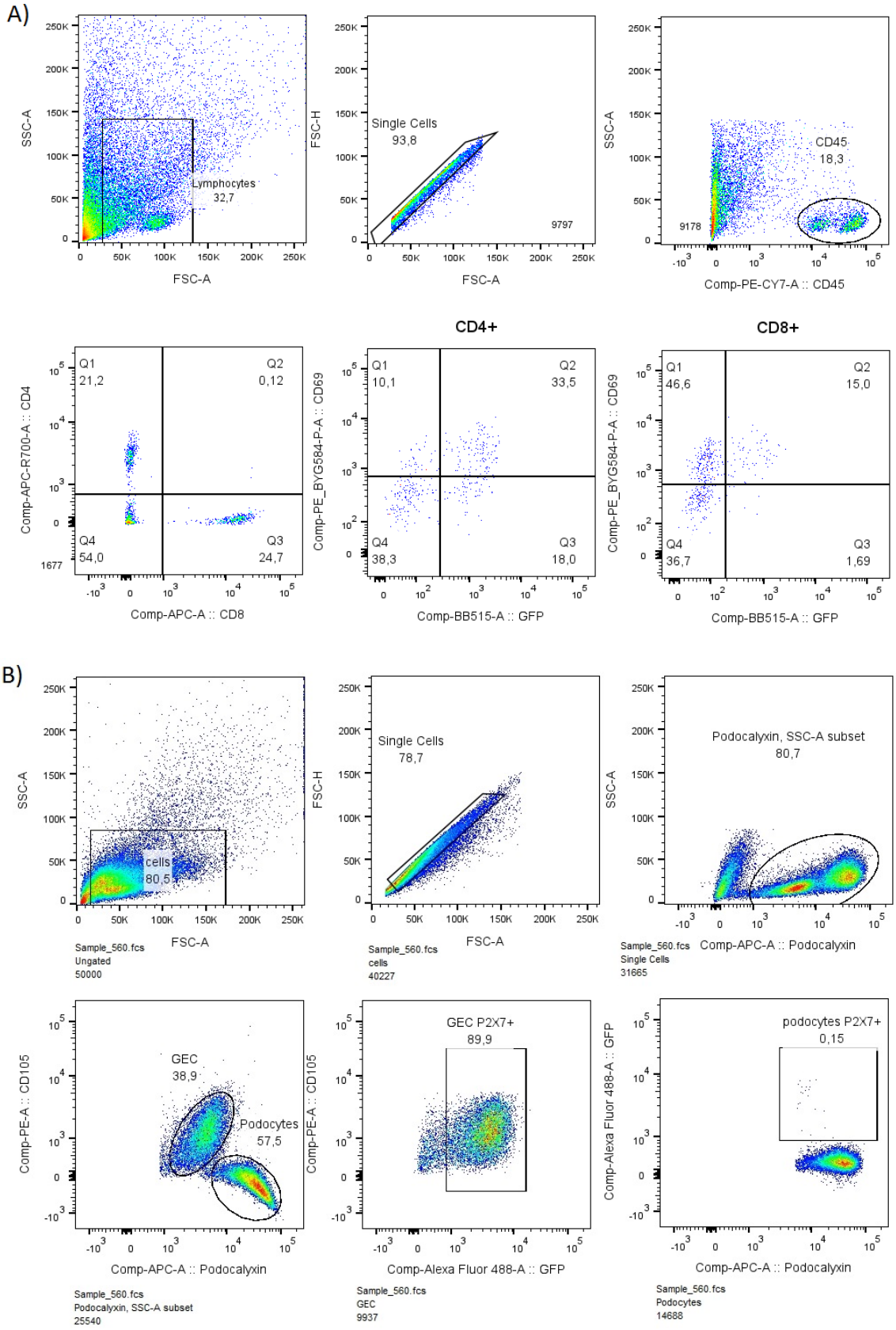

Figure 9. Flow cytometry gating strategy of isolated renal resident immune and glomerular cells. A) Gating strategy for renal T cells. B) Gating strategy for isolated GEC and podocytes. P2X7 expression on the cells was analysed within GFP signal.

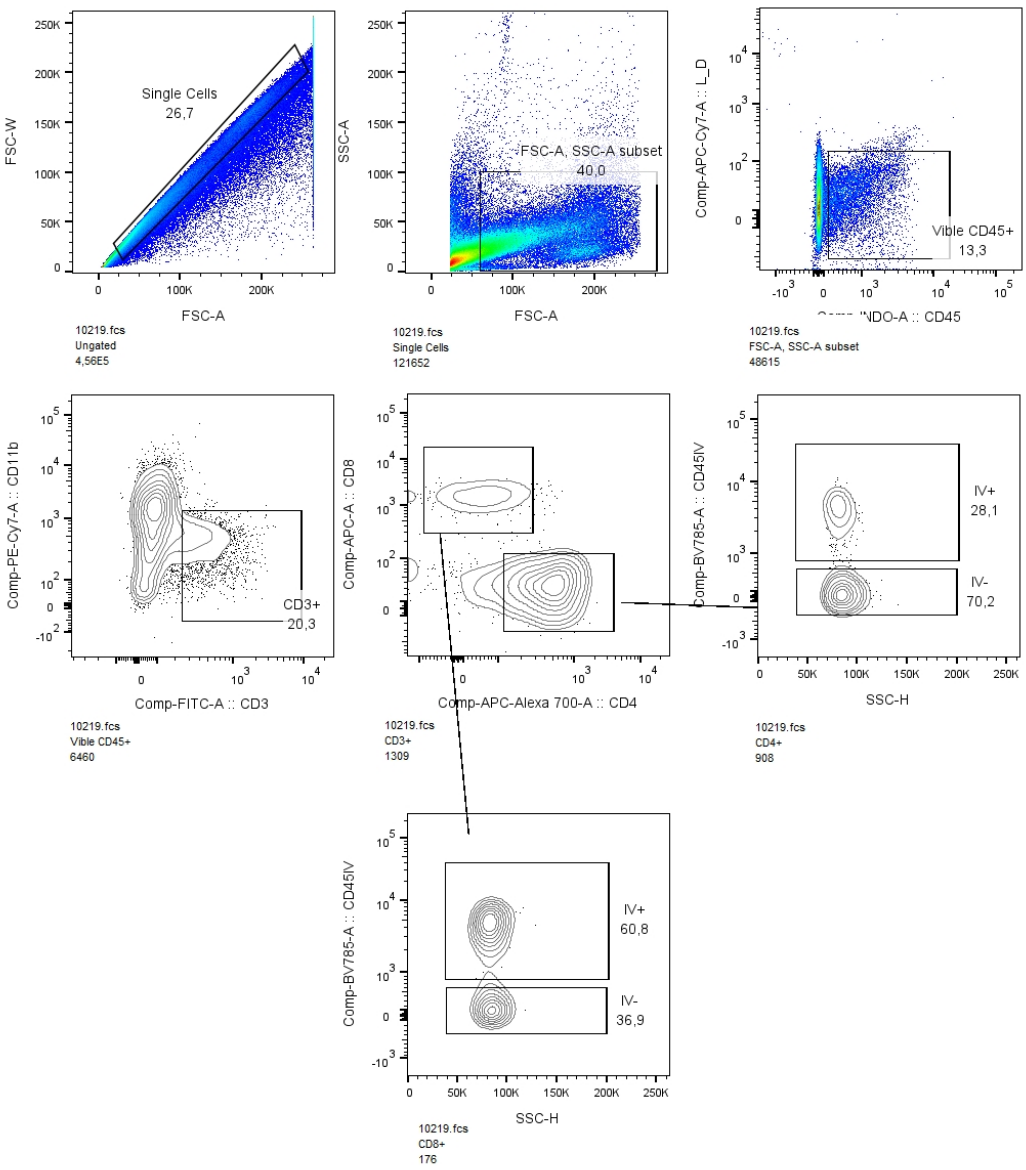

Figure 10. Gating strategy for FACS sorting of kidney resident T cells. Living $CD3^+$ T cell population was separated from the $CD11b^+$ population, divided into $CD4^+$ and $CD8^+$ subsets, which then were split into CD45 i. v. positive and negative populations. CD45 i. v. negative $CD4^+$ and $CD8^+$ T cells were sorted for subsequent RNA sequencing.

2.2.4 Molecular and genetic analysis

Since the number of isolated renal T cells was low and insufficient for proper RNA isolation, SMART-Seq (Switching Mechanism at 5' End of RNA Template) technology was applied. This technology enables high-sensitivity mRNA sequencing from very low inputs of RNA or intact cells.

The ***SMART-Seq method*** relies on a template-switching mechanism during reverse transcription. When the reverse transcriptase enzyme reaches the 5' end of the RNA template, it adds a few additional nucleotides to the cDNA. These nucleotides act as an anchor for the template-switching

oligonucleotide (TSO), which allows the enzyme to switch templates and continue synthesizing cDNA from this new primer.

Isolated kidney-resident $CD4^+$ and $CD8^+$ T cells were sorted into PCR tubes containing 12.5 µl of sorting buffer, which included 10x lysis buffer, RNase inhibitor, 3' SMART-Seq CDS Primer, and nuclease-free water. After pulse vortexing and brief centrifugation, the cells were stored at -80 °C until the subsequent steps of cDNA synthesis and RNA sequencing, which were performed at the Leibniz Institute of Virology. Quality control was done with FastQC (Barbraham Bioinformatics). Raw reads were mapped with RNA Star to mm9 using Galaxy Freiburg. Read counts were extracted with htseq-count (Anders et al. 2015), and differential gene expression was done with DESeq2 (Love et al. 2014). Gene set enrichment analysis was performed with Shiny GO (Ge et al. 2020)

2.2.5 Biochemical and analytical assays

The amount of albumin in urine and antibodies against huPLA2R in blood were analysed using the ***enzyme-linked immunosorbent assay (ELISA)*** method. A 96-well ELISA high binding plate was coated with primary antibody diluted in coating buffer (100 µl/well) and stored at 4 °C overnight. After the plate and reagents warmed up at RT for 1 hour, the coating buffer was removed, and the plate was washed three times with washing buffer (200 µl/well). The plate was filled with postcoat buffer (150 µl/well) and incubated for 30 minutes at RT on a shaker with subsequent 3 x washing. 100 µl/well of previously diluted in sample diluent standards and samples were added to the plate in duplicates and left for incubation on the shaker by RT for 1 hour. The plate was then washed 5 times with washing buffer, and incubated on the shaker with HRP conjugated antibody solution (100 µl/well) in the dark, for 1 hour at RT. After washing 5 times, the plate was filled with 100 µl/well TMB substrate and incubated in the dark for 3 minutes (albumin ELISA) or 2 minutes (mouse IgG ELISA). The reaction was stopped with 100 µl/well Stop Solution and measured within 30 minutes on an ELISA reader.

Creatinine level in urine was measured using a ***creatinine test*** kit. Previously diluted in water samples (1:10 or 1:20) and standards were added to the 96-well plate in the amount of 4 µl with subsequent pipetting of 100 µl/well Reagent-1. After incubation for 5 minutes at RT on the shaker, the plate was filled with 50 µl/well Reagent 2. The primary absorbance was evaluated after 1 minute on ELISA reader. The secondary absorbance was evaluated after additional incubation on the shaker for 20 minutes at RT.

To identify ***nanobodies in urine and blood serum***, the cell culture method was used. Detached P2X7-expressing HEK293 cells were washed with 10 ml FACS buffer at 1500 rpm for 5 minutes. The cell pellet was diluted in FACS buffer, split into FACS tubes (100 µl/sample) and incubated for 20 minutes at 4 °C with 1 µl urine or blood serum sample of nanobody-injected mice. After washing with FACS buffer, the cells were incubated with a-HLA antibody (0.2 µg/sample Mab77) for 20 minutes at 4 °C. The cells were washed and stained with fluorochrome-conjugated secondary antibody for Mab77 (a-mouse IgG) for 20 min at 4 °C, and analysed on flow cytometry.

2.2.6 Animal handling

All mice were bred in the University Medical Center Hamburg-Eppendorf animal facility. Animals had access to water and standard animal chow ad libitum. All experiments complied with national and institutional ethical standards and animal care guidelines and were approved by the Veterinarian Agency of Hamburg and the local committee for animal care (registration numbers N059/21, N020/2019).

Urine was collected by spontaneous urination, or using a metabolic cage, where mice were placed for up to two hours in a small cage (8 x 12 cm) and up to four hours in a big cage (half of type II long cage). Urine was collected into 1.5 ml tubes and stored at -20 °C.

During the experiment, blood from MN mice was collected via cheek puncture. On the final day of the experiment, blood collection from all mice was conducted either through the heart puncture (NTN mice) or aorta puncture (MN mice).

The blood was collected into 1.5 ml tubes containing 5µl Heparin. After 20 min of incubation at RT, the blood was centrifuged by 1500 x g for 10 minutes. The supernatant was collected into new 1.5 ml tubes and stored at -20 °C.

NTN mice were anaesthetized by isoflurane inhalation for blood collection through heart puncture and subsequent euthanasia in cervical dislocation. Isolated kidneys were perfused with PBS under an optical microscope via *arteria renalis* using a thin plastic needle attached to a 1 ml syringe.

MN mice were anaesthetised by isoflurane inhalation with subsequent urine collection through urinary bladder puncture and blood collection through aorta punction. Kidney perfusion was conducted with a 20 ml PBS through the heart puncture.

2.2.7 Statistical analysis

All statistical analysis was performed in GraphPad Prism 8.3.0. The cell quantity, GSI, and protein expression levels between the healthy control, diseased and therapeutic groups were compared using the Mann-Whitney U test due to the small sample sizes. Survival rates among the groups were compared using Kaplan-Meier survival analysis with the log-rank (Mantel-Cox) test. Changes in urine and blood parameters over time between the groups were analysed using ANOVA test. Correlation analysis was assessed using Spearman's rank correlation coefficient. Data were expressed as mean with the standard error of the mean (SEM). A p-value of < 0.05 was considered statistically significant for all analyses.

3. Results

3.1 Characterisation and visualization of P2X7 expression in kidney resident cells

3.1.1 Distribution of P2X7 expression by kidney-resident cells

To better understand the role of P2X7 for kidney-resident cells, histological sections of previously engineered P2X7-EGFP transgenic mice were analysed (Kaczmarek-Hajek et al. 2018). These mice overexpress a P2X7-EGFP fusion protein from a bacterial artificial chromosome encompassing the entire P2X7 gene locus. Immunofluorescent staining of healthy kidney sections revealed P2X7 expression mostly on resident immune cells: Co-staining of markers for T cells and macrophages with a GFP-specific antibody confirmed the expression of P2X7 by interstitial $CD3^+$ and $CD4^+$ T cells and by $IBA1^+$ macrophages. In addition, P2X7 receptor is widely expressed on glomerular cells, which was shown in co-expression with endomucin, a marker for endothelial and hematopoietic stem cells. Among all P2X7-expressing cells, macrophages constituted the largest population, accounting for 60 %. Other 40 % of P2X7-expressing kidney cells constituted $CD3^+$ T cells and glomerular cells (19.4 % and 20.6 % respectively), with 12.25 % in $CD4^+$ T cells (n = 4) (Figure 11).

3.1.2 Targeting of P2X7-expressing cells with alfa-tagged 13A7 nanobody

13A7 nanobody is a selective antagonist for P2X7, developed by the group of Prof. Friedrich Koch-Nolte (Danquah et al. 2016). To analyse 13A7 nanobody in Paraffin-embedded mouse samples, the construct used in this study was edited to include an alpha-tag, a protein fusion tag commonly used for scientific visualisation and identification in biological samples; two anti-P2X7 domains to enhance avidity towards P2X7, and an anti-albumin domain to extend its half-life by preventing rapid clearance through the renal filtration barrier (Figure 12).

As a control nanobody without binding ability to antigens in mice, L-10 (a nanobody against Clostridium difficile toxin) was also edited to contain an alfa-tag, two L-10 domains and an anti-albumin domain.

To analyse and prove the P2X7-binding capacity of the generated alfa-tagged 13A7 nanobodies in the kidney, the immunofluorescence analysis was performed. For this purpose, P2X7 transgenic (Tg) and P2X7 knockout (KO) mice were used. 20 µg of alfa-13A7dim-alb nanobodies were injected i. v. and the kidneys were isolated 24 hours after injection.

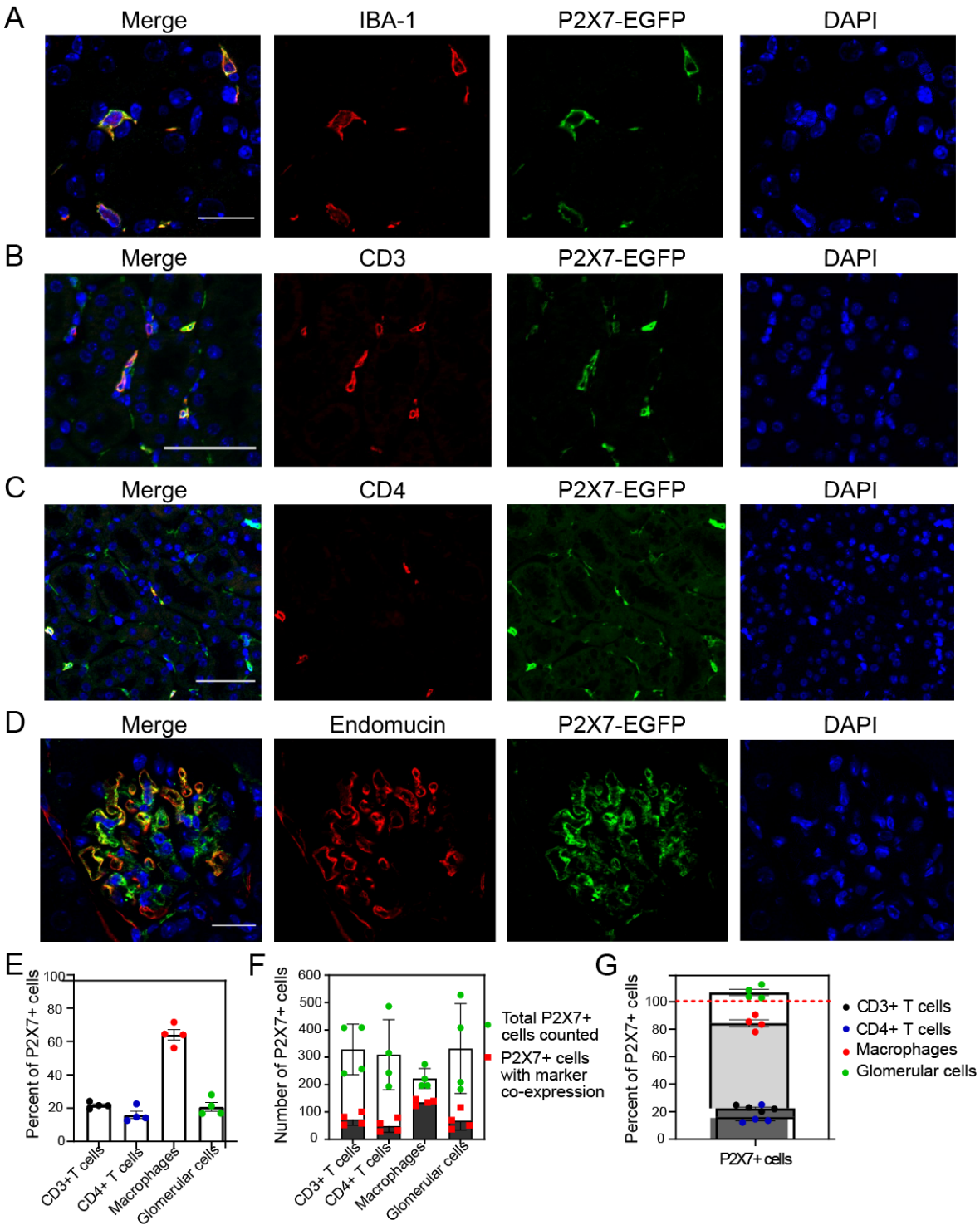

Figure 11. Co-expression of P2X7 with T cells, macrophages, and glomerular cells in healthy mice kidney. A-D) Kidney sections were stained with a-GFP and with A) a-CD3 antibodies, Scale bar: 10 µm; B) a-CD4 antibodies, scale bar: 10 µm; C) a-iba-1, scale bar: 20 µm; D) a-endomucin, scale bar: 30 µm. E) The percentage of P2X7+ cells expressed in $CD3^+$ and $CD4^+$ T cells, iba-1^+ macrophages and glomerular cells. F) Absolute number of P2X7+ cells co-expressed with CD3, CD4, iba-1 and endomucin and without co-expression. G) Total relative amount of P2X7+ cells expressed on T cells, macrophages, and glomerular cells (cumulative percentage: 102-113%).

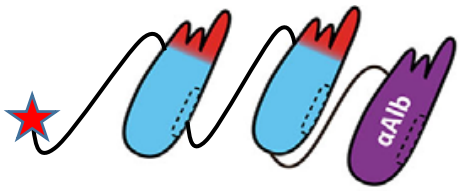

Figure 12. 13A7 nanobody construction. The alfa-tag is shown as a star; 13A7 domains (P2X7-blocking site) are shown in blue and the anti-albumin domain in violet.

Immunostaining showed the binding of P2X7-blocking nanobody to P2X7-GFP-expressing cells in the renal interstitial and glomerular cells (Figure 13, A). As expected, 13A7 nanobody did not bind to P2X7 KO kidney tissue (Figure 13, B).

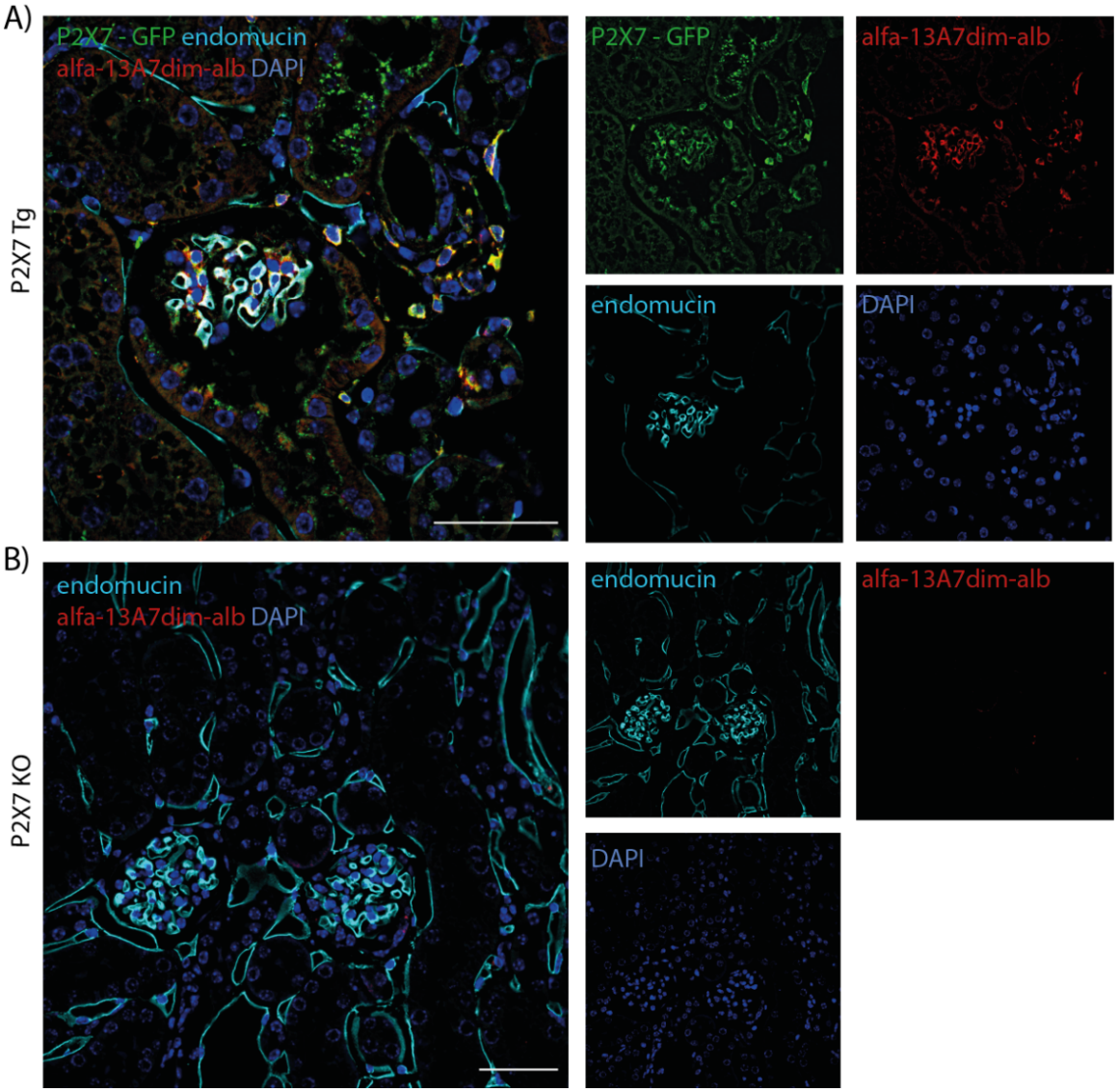

Figure 13. Visualization of 13A7 nanobodies in the kidney. A) 13A7 covers P2X7-expressing cells in P2X7 Tg mice and B) does not bind to kidney cells in P2X7 KO mice. Scale bar 50 µm.

Functional tests using P2X7-expressing HEK cells confirmed the effective binding and blocking of alfa-tagged 13A7 nanobody, preventing large pore formation and DAPI uptake in the presence of ATP at high and low concentrations (Figure 14, A). Conversely, control nanobody L-10 did not prevent these effects, resulting in an increased DAPI signal when analysed in flow cytometry (Figure 14, B).

These data confirm the capacity of alfa-tagged 13A7 nanobodies to bind specifically to P2X7-expressing cells and effectively prevent P2X7 activation in the presence of eATP.

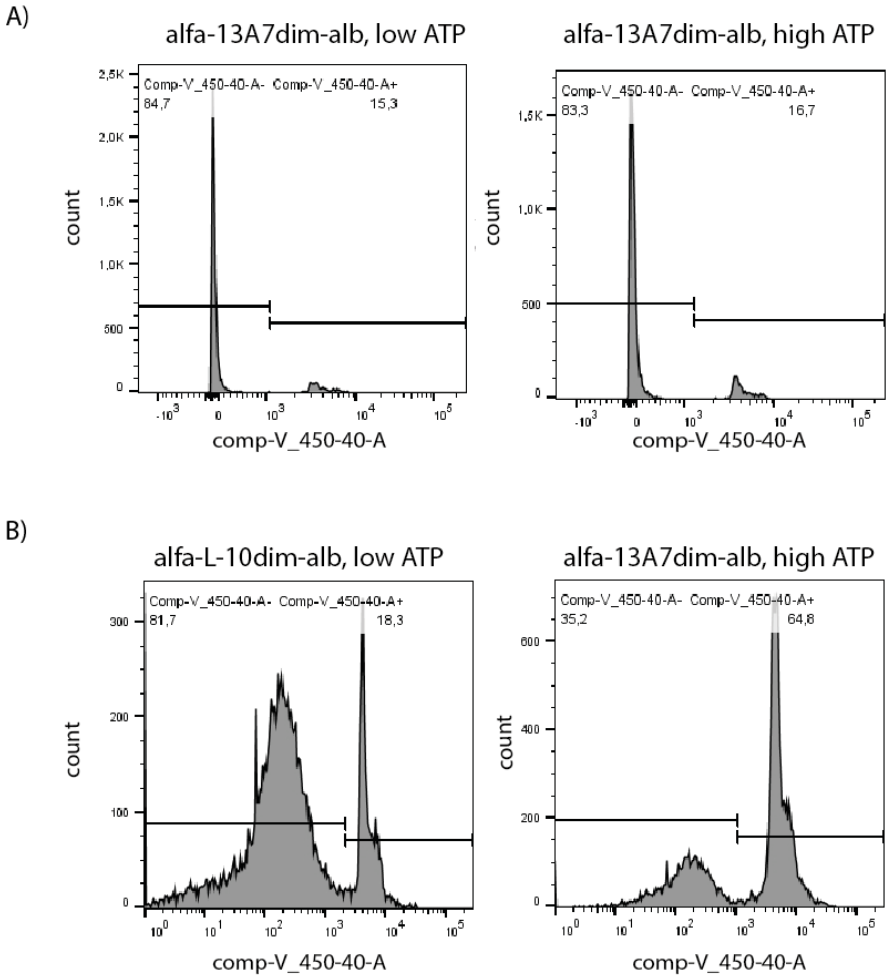

Figure 14. Functional test of alfa-tagged nanobodies. eATP at low and high concentrations when binding to P2X7 leads to large pore formation and DAPI uptake. 13A7 nanobody effectively prevents this effect (upper row), while the L-10 control nanobody does not (bottom row). This effect is seen in the flow cytometry analysis of DAPI signal.

3.2 Impact of nanobody therapy on T cell dynamics in NTN progression

To analyse the therapeutic potential of the P2X7 blocking nanobody in glomerulonephritis and investigate the role of P2X7 in kidney inflammation, the well-established immune-mediated kidney disease model of nephrotoxic nephritis (NTN) was employed. This model is induced via the administration of nephrotoxic serum (NTS), which contains antibodies against components of the GBM. Binding of antibodies to the GBM triggers complement activation and immune cell recruitment, leading to inflammation and glomerular injury.

A higher dose (75 µl) and lower dose (35 µl) of NTN, diluted 1:1 in NaCl, were administered by intraperitoneal (i. p.) injection to the mice to induce a more severe and a milder form of NTN, respectively.

Based on the experimental scheme (Figure 15), the mice were sacrificed twelve days after induction of NTN. Disease progression was monitored by urine analysis using urine stix and ELISA analysis, starting from day 0 before disease induction. Control and NTN mice receiving nanobody therapy were injected with 50 µg of half-life extended alfa-13A7dim-alb nanobody every two days before urine collection. Nanobody-treated NTN mice received the first dose of 13A7 nanobody two hours before NTS injection.

Kidney and blood collection for subsequent analyses was performed on day 12 of the experiment. The mice were euthanized beforehand if they experienced severe disease symptoms (stress and pain signs combined with weight loss ≥ 10%; development of ascites; or weight loss ≥ 20%).

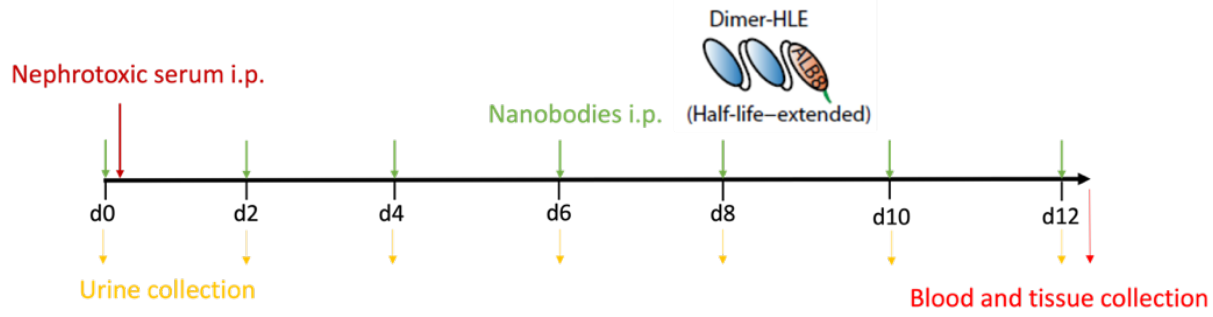

Figure 15. Experimental scheme of nanobody therapy in NTN model. NTS was injected i. p. at the day 0. Urine collection and nanobody application were performed every second day starting from day 0. The experiment was ended after twelve days of NTN followed by blood and tissue collection for further analysis.

3.2.1 P2X7 blocking therapy does not alleviate proteinuria but shows a trend towards increased survival in severe NTN

To investigate the progression of NTN, albumin-ELISA analysis of collected every two days urine was performed.

Mice with high dose NTN (severe NTN: sNTN) experienced fast-developing nephrotic syndrome with severe proteinuria shortly after disease induction: on day 2, albumin-creatinine ratio (ACR) level in sNTN mice with and without nanobody therapy reached 380 mg/mg and remained severe during the whole course of the disease. While untreated sNTN mice manifested stable high proteinuria (400 - 500 mg/mg), 13A7-treated sNTN mice experienced fluctuating ACR levels with its peak on day 8 (726 mg/mg), which levelled up with untreated mice on day 12 (520 mg/mg) (Figure 16, A). This can be explained by a low number of sNTN-treated mice (n = 4) showing higher variability in proteinuria levels.

Mice receiving a lower dose of NTN (milder NTN: mNTN) also experienced severe proteinuria on the entire course of the experiment, with the highest peak on day 2 for untreated mNTN mice (242 mg/mg) and on day 4 for treated mNTN mice (552 mg/mg). Starting from day 6 albuminuria levelled up in both groups of mice and remained at 170-230 mg/mg (Figure 16, A).

Despite severe NTN symptoms and high proteinuria, 100 % of anti-P2X7 nanobody-treated sNTN mice (n = 4) survived the whole experiment, while 27.3 % of control nanobody-treated sNTN mice (n = 11) died within three days after NTS injection. mNTN appeared with smaller disease manifestations with 100 % survival in both groups with and without nanobody therapy (n = 9 and n = 10 respectively) (Figure 16, B).

Thus, 13A7 therapy in both severe and milder NTN did not improve proteinuria, however, while not statistically significant ($p = 0.272$) there might be a trend to increased survival in sNTN mice with anti-P2X7 nanobody therapy.

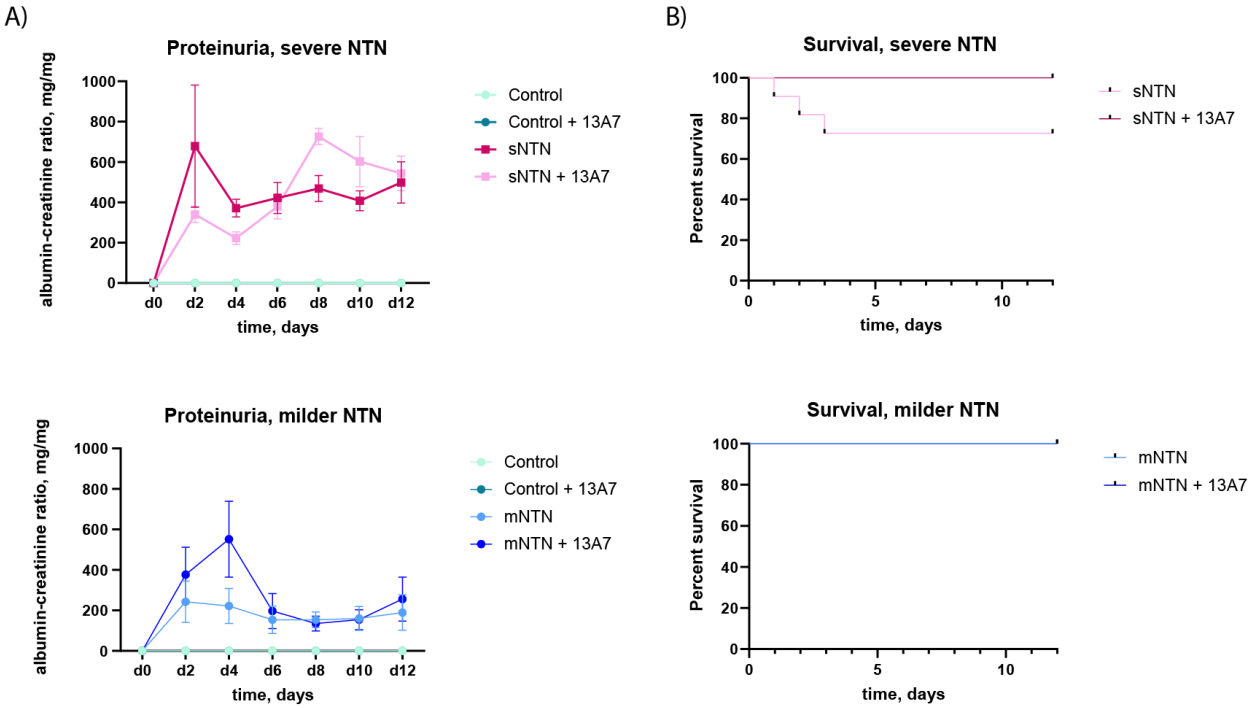

Figure 16. Proteinuria and survival in NTN mice. A) Albuminuria in severe (upper panel) and milder (bottom panel) forms of NTN shows no difference in treated and untreated groups. B) The application of 13A7 nanobodies shows a trend toward increased survival in sNTN mice (upper panel, log-rank test p = 0.272). Both treated and untreated mNTN mice demonstrated 100% survival (bottom panel).

3.2.2 Blocking of P2X7 does not reduce immune cell infiltration and immune-mediated renal damage

To investigate the extent of inflammation and immune response within the NTN kidney and assess the impact of 13A7 therapy, histological and flow cytometry analyses of infiltrated immune cells were performed.

Macrophage analysis showed that, compared to healthy mice where F4/80-stained macrophages were distributed throughout the kidney evenly in small amounts, the infiltration was highly increased in severe and milder NTN mice and located periglomerularly (Figure 17). Mice with and without 13A7 nanobody therapy did not show differences in macrophage quantity and distribution.

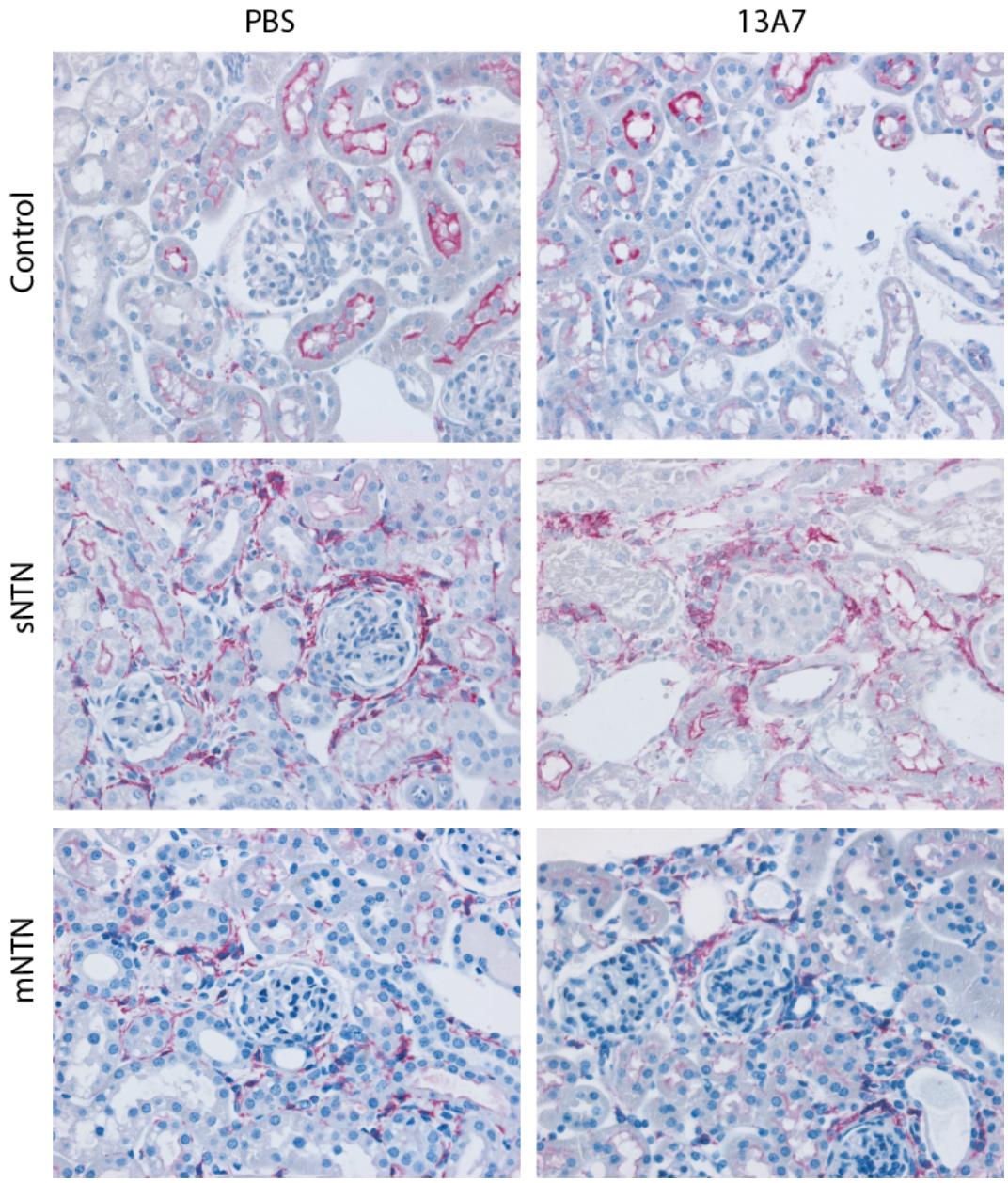

Figure 17. Macrophage infiltration is increased in NTN kidneys independent of therapy. The graphs show no effect of 13A7 nanobody on macrophage proliferation, indicating increased inflammatory reactions. Macrophages were stained with F4/80 antibody.

Immunofluorescent analysis of T cells revealed their extreme infiltration into NTN kidneys with scattered interstitial locations in sNTN and to a lower extent in mNTN mice without difference in treated and untreated groups. T cells in healthy control mice were distributed through the kidney tissue in a small number. Only a part of renal T cells expressed the P2X7 receptor (Figure 18).

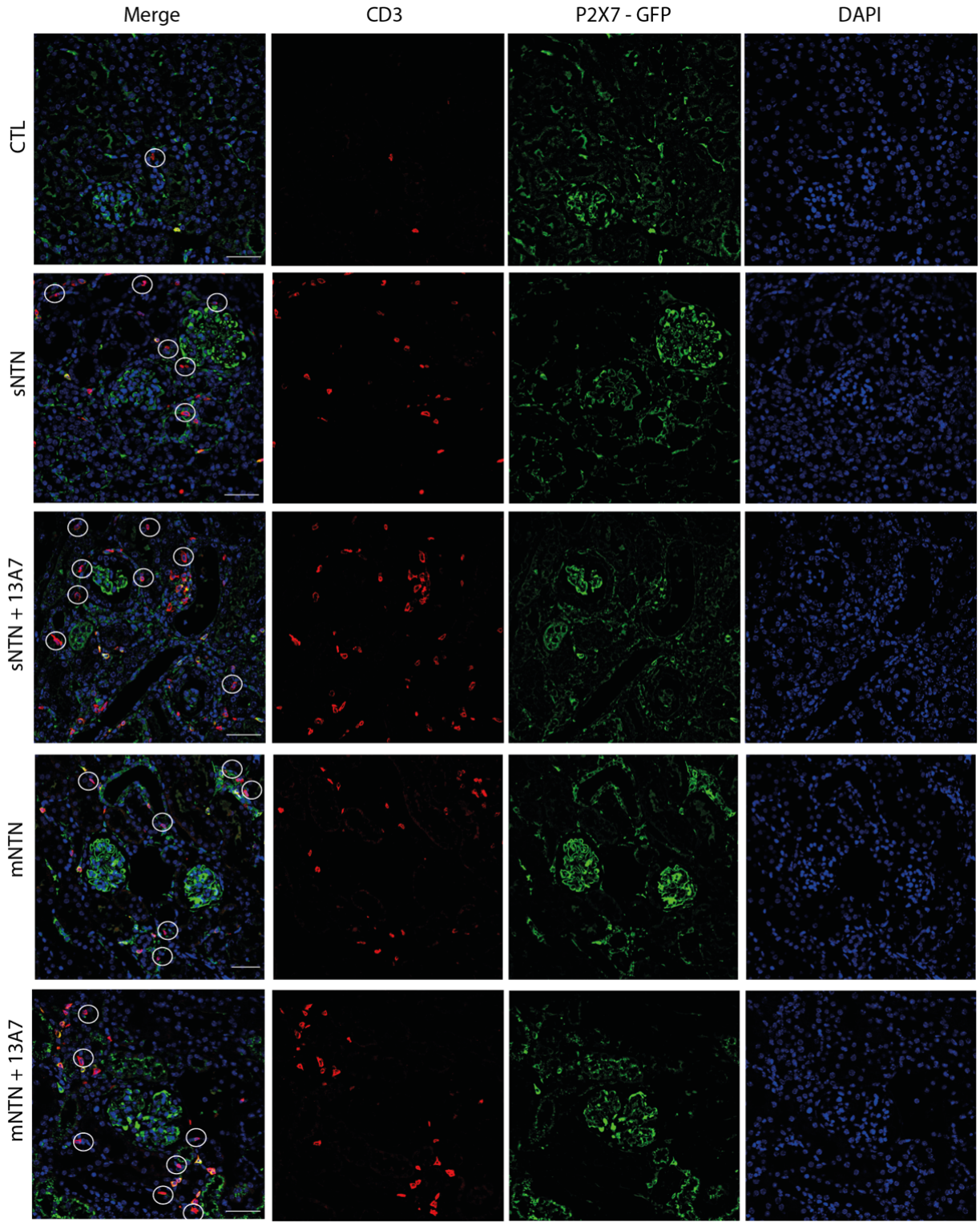

Figure 18. Increased CD3⁺ T cell infiltration into NTN kidneys. The images show no difference in 13A7 treated and untreated groups. Part of the infiltrated T cells did not express P2X7 (shown in white circles). Scale bar 50µm.

Flow cytometry analysis confirmed an increased infiltration of T cells in the kidneys of NTN mice: the percentage of $CD4^+$ T cells was statistically higher in both treated and untreated sNTN groups (28.6 %, $p = 0.005$ and 26.8 %, $p = 0.004$, respectively) and in the 13A7-treated mNTN group (37 %, $p = 0.006$) compared to 16.1% in the control. Additionally, the percentage of $CD4^+$ T cells in

the 13A7-treated mNTN group was higher than in untreated mNTN mice ($p = 0.002$) (Figure 19, A).

The percentage of $CD8^+$ T cells was statistically higher in the mNTN + 13A7 group (23.6%) compared to the healthy control (13%, $p = 0.019$) and untreated mNTN (17 %, $p = 0.03$) (Figure 19, A). This finding parallels the increased rate of $CD4^+$ T cells observed in mNTN mice receiving therapy.

The increased number of isolated T cells in the mNTN 13A7-treated group can be attributed to enhanced lymphocyte survival during isolation, facilitated by P2X7 blockade. Elevated eATP levels released by injured and dying cells, a common occurrence during immune cell isolation, activate P2X7 receptors, leading to pyroptosis. Our recent study demonstrated that blocking of P2X7 receptor using 13A7 nanobodies prior to cell isolation prevents immune cell death and enhances cell yields (Junge and Liaukouskaya et al., Manuscript under revision).

To determine the role of P2X7 in kidney inflammation, its expression on immune cells was analysed under healthy and inflammatory conditions (NTN). Mice with mNTN without nanobody therapy showed an increased percentage of P2X7-expressing $CD4^+$ kidney T cells (77 %) compared to the healthy control group (30.3 %), $p = 0.0159$. The rate of $P2X7^+CD8^+$ T cells was also higher in untreated sNTN and mNTN groups *vs.* control (44.4 % and 41.4 % *vs.* 8.9 %, $p = 0.071$ and $p = 0.016$.) (Figure 19, B).

Mean fluorescent intensity (MFI) analysis of the P2X7 receptor on $CD8^+$ T cells also revealed its increased expression levels in untreated sNTN and mNTN groups (949.7 RFU and 700.6 RFU) *vs.* 154 RFU in the control mice, $p = 0.016$ and $p = 0.036$ respectively. Interestingly, 13A7 application resulted in the tendency to decrease P2X7 expression on $CD4^+$ and $CD8^+$ kidney T cells in severe and milder NTN, compared to their untreated related groups. In the case of $CD4^+$ T cells, nanobody therapy aligned the expression of P2X7 in sNTN and mNTN to its expression in healthy mice. Moreover, the healthy group that received nanobody therapy also showed a trend to decrease the expression of P2X7 on $CD4^+$ T cells compared to untreated healthy control (Figure 19, C).

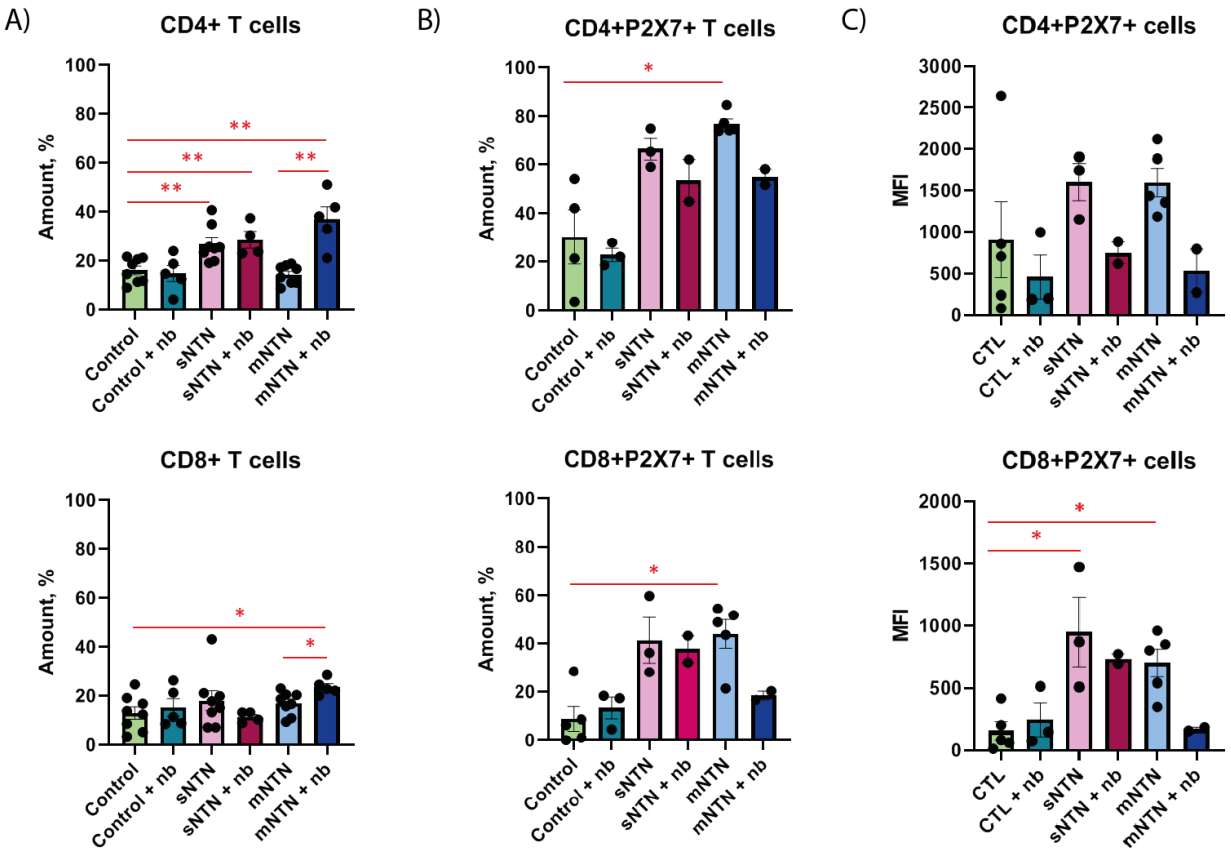

Figure 19. NTN kidneys express the increased total number of T cells with an elevated expression of P2X7. A) Flow cytometry analysis of kidney $CD4^+$ and $CD8^+$ T cells shows their increased levels in NTN mice. B) The percentage number of P2X7-expressing kidney resident $CD4^+$ and $CD8^+$ T cells is increased in mNTN mice without nanobody therapy. C) P2X7 expression level analysis on $CD4^+$ and $CD8^+$ renal T cells. CD8+ T cells express higher levels of P2X7 in untreated NTN groups. The number of all samples ranged from four to eight per group; transgenic mice samples from two to five per group.

As a result of immune cell infiltration, compared to the healthy mice, both groups of NTN mice with and without nanobody therapy were affected by intense kidney damage. Histological analysis revealed severe glomerulosclerosis, tubulointerstitial sclerosis, tubular necrosis, increased cellular infiltration in parenchyma, tubular enlargement or contraction with visible protein lesions and cellular infiltrates on PAS staining on the entire section in the sNTN group and in a lesser degree in mNTN mice with mostly segmental location (Figure 20, A – C).

Glomerulosclerosis analysis revealed severe glomerular damage in all NTN groups without differences in treated and untreated animals: Glomerular sclerosis index (GSI) was 2.3 in sNTN *vs*. 2.87 in sNTN + 13A7 nanobody; and 1.82 in mNTN *vs*. 1.53 in mNTN + 13A7 nanobody. Healthy mice experienced minimal sclerosis (GSI = 0.18 with 16.13 % sclerotic glomeruli) related to the natural ageing process. The percentage analysis of sclerotic glomeruli did not show a difference in

the group of sNTN, however, this rate was decreased in the 13A7-treated mNTN group compared to mNTN control animals (75.43 % *vs.* 89.52 % respectively, p = 0.014) (Figure 20, D).

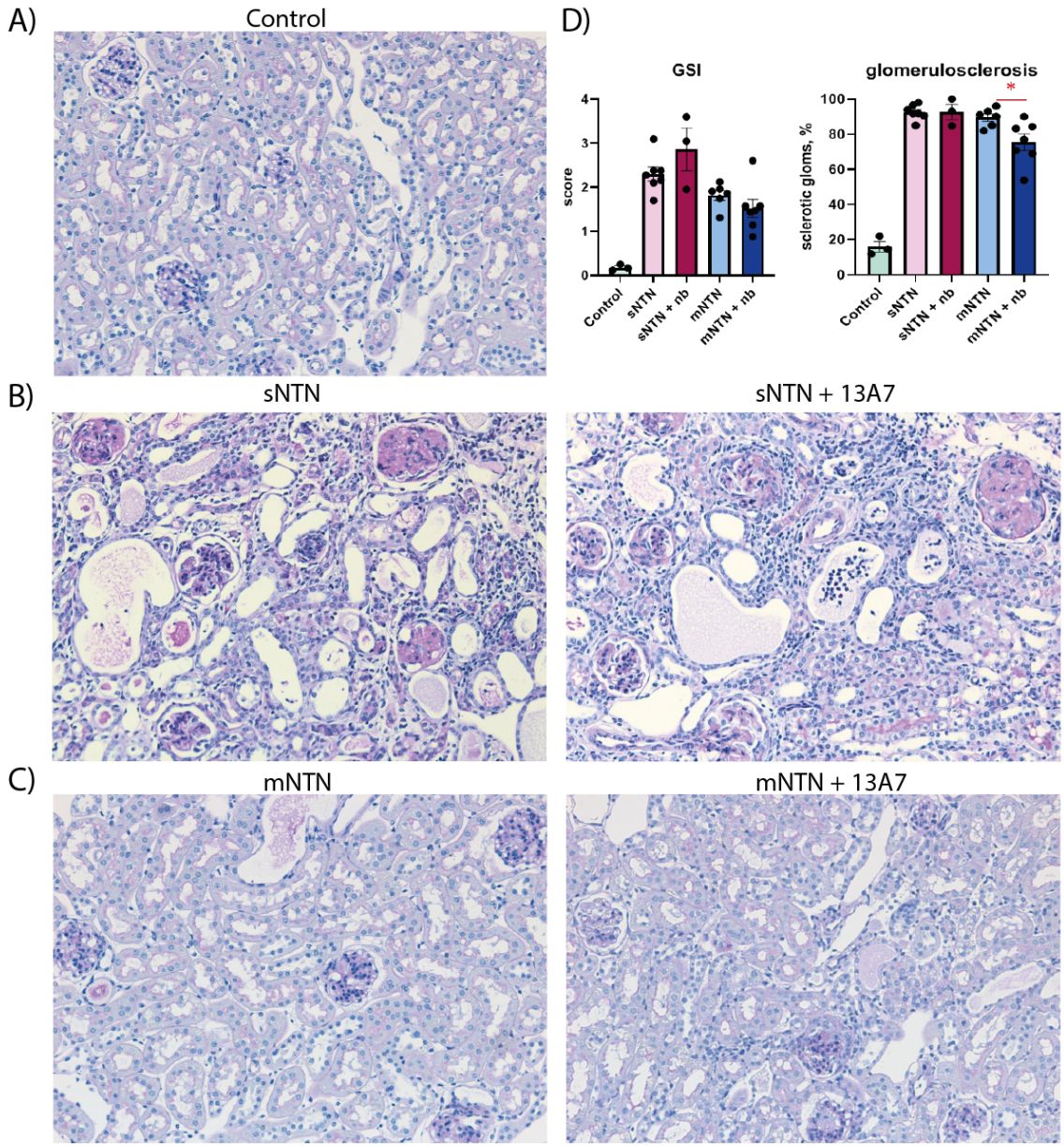

Figure 20. 13A7 nanobody decreased glomerulosclerosis in mNTN despite severe renal damage. A) PAS kidney staining of a healthy mouse; B) PAS kidney stainings show increased renal damage in both, untreated and 13A7 treated mice with sNTN (left and right panels respectively); C) PAS kidney stainings express mild renal damages in mNTN mice without and with nanobody therapy (left and right panels respectively); D) Glomerulosclerosis index (left graph) is increased and shows no difference in all NTN groups; the percentage of sclerotic glomeruli in mNTN mice is decreased upon 13A7 therapy (right graph). The number of all samples ranged from three to seven per group.

Thus, 13A7 nanobody therapy does not reduce immune cell infiltration into NTN kidneys and as a result, immune-mediated renal damage. While nanobody-treated mNTN kidneys show a reduced percentage of sclerotic glomeruli, there is no reduction of disease severity.

3.2.3 Nanobodies are not depleted with high proteinuria

P2X7-blocking nanobodies used in this study consist of two P2X7-blocking domains and an albumin-binding domain for extended half-life. We hypothesised, that severely proteinuric mice may lose therapeutic nanobodies in the urine by binding to albumin and passing through the damaged filtrating barrier. Urine analysis of mice treated with nanobodies showed an increased amount of nanobodies on day 2 in the group of sNTN (MFI = 2000 RFU *vs.* 400 RFU in CTL, p=0.002), which slightly decreased on day 4 and was continuously higher through the experiment compared to the control group (1000 RFU *vs*. 400 RFU respectively). mNTN mice displayed slightly increased MFI levels only on day 2 (600 RFU), which levelled up with control starting from day 4 (Figure 21, A). However, the analysis of blood serum taken on day 12 showed high MFI levels of 13A7 in all three groups of mice, where the highest nanobody level was presented in the group of sNTN mice (8345 RFU *vs*. 4455 RFU in CTL and 3123 RFU in mNTN) (Figure 21, B).

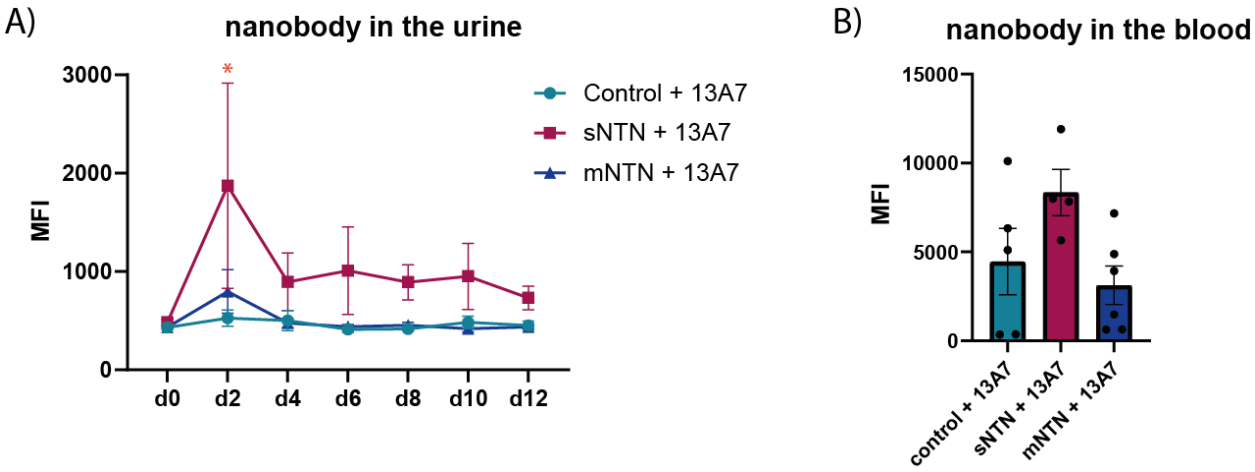

Figure 21. The common amount of nanobodies was not depleted in severely proteinuric mice. A) 13A7 nanobody level was partially increased in the urine of sNTN and not present in mNTN mice. B) 13A7 nanobodies were present at a high level in the blood serum of NTN and control mice. The number of all samples ranged from four to six per group.

These data showed that despite high proteinuria levels, 13A7 nanobodies were not all cleared through the renal filtration barrier and remained at a high concentration in the blood. Altogether, the results showed that P2X7 blockage alone was not enough to prevent or ameliorate renal damage in NTN, indicating the need for additional therapeutic strategies to effectively treat GN.

3.2.4 Blocking of P2X7 in T cells mediates their survival and proliferation

Although P2X7-blocking nanobody therapy was insufficient to reduce kidney damage, it showed a reduction of P2X7 expression on kidney resident T cells in NTN compared to untreated NTN

mice. Therefore, bulk RNA sequencing of kidney resident $CD4^+$ and $CD8^+$ was performed to investigate which genetic mechanisms were activated in mNTN conditions alongside P2X7 blockage.

For this, $CD4^+$ and $CD8^+$ T cells were isolated from healthy untreated, healthy nanobody-treated, untreated mNTN and nanobody-treated mNTN kidneys and used for library preparation and RNA-sequencing.

The analysis revealed significant differences in gene expression between mice treated with P2X7-blocking nanobodies and untreated mice, both in healthy and NTN conditions. The results indicated that the nanobody treatment had a greater effect on T cells than the disease itself (Figure 22, A and B). These differences were primarily observed in $CD4^+$ T cells, while gene expression in $CD8^+$ T cells mostly did not differ among the studied groups. The analysis showed upregulation of WNT signalling in $CD4^+$ T cells (*Narf*, negative WNT regulator; *Apc2*, positive WNT regulator), which regulates cellular activation, migration and proliferation; increased sensitivity to TNF-inflammatory signalling (*Spata2*), but at the same time, increased TNF-induced apoptosis (*Mtx1*). Blocking of P2X7 upregulated some unspecific immune cell genes, such as *Nhs* (responsible eyes and teeth development), *Arhgef9* (neuron development) and *Olfr707* (odour), and at the same time upregulated the p53 signalling pathway (*Herc2*), essential for DNA repair, apoptosis and development (Figure 22, C).

Comparative analysis of immune-related genes showed their upregulation in T cells of NTN (at a higher level) and CTL mice that received 13A7 therapy (Figure 22, D). The upregulation of immune genes in 13A7-treated mice suggests activation and memory formation in various T cell subsets: Th1 (*Ifng, Cxcr3, Cxcr4, Tbx21*), Th2 (*Il-4, Gata3*), Th17 (*Rorc*), and Treg (*Foxp3*).

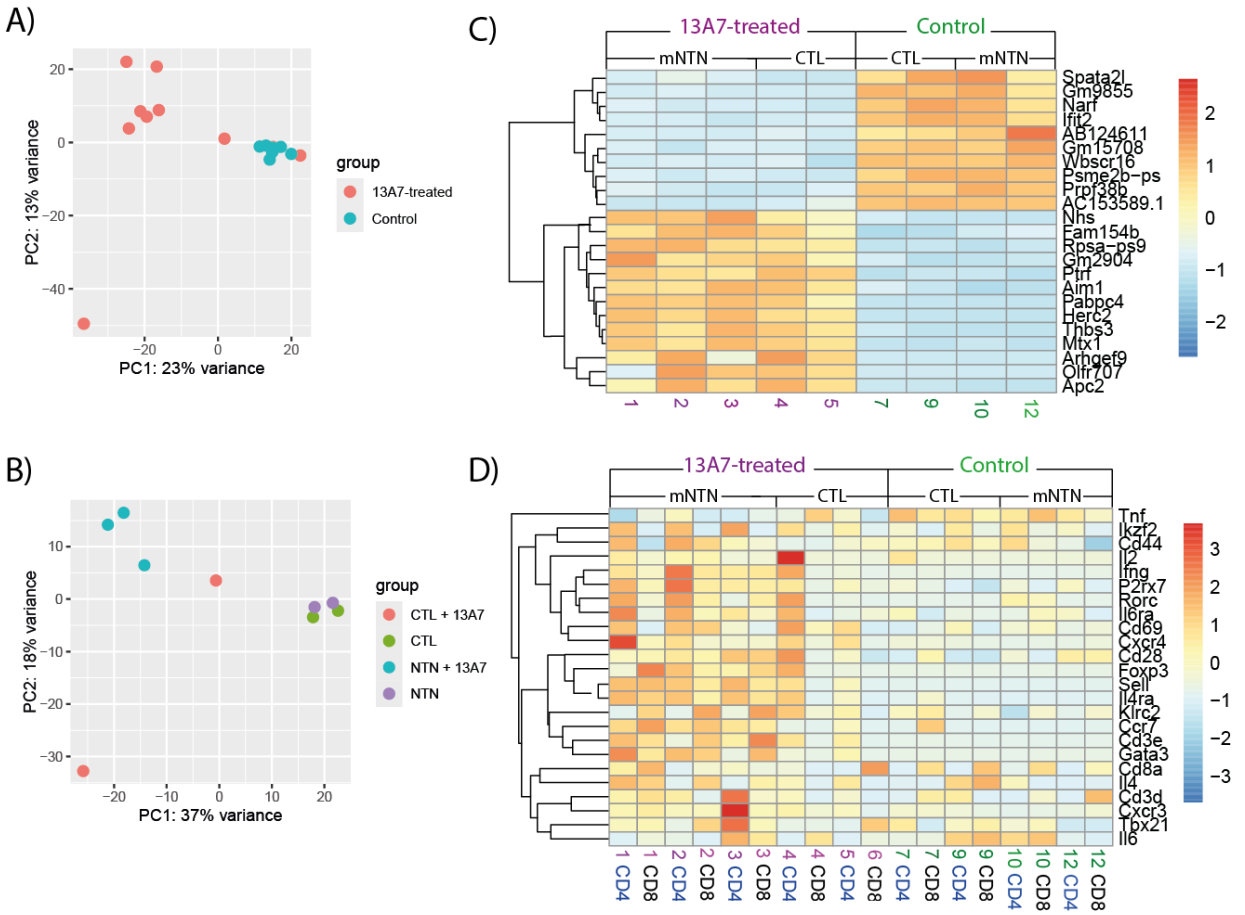

Figure 22. RNA sequencing of kidney resident T cells. A) PCA plot of kidney T cells shows the separation of 13A7-treated from the untreated (CTL) group. B) PCA plot of $CD4^+$ renal T cells shows the separation of 13A7 CTL and NTN groups from CTL and NTN untreated groups. C) Up- and downregulated genes in kidney resident $CD4^+$ T cells. The graph shows the difference in gene regulation in CTL and NTN groups based on 13A7 therapy. D) Immune-related genes were upregulated in $CD4^+$ and $CD8^+$ kidney T cells in mice with 13A7 nanobody therapy compared to the untreated group.

Gene enrichment analysis revealed upregulated signalling pathways in T cells of control and NTN mice treated with 13A7 therapy compared to untreated mice. The most prominent pathways included WNT, Hippo, cancer, MAPK, calcium, RAS and metabolic signalling pathways (Figure 23).

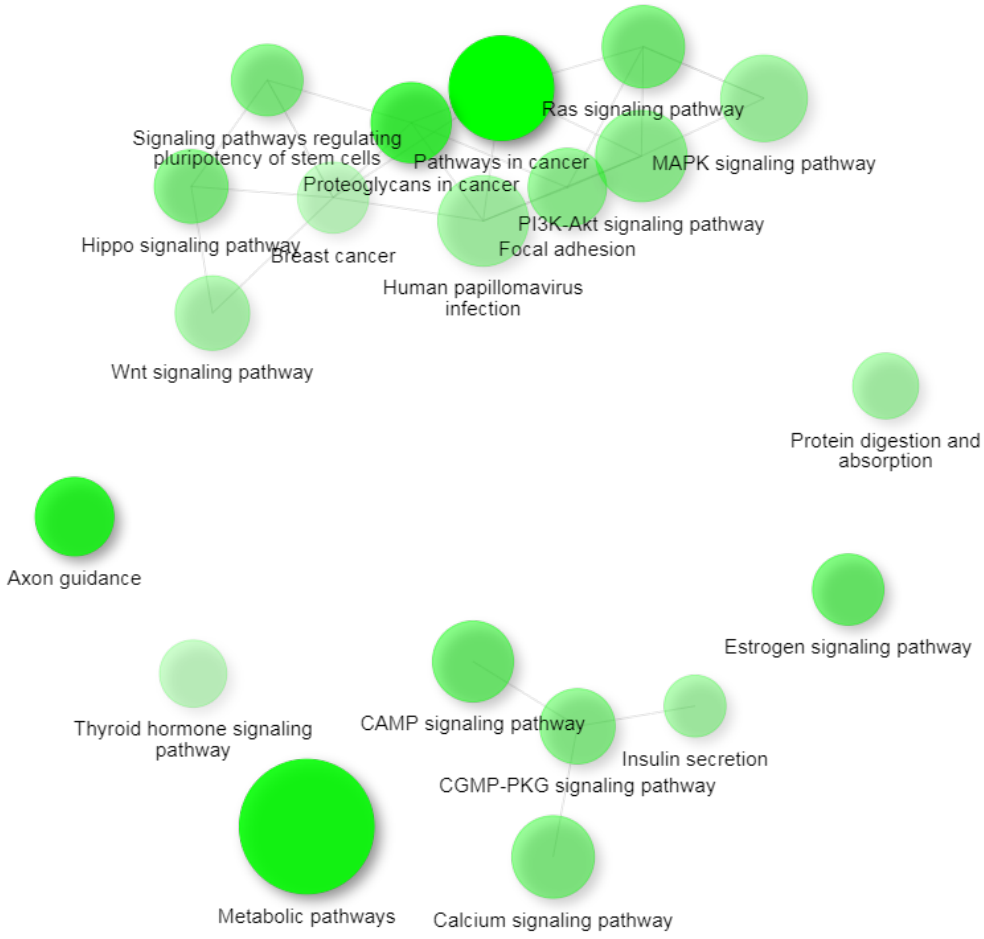

Figure 23. Upregulated signalling pathways in renal T cells of NTN and control mice treated with 13A7 nanobodies. Enrichment analysis from shinyGO shows the upregulation of several pathways with such common outcomes, as cellular activation, proliferation, migration, spreading and survival.

These upregulated pathways are known for promoting cell survival, adhesion, cell spreading, migration, invasion, proliferation, cell growth, regulation of cytoskeleton, and microtubule reorganisation. Some of those common mechanisms are shown in one of many cancer signalling pathways upregulated in T cells of 13A7-treated mice in Figure 24.

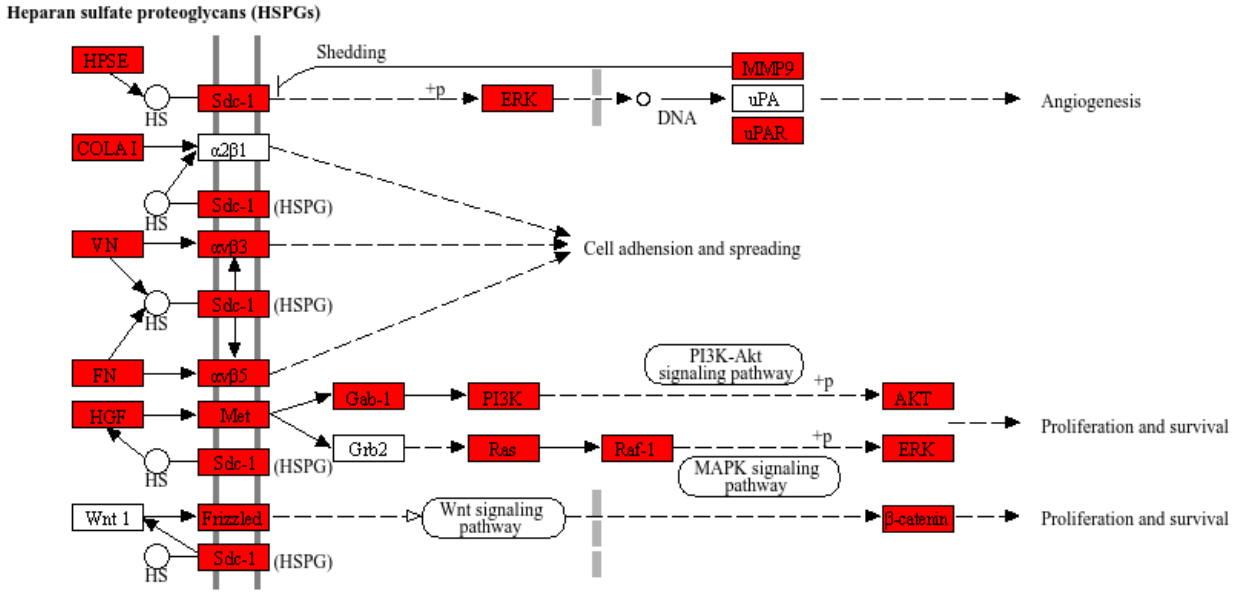

Figure 24. Signalling pathway within upregulated heparan sulfate proteoglycans in kidney T cells of mice treated with 13A7. The cancer signalling pathways result in increased proliferation, survival and spreading in T cells of healthy and NTN mice after nanobody therapy.

Furthermore, Hippo and WNT signalling pathways exhibited upregulation of several anti-apoptotic and proliferative genes, even though some signalling-inhibitory genes were upregulated as well (Figure 25).

cGMP-PKG signalling indicated the activation of multiple membrane channels and receptors that regulate the transport of calcium, sodium, and potassium ions. Calcium transport led to the activation of nuclear factor NFAT and other transcription factors, which is particularly important, as the main aim of P2X7 blocking on T cells in this study was to prevent NFAT activation, thereby inhibiting T cell activation, proliferation and reduction inflammatory cytokine production.

These results suggest significant changes in gene expression in renal T cells of NTN and control mice treated with nanobodies, including increased survival, proliferation, migration and spreading.

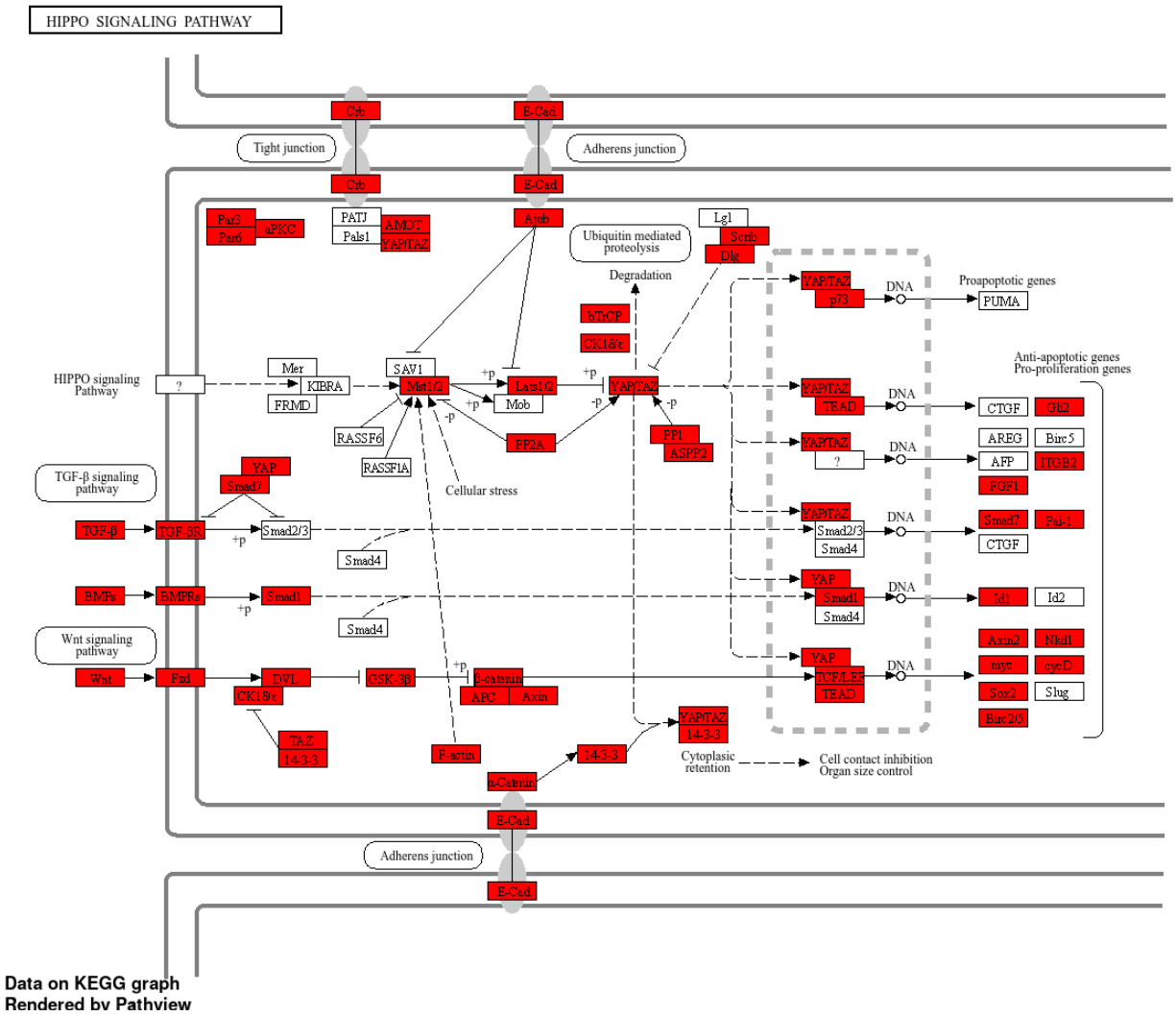

Figure 25: Leading signalling pathways overactivated in kidney T cells in mice with P2X7 blockage. WNT and Hippo pathways activate several anti-apoptotic and proliferative genes.

3.3 Inflamed glomeruli express increased levels of P2X7

To better understand the role, localization, and expression of P2X7 within the glomerulus in the inflamed kidney, immunofluorescent staining and flow cytometry analysis using markers for P2X7, podocytes and endothelial cells were performed.

Immunofluorescent images in all groups of NTN mice, compared to healthy group, showed severely destroyed nephrin, a key structural component of the slit diaphragm in podocytes, essential for the proper functioning of the filtration barrier. P2X7 expression in healthy mice was distributed at a low level in glomeruli, mostly on glomerular endothelial cells (GEC), however, its expression was highly increased in damaged glomeruli. The milder glomerular damage caused a uniform distribution of P2X7 along with nephrin and endomucin. Interestingly, severely damaged sclerotic glomeruli expressed higher levels of P2X7 on the sides of sclerosis, where nephrin and endothelial cells were absent (Figure 26). Both severely and less severely damaged glomeruli were observed in sNTN and mNTN mice.

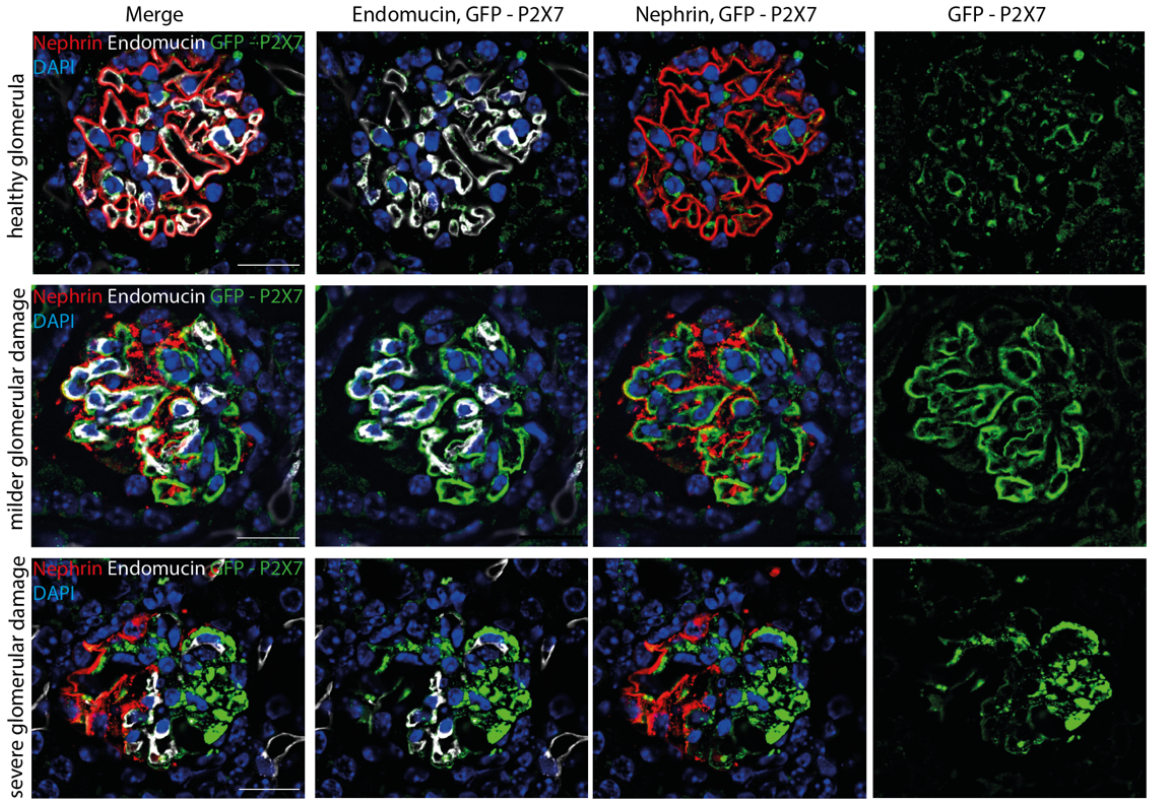

Figure 26. P2X7 expression is increased in NTN glomeruli. NTN kidney sections were stained with a-GFP-P2X7 (green), a-nephrin (red) and a-endomucin (white) antibodies for detection of P2X7 in co-localisation with glomerular cells (podocytes and endothelial cells). Staining shows low P2X7 expressions in healthy glomerulus (upper row) compared to its increased expression in mildly (middle row) and severely (bottom row) damaged glomeruli in sNTN and mNTN mice with 13A7 therapy respectively. Scale bar 20µm.

Additional flow cytometry analysis of glomerular cells confirmed previously described glomerular damage in NTN mice and showed an extreme decrease of podocytes in sNTN and mNTN mice compared to control (9.35 %, p = 0.006 and 8.45 %, p = 0.036 in untreated and treated sNTN; 8.67 %, p = 0.003 and 16.05 %, p = 0.008 in mNTN groups *vs.* 45.27 % in CTL) (Figure 27, A).

The percentage of GEC ranged between 30 % and 60 % in all groups of mice without a statistical difference, however, the percentage of P2X7 expressing GECs was higher in mNTN untreated group (93.13 %) vs control (55.01 %), p = 0.029 (Figure 27, B and C). P2X7 expression level in mNTN untreated group was also higher compared to the control (6855.5 RFU vs. 3608.7 RFU, p = 0.029). Interestingly, the 13A7 therapy showed a tendency to suppress the expression of P2X7 on GEC in severe and mild NTN, levelling it to the MFI of healthy mice (with MFI 2340 RFU and 2154 RFU respectively) (Figure 27, D).

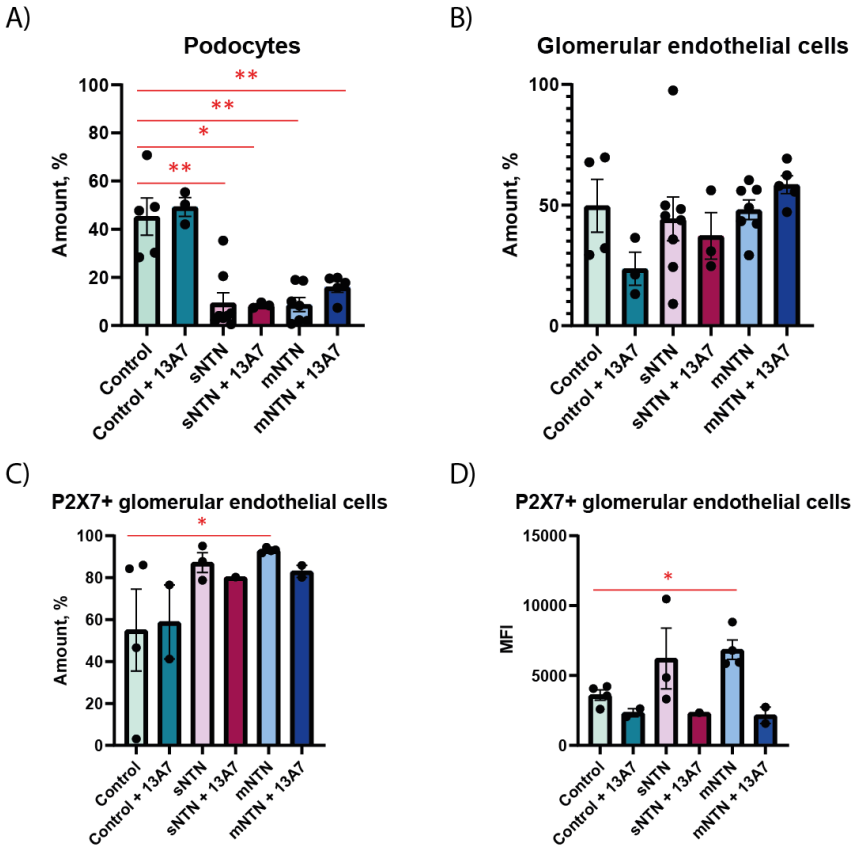

Figure 27. NTN kidneys express podocyte loss and increased P2X7 levels in GEC. A) The percentage analysis of podocytes shows their depletion in NTN. B) The rate of GEC did not differ in the groups. C) The percentage of P2X7-expressing GEC and D) the expression level of P2X7 on GEC are increased in untreated mNTN and show the tendency to decrease in 13A7 treated NTN groups. The number of all samples ranged from three to eight per group; transgenic mice samples from one to four per group.

These data show increased levels of P2X7 on GEC under inflammatory conditions, highlighting its role in the pathophysiology of GN.

3.3.1 13A7 nanobody binding enhanced in inflamed glomeruli

To determine 13A7 nanobody distribution under conditions of increased P2X7 expression by kidney resident cells in inflammation, histological immunostaining was performed.

Despite the high expression levels of P2X7 on immune cells and GEC, visualisation of alfa-tagged 13A7 nanobodies in NTN kidneys showed their highly increased binding only to glomerular cells, while their binding to the interstitial immune cells was not observed (Figure 28, A). Compared to immunofluorescent stainings of nanobodies in healthy mice, where 13A7 were distributed through the P2X7-expressing cells evenly in NTN mice (see chapter 3.1.2).

The detailed fluorescence microscopy images revealed that nanobody binding was sometimes observed on the slit diaphragm of podocytes, as indicated by co-localization with nephrin. In other instances, binding was observed on endothelial cells, evidenced by co-localization with endomucin. This variability in binding localization made it challenging to definitively determine the primary cellular target of the nanobodies within the glomerulus (Figure 28, B).

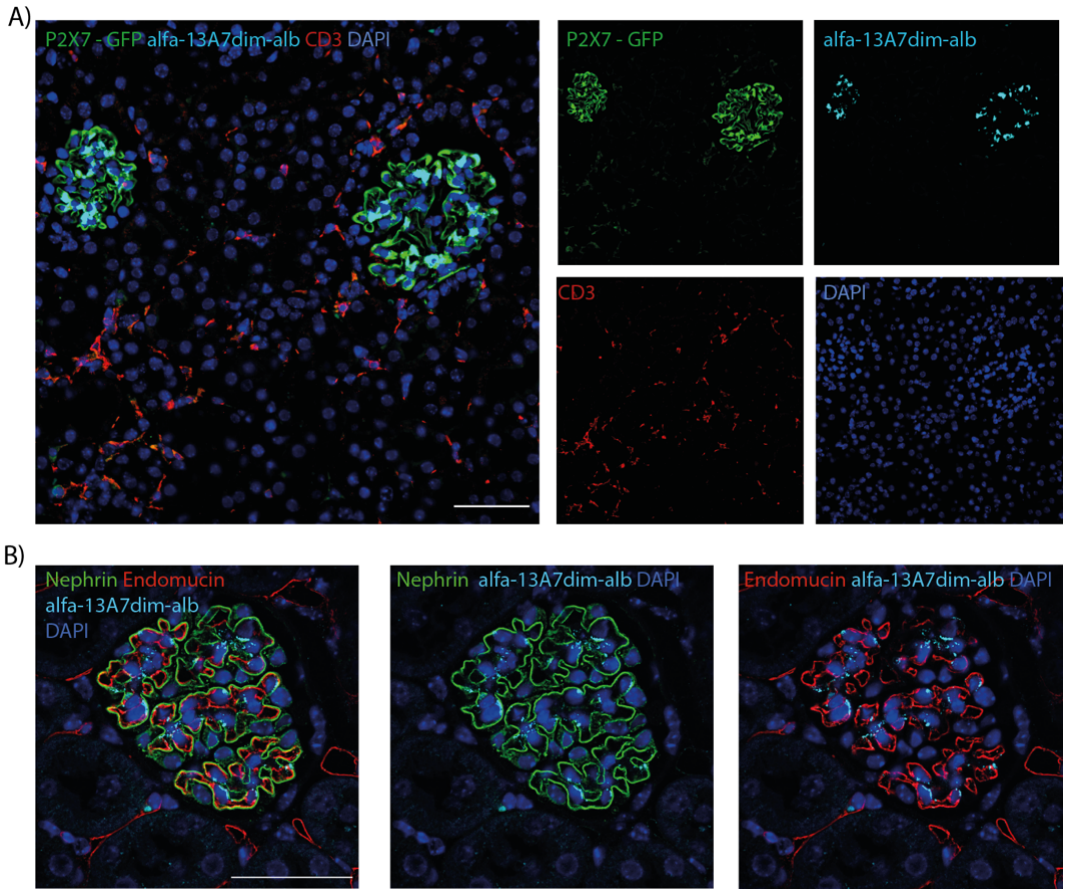

Figure 28. Nanobody visualisation in NTN kidney. A) NTN kidney sections were stained for P2X7-GFP, CD3, and alfa-tag for nanobody visualization. 13A7 nanobodies expressed an increased binding to glomerular cells. Scale bar: 50 µm B) Immunofluorescent staining of glomerular cells was made with antibodies to nephrin and endomucin showing a more detailed picture of 13A7 nanobodies binding to glomeruli. Scale bar: 50µm.

Previous flow cytometry analysis demonstrated that the nanobody target protein P2X7 was expressed on GEC. These data provide a clearer indication that the nanobodies preferentially may bind to endothelial cells within the glomerulus. However, further investigation is needed to fully understand the distribution and functional implications of nanobody binding within the glomerular cells.

3.3.2 The absence of P2X7 on glomerular endothelial cells does not affect NTN outcome

To establish the role of P2X7 in renal endothelium on disease outcome, we generated P2X7 -/- on GEC using endothelial-specific Cdh5.Cre lines, floxed *P2rx7* mouse lines and mTomato/mEGFP reporter line (Figure 29, A) and analysed the progression of the milder form of NTN (Alva et al. 2006, Kaczmarek-Hajek et al. 2018).

For CdH5.Cre line induction, eight-week-old P2X7 fl/fl and heterozygous mice were injected i. p. with Tamoxifen in corn oil (20mg/ml) with a maximal volume of 100µl. The injection was performed daily for five consecutive days. 35µl NTS diluted in PBS 1:1 was injected seven days after the primary Tamoxifen application (Figure 29, B).

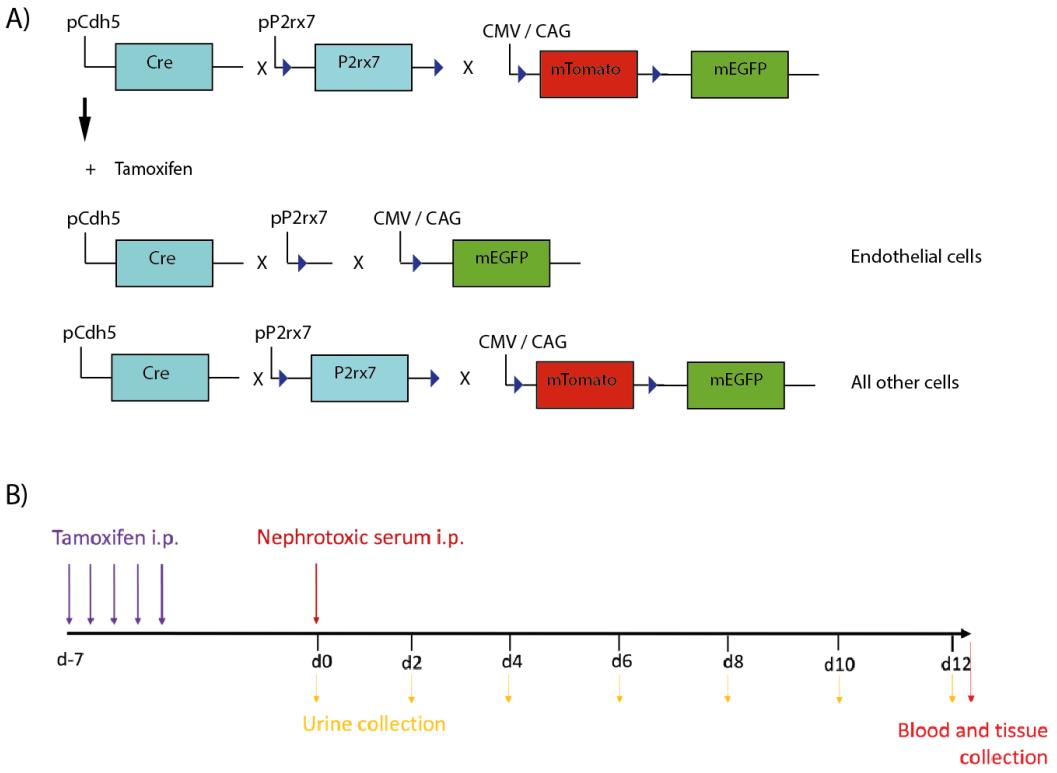

Figure 29. Cdh5.Cre induction scheme in NTN model. A) Tamoxifen-inducible pCdh5-Cre system drives Cre expression in endothelial cells, excising floxed *P2rx7* and mTomato leading to a conditional KO of P2X7 and expression of mEGFP in endothelial cells, while other cells retain P2X7 and mTomato expression. B) Tamoxifen was injected i. p. daily for five days one week before NTN induction. Urine collection was performed every second day after the NTS injection. Terminal blood and tissue collection was performed on day 12.

Cdh5.Cre mice lacking P2X7 on GECs showed the tendency to decrease proteinuria level at each urine sampling point compared to P2X7 heterozygous mice, with the biggest difference on day 2: (380 mg/mg *vs*. 939 mg/mg respectively). ACR level of P2X7 +/+ mice decreased sharply after day 2 to the level of 328 mg/mg and gradually decreased over time, as well as the ACR of P2X7 fl/fl mice. In contrast to P2X7 Tg mice from the previous experiments, where proteinuria remained high until the last day of the experiment (170-230 mg/mg), the ACR level of Cdh5.Cre mice decreased greatly and reached 31 mg/mg in P2X7 fl/fl mice (n = 6) and 105 mg/mg in P2X7 heterozygous mice (n = 6) (Figure 30, A).

Although the albumin-creatinine ratio in P2X7 fl/fl Cdh5.Cre mice was slightly lower than in heterozygous mice throughout the experiment, statistical analysis did not reveal a significant difference.

Histological analysis of PAS stainings showed minimal damage in both groups of mice, which correlated with low proteinuria levels. Kidney sections of most NTN mice from both groups showed minimal interstitial and glomerular sclerosis, thickening of GBM with a small number of enlarged tubuli and cellular infiltration (Figure 30, B). Despite slightly decreased proteinuria in Cdh5.Cre P2X7 fl/fl mice, three out of six mice (*vs.* one mouse out of six in Cdh5.Cre P2X7 heterozygous mice) experienced significant kidney damage, comparable to those in mNTN P2X7 Tg and WT mice. However, GSI did not differ in both NTN groups (0.69 in P2X7 fl/fl *vs.* 0.75 in P2X7 +/+). The sclerotic glomeruli level did not differ (39,3 % *vs.* 41,2 % respectively) (Figure 30, C).

In contrast to Cdh5.Cre mice, NTN P2X7 Tg and WT mice in previous experiments showed severely sclerotic glomeruli with 75 – 89 % of affected gloms (see chapter 3.2.2).

The NTN mouse model in Cdh5.Cre mice was significantly less severe than those in P2X7 Tg and WT mice from the previous experiment (chapter 3.2). Despite the tendency to decreased proteinuria levels in mice lacking P2X7 on GEC, statistical analysis did not reveal significant differences between the two groups with and without P2X7 expression on GEC. These data indicate that even though P2X7 expression was severely increased in GEC in WT NTN mice, its absence alone is not sufficient to affect disease outcome.

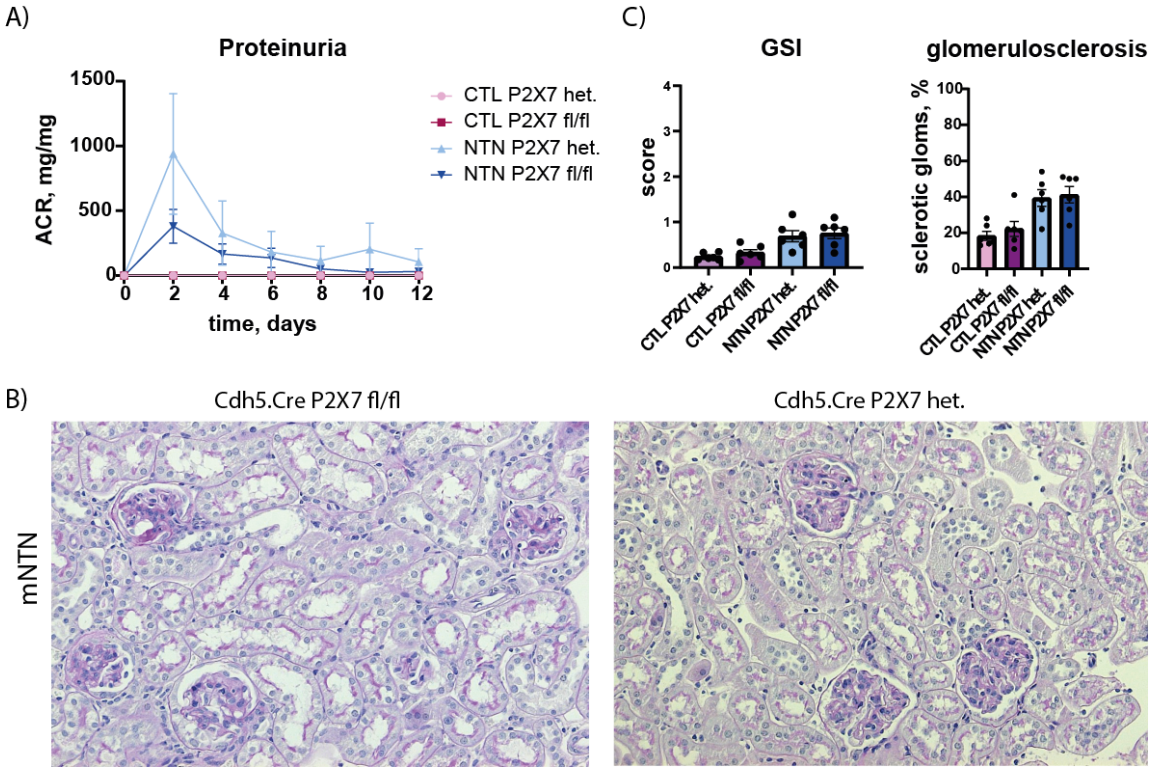

Figure 30. Characteristic of renal function in Cdh5.Cre mice with and without P2X7 expression on GEC. A) Albuminuria in Cdh5.Cre P2X7 fl/fl mice tend to decrease compared to P2X7 heterozygous mice, without statistical significance. B) PAS kidney staining of Cdh5.Cre P2X7 fl/fl mNTN mouse (left panel) and P2X7 heterozygous mouse (right panel). The histology analysis shows minimal interstitial and glomerular damage in both groups. C) Glomerulosclerosis index and the rate of sclerotic gloms show no difference in analysed groups of mice.

3.4 Blocking of P2X7 does not ameliorate acute autoimmune membranous nephropathy

Next to experimental NTN, P2X7 might play a role in other forms of glomerulonephritis. To establish the possible role of P2X7 in MN development and progression, and to evaluate the therapeutic capacity of P2X7-blocking nanobodies in autoimmune glomerulonephritis, 13A7 therapy was applied in the spontaneous (acute) and active (chronic) experimental forms of MN.

Since the major autoantigen in the MN, PLA2R, is not expressed on podocytes of widely used experimental animals, such as mice and rats, the group of PD Dr. Gunther Zahner recently developed a transgenic mouse strain expressing the full-length huPLA2R1 on the podocytes of BALB/c mice (Tomas et al. 2023 a) (Figure 31, A). These transgenic mice spontaneously develop signs of MN from the fourth week after birth (proteinuria and IgG deposition on GBM) with the first autoantibody detection in the blood on the third week of age. Starting from the fifth to sixth week of age, some of those mice develop ascites and severe health deterioration, which requires termination of the experiment until the eighth week (Figure 31, B). The spontaneous development of MN

makes this model suitable for disease investigation and drug testing, making it comparable to spontaneous disease development in humans.

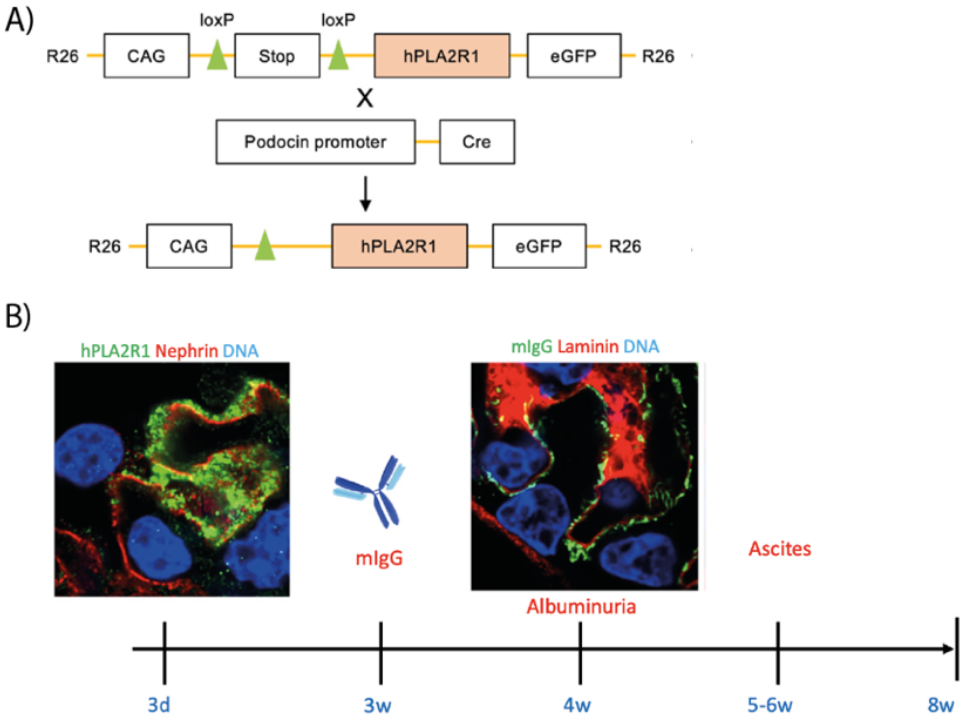

Figure 31. Schematic of spontaneously developing MN in huPLA2R-positive mice. A) Schematic depiction of the Rosa 26 (R26)–based hPLA2R1 full-length knock-in target construct including the transactivation by the CAG promoter. After breeding hPLA2-negative mice with podocin Cre deleter mice, hPLA2R1-positive mice are obtained that express hPLA2R1 specifically in podocytes. B) Schematic of MN development in huPLA2R-positive mice (adapted from Tomas et al. 2023a).

huPLA2R-positive mice were split into three groups: MN control; MN + therapeutic 13A7 nanobody; and MN + control nanobody L-10. P2X7-blocking therapy on spontaneous MN was started at three weeks of age. The experiment began with control urine collection and 50µg 13A7 nanobody (or control L-10 nanobody) i. p. injection. Based on the experimental scheme (Figure 32), urine collection and nanobody injection were performed twice weekly with blood collection once a week. The disease progression was controlled using urine stix, every time after urine collection. The ethical endpoint was evaluated in each mouse individually, considering health conditions (ascites, pain, and stress signs), and proteinuria severity with the maximal duration of the experiment of five weeks, when mice reached eight weeks of age.

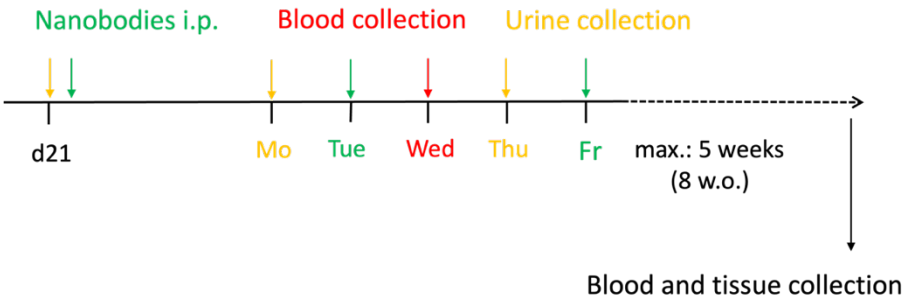

Figure 32. Experimental scheme of nanobody therapy in spontaneous MN model. The experiment with huPLA2R-positive mice started on the 21st day of age followed by urine collection (Mondays and Thursdays), blood collection (Wednesdays), and nanobody application (Tuesdays and Fridays). The experiment ended with terminal blood and tissue collection.

3.4.1 13A7 nanobodies do not alleviate proteinuria and renal damage in acute MN

The first signs of proteinuria in all three groups of MN mice occurred in the fifth week of age with a fast, but gradual increase of ACR. In week 6.5, the ACR level reached 966.5 mg/mg in the L-10 treated group (n = 5), 595.6 mg/mg in the 13A7 treated group (n = 12) and 439.6 mg/mg in the control MN group (n = 13), showing no statistical difference. Interestingly, MN female mice expressed seventeen-fold severe proteinuria (950 mg/mg) compared to MN males (55 mg/mg) at the 6.5 week of the experiment (Figure 33, A). The survival rate did not differ in all three groups of mice with mean survival in the control MN group of 7 weeks and 6.5 weeks in groups with 13A7 and L-10 nanobodies (Figure 33, B).

The analysis of mouse autoantibodies against huPLA2R revealed a gradual increase of mIgG in the blood, reaching 40 U in the 6.5 week in all three groups of mice, showing no difference in the treated and control groups (Figure 33, C). Immunofluorescent staining confirmed the increased presence of autoantibodies in the glomeruli together with severely damaged nephrin in all mice showing no differences regardless of therapy. The positive staining of hPLA2R on the podocytes confirmed the genotype of huPLA2R-positive mice (Figure 33, D).

Despite numerous research focusing on the role of P2X7 in an autoimmune pathology (Grassi/Salina 2023), its blocking did not prevent or ameliorate renal damage in MN, indicating that P2X7 blockade alone is ineffective in mitigating MN progression. The reason for this outcome could be the rapid and severe onset of MN development in this model, and the complex nature of autoimmune kidney diseases.

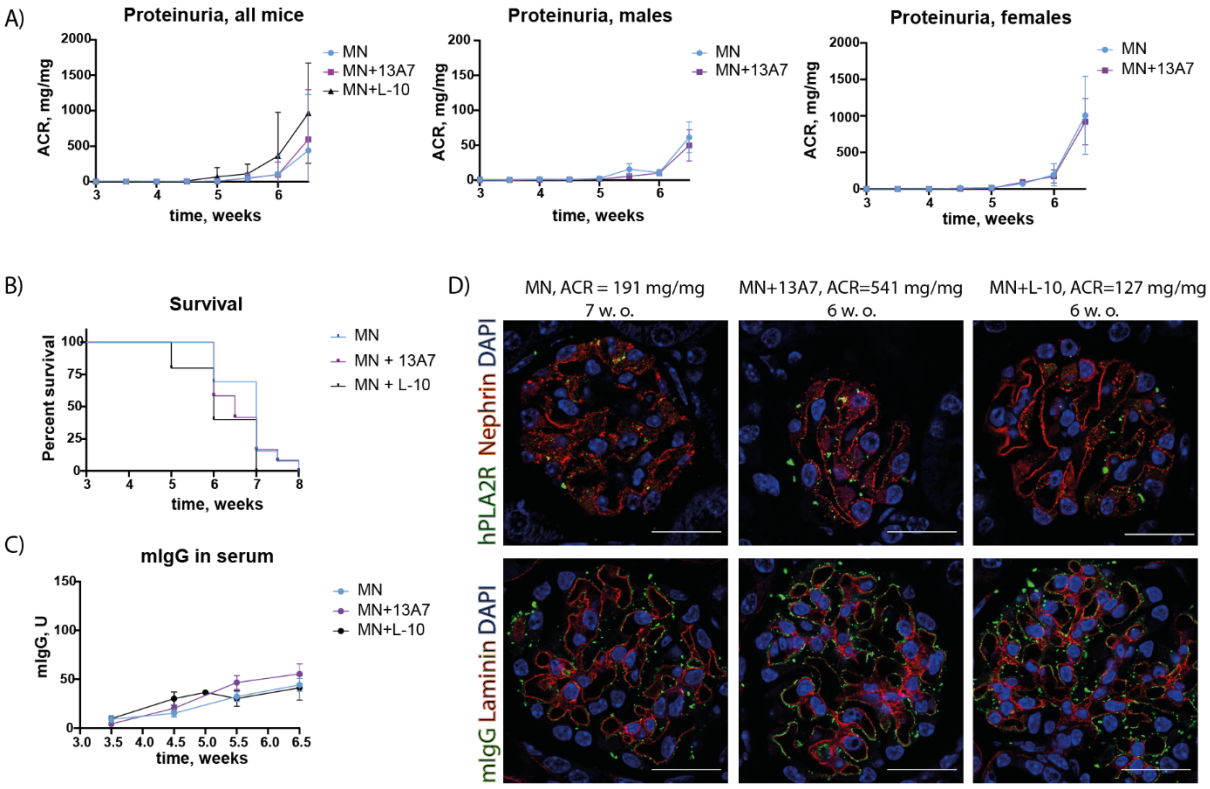

Figure 33. P2X7 blockage with nanobodies did not affect spontaneous MN. A) The common ACR level in MN control and nanobody (13A7 and L-10) treated mice shows the same progression with slightly increased proteinuria in L-10 treated group. Albuminuria in MN females (right panel) is seventeen-fold higher compared to MN males (middle panel). B) The survival rate of MN mice shows no difference in all three groups of MN mice. C) Mouse PLA2R-specific antibodies (mIgG) in blood serum over time increased and did not differ in analysed groups of mice. D) Glomerular immunofluorescent staining of MN control mouse (left column), MN mouse treated with 13A7 (middle column) and MN mouse treated with control L-10 nanobody (right column). The stainings were made using antibodies for hPLA2R and Nephrin (upper row); and mIgG and laminin (bottom row) and show increased immunocomplex deposition in glomeruli with damaged nephrin and PLA2R expression in all three groups without differences.

3.4.2 Depletion of P2X7 blocking nanobody in the blood is correlated with increased proteinuria in MN mice

The nanobody analysis in the blood serum and urine taken once and twice a week respectively, showed the first signs of 13A7 in the urine in the seventh week of age (four weeks after the first nanobody injection), suggesting that injected 13A7 remained in the body despite the disrupted filtration barrier and increased proteinuria (Figure 34, A). However, the nanobody level in blood serum sharply decreased starting from 5.5 weeks of age (2.5 weeks of treatment) (5441.4 RFU), to the minimal level at week 7 (528 RFU) (Figure 34, B). 13A7 nanobody level in the blood serum negatively correlates with proteinuria in MN mice, the first signs of both, proteinuria development and nanobody decrease start at week 5.5 (r = -1) (Figure 34, C).

In this model, in contrast to the NTN model, kidney immunofluorescent staining showed a uniform distribution of 13A7 nanobodies on immune and glomerular cells, proving the binding to P2X7. However, binding and blocking of P2X7 did not positively affect the disease progression and outcome. Control L-10 nanobodies in MN mice were neither detectable in the urine or blood, nor in the kidney sections (Figure 34, D).

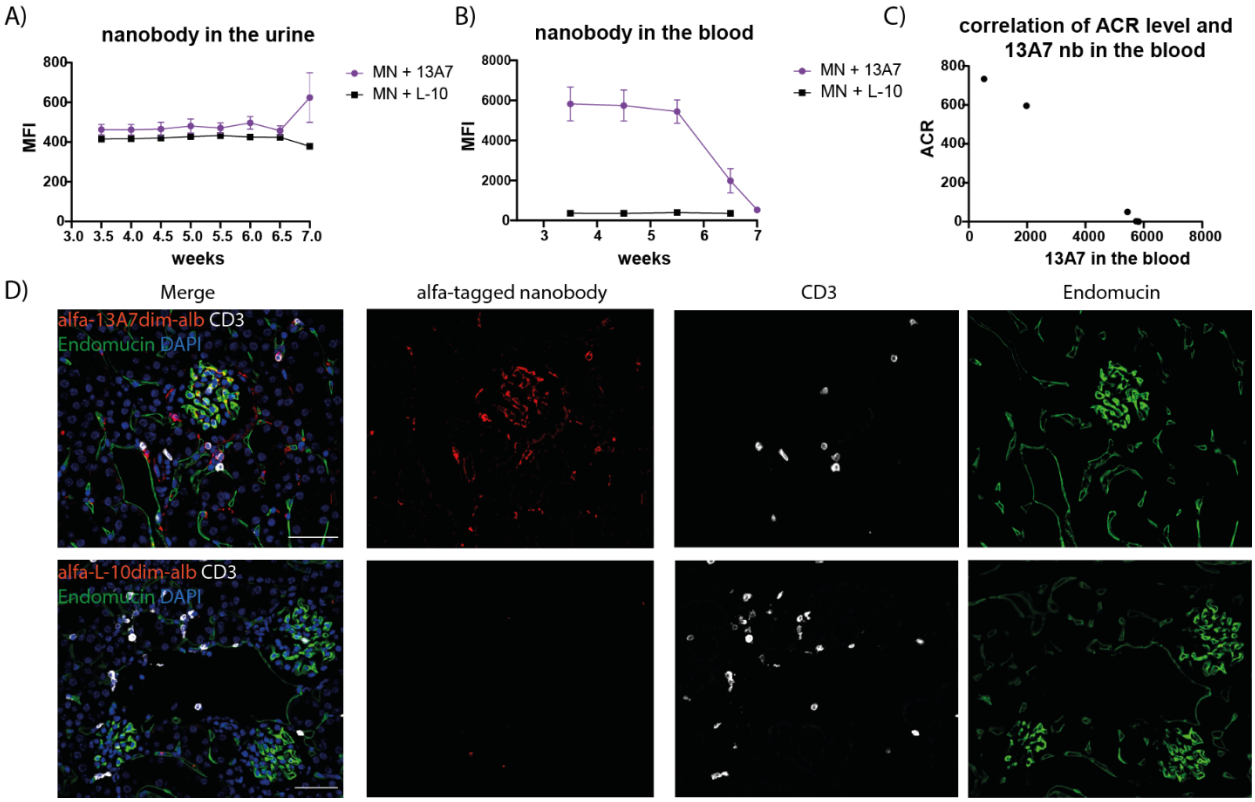

Figure 34. Nanobody identification in MN murine samples. A) Nanobody levels in the urine of MN mice show the first signs of 13A7 in the urine in the seventh week of the experiment (four weeks after the first injection). B) Nanobody levels in the blood serum of MN mice sharply decrease after 5.5 weeks of age. C) Correlational analysis of ACR and nanobody level in the blood serum, r = -1. D) Kidney immunofluorescent staining of MN mice injected with P2X7-blocking 13A7 nanobody (upper row) and L-10 control nanobody (bottom row) show the binding of 13A7 to glomerular and interstitial cells, while L-10 has no signal in the kidney. The tissue was stained with antibodies to CD3, endomucin and alfa-tag. Scale bar: 50 µm.

Despite the nanobody level in the blood serum sharply decreased with the development of proteinuria, its presence in the urine was not observed. Moreover, immunofluorescence staining revealed 13A7 nanobody in the kidney binding to glomerular and interstitial cells, proving that nanobodies bound to P2X7 and mediated their functions. However, this blocking was insufficient to prevent MN development and ameliorate disease outcome.

3.5 Blocking of P2X7 in insidious membranous nephropathy might ameliorate disease progression

Since the spontaneous MN model expressed fast-developing proteinuria and nephrotic syndrome with severe health deterioration, the therapeutic potential of P2X7-blocking nanobodies might have been not enough to prevent kidney damage. For this reason, a second, active slow-developing mouse model of MN was used (Tomas et al. 2023 b) (Figure 35, A).

This MN model was generated by active 2-stage immunization of BALB/c mhPLA2R Pod.Cre mice with the 1 µg of recombinant PLA2R in TMG 1:1 sub-cutaneous (s. c.). The boost immunisation contained a mix of 4:1 PLAR2 and TMG with NaCl in 60µl of total volume and was injected s.c. three weeks after the primary immunisation (Figure 35, B).

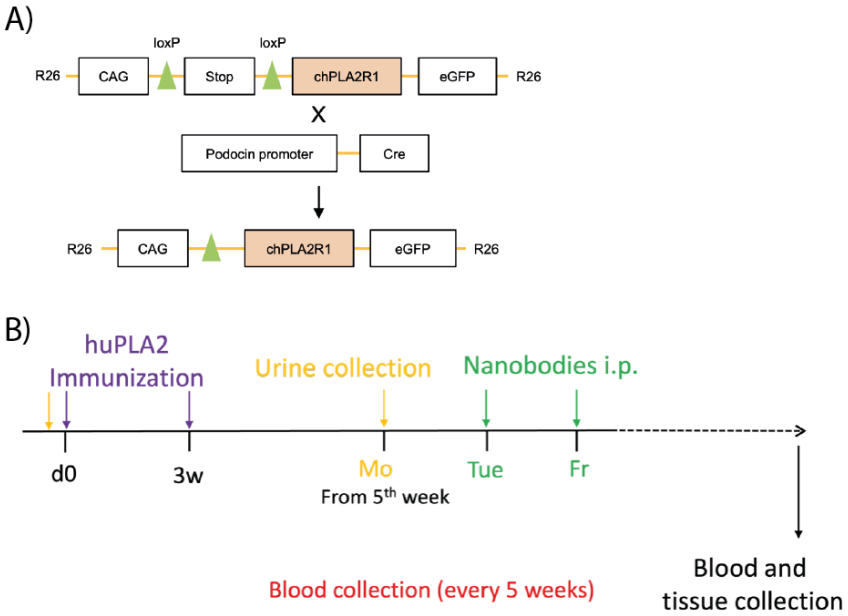

Figure 35. Schematic of active MN mouse model. A) Schematic depiction of the Rosa26 (R26)-based chPLA2R1 full-length knock-in target construct including the transactivation by the CAG promoter. After breeding chPLA2R1-negative mice with podocin Cre deleter mice, chPLA2R1-positive mice are obtained which express chPLA2R1 specifically in podocytes (Tomas et al. 2024b). B) Therapeutic scheme of nanobody therapy in the active MN model.

Urine was collected before the start of the experiment and once a week starting from the fifth week after the primary immunisation, when the first signs of disease appeared. The blood was collected every five weeks after the primary immunisation. Because the active MN developed at different time points in mice, where up to 30% of immunised mice did not express disease development, nanobody therapy, including twice-weekly i. p. injection of 50µg therapeutic 13A7 or control L-10, was started individually when a mouse reached ACR 3 mg/mg. Mice insensitive to recombinant PLA2R that remained healthy by the ninth week after primary immunization were removed

from the experiment. The ethical endpoint was evaluated in each mouse separately, based on health conditions (ascites, pain, and stress signs) and proteinuria level (ACR ≥ 500 mg/mg).

The administration of P2X7-blocking nanobodies in the slowly developing MN, in contrast to the acute MN form, showed increased survival compared to mice receiving L-10 control nanobodies ($p = 0.03$) (Figure 36, A). The mean survival time of mice with P2X7 blockage was 13 weeks ($n = 10$) *vs.* 10 weeks in the control group ($n = 7$). In addition, two mice that received 13A7 nanobodies survived an unusually long time, experiencing remission after 11 – 12 weeks and were eliminated from the experiment in the 21st week of the trial.

The first signs of proteinuria in most MN mice occurred in the seventh to ninth week of the experiment. As shown in Figure 36, B, proteinuria in the group of mice that received 13A7 therapy developed slower than in the L-10 control group and showed a statistically significant reduction on week 12 (141.9 mg/mg vs. 882.5 mg/mg in the control group, $p = 0.015$) and on week 14 (428.1 mg/mg vs 1383.8 mg/mg in L-10 group, $p = 0.009$).

As mentioned before, two out of ten mice with 13A7 therapy experienced remission after 11 – 12 weeks of the experiment, with their mean ACR = 18.8 mg/mg on week 15 and ACR = 0.8 mg/mg on week 20 (Figure 36 B, right panel). This sharply decreased mean ACR in Figure 36 B (left panel) was shown after 14 weeks when the rest of the MN mice with higher proteinuria were eliminated.

Immunofluorescent analysis showed nephrin disruption and increased deposition of immune complexes in the glomeruli in 13A7- and L-10-treated mice (Figure 36, C). The expression level analysis of mIgG in glomeruli did not show a statistical difference in both groups of mice (mean expression value = 6.3 a. u. in both groups) as well as nephrin expression (mean expression value = 16.6 a. u. in 13A7 group *vs.* 16 a. u. in L-10 group), indicating a similar level of glomerular damage in both groups (Figure 36 D, E).

Analysis of blood serum showed increased anti-PLA2R antibody (mIgG) circulation in 13A7 and L-10-treated mice with its peak on week 10 (mean 121,5 U), without differences in both groups (Figure 36, F). The decrease in mean IgG level after 10 weeks of the experiment can be explained by eliminating severely proteinuric mice at that time, leaving animals with less developed MN. Two MN mice from the 13A7-treated group (1690, 1706), that experienced remission in albuminuria, showed severely increased mIgG levels in the blood despite mildening symptoms (mean mIgG = 367,7 U). The common autoantibody levels on the last day of the experiment also indicated

no difference in both groups of mice, with mean mIgG level 128,8 U in 13A7- and 82,6 U in L-10-treated groups (Figure 36, G).

During the trial, two mice in the 13A7 therapeutic group exhibited allergic reactions after the PLA2R immunisation, which manifested in aggressive behaviour accompanied by pruritus, which led to intense self-mutilation (mouse 1901). The animal repeatedly bit its tail, resulting in the loss of approximately one-third of the tail length. The mouse 1901 received Tramal in water in weeks 3 and 4 to weaken the pain reactions. ACR level of this mouse was increased on week 5 (7.2 mg/mg), compared to other mice, which developed the first signs of proteinuria in week 7. The administration of 13A7 nanobodies starting from week 5 weakened allergic symptoms and reduced proteinuria to 1.2 mg/mg (week 6), gradually increasing to 3.6 mg/mg (week 7) and more in the next weeks. This mouse lost all signs of allergy by week 7, did not express signs of health deterioration through the experiment and had a prolonged survival of 14 weeks. The second mouse (1920) exhibited allergic reactions characterized by localized hair loss on the back. The initial signs of proteinuria were detected in week 8 of the experiment (4.5 mg/mg). Following the administration of 13A7 nanobodies, there was a reduction in proteinuria to 1.4 mg/mg by week 9. Over time, proteinuria levels gradually increased, and complete hair regrowth on the back was observed after two weeks of therapy. Additionally, the mouse had a prolonged survival of 14 weeks.

Despite the initially promising effects of 13A7 nanobody therapy in slowly developing MN, which included increased survival, lower proteinuria, and reduced allergic reactions, the treatment did not reduce kidney damage and mIgG production in MN. However, two out of ten mice treated with 13A7 nanobody experienced remission and a decrease in MN symptoms, despite having high mIgG levels in their blood. This indicates that while 13A7 blockage may not be effective by itself/alone in most cases of MN, it holds potential for certain subsets of patients or under specific conditions, warranting further research and optimization of this therapeutic approach.

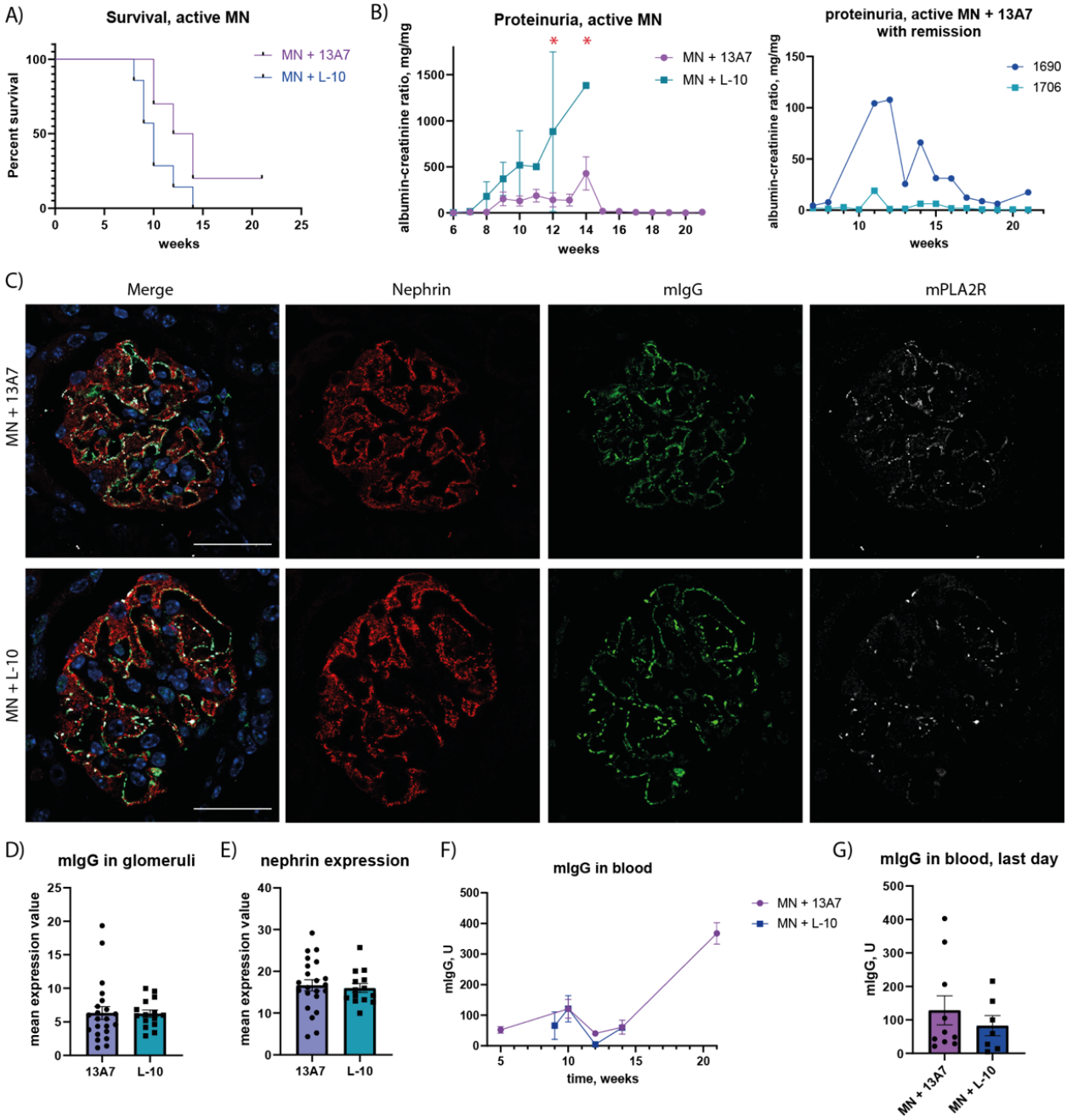

Figure 36. 13A7 therapy partially ameliorated chronic MN. A) The survival graph shows increased survival in mice with 13A7 therapy. B) Proteinuria in mice with 13A7 therapy and L-10-treated control MN (left panel) shows the tendency to decrease proteinuria within P2X7 blockage. Proteinuria in 2 mice with 13A7 therapy that developed remission after 12 weeks of trial (right panel). C) Renal immunofluorescent staining of 13A7- (upper row) and L-10-treated mice (bottom row) with antibodies to nephrin (red), mIgG (green) and PLA2R (white). Staining shows damaged nephrin, increased immunocomplex deposition and PLA2R expression on the slit diaphragm in both groups of mice. Scale bar: 20 µm. D) The mean expression value of mIgG in glomeruli shows no difference in 13A7 and L-10 treated groups. Glomeruli n = 22 and 15 from 8 13A7 and 7 L-10 mice respectively. E) The mean expression value of nephrin shows no difference in both groups of mice. Glomeruli n = 22 and 14 from 8 13A7 and 7 L-10 mice respectively. F) P2A2R-specific antibodies (mIgG) level in the blood serum of mice receiving 13A7 and L-10 therapy through the experiment shows no difference in both groups. Mice with developed remission express increased levels of mIgG in the blood on week 21. G) mIgG level in the blood serum in both groups of mice on the individual last day of the experiment (9-21 weeks) shows no difference between the two groups.

4. Discussion

Glomerulonephritis represents a heterogeneous group of immune-mediated renal disorders characterised by the inflammation and subsequent damage of the glomeruli. Despite advances in understanding the pathophysiology of GN, therapeutic options remain limited. Conventional treatments primarily focus on immunosuppression and symptom management. Corticosteroids and other immunosuppressive agents are commonly employed to mitigate the immune response. However, these treatments are associated with considerable adverse effects and variable efficacy, necessitating the exploration of novel therapeutic targets and strategies that can more effectively halt or reverse the progression of glomerular damage.

One such promising target is the P2X7 receptor, predominantly expressed on tissue-resident immune cells and known to trigger inflammatory responses in various diseases. Suppression of P2X7 activity in animal models has been shown to reduce inflammation and improve clinical outcomes in several inflammatory conditions, including GN, highlighting the potential of P2X7 modulation as a therapeutic strategy (Savio et al. 2018, Taylor et al. 2009, Danquah et al. 2016).

In the present study, we showed that P2X7 blocking therapy was insufficient to alleviate kidney damage in the fast-developing GN models (NTN and spontaneous MN), however, the therapy showed a positive effect in slowly-developing MN, where MN mice experienced decreased proteinuria and allergic reactions as well as increased survival compared to the MN control group.

4.1 Role of P2X7 blockade in treating glomerulonephritis

Initially, due to limited method sensitivity, it was believed that P2X7 expression was absent in renal cells (Collo et al 1997). However, modern techniques have revealed low-level P2X7 expression in mesangial cells, endothelial cells, and macrophages under healthy conditions (Harada et al. 2000; Di Virgilio et al. 2001). In this study, using P2X7-GFP Tg mice, we observed its expression on renal resident T cells, macrophages and GEC, with its increased expression under inflammation (NTN). This finding supports the growing body of evidence indicating the importance of P2X7 in GN pathogenesis and aligns with previous data showing increased P2X7 expression in lupus nephritis, primary minimal change disease and focal segmental glomerulosclerosis (Zhu et al. 2021; Solini et al. 2013; Vonend et al. 2004, Turner et al. 2007, Taylor et al. 2009, Danquah et al. 2016).

The 13A7 nanobodies used in this study were modified to include an alfa-tag (alfa-13A7dim-alb), enabling their visualization in histological samples post-injection using an anti-alfa AF 647 antibody (NanoTag). This modification allowed the detection of those nanobodies via immunofluorescent staining, showing their evenly distribution across all P2X7-expressing renal cells, including glomerular endothelial cells (GEC), T cells, and macrophages. Interestingly, histology analysis revealed an increased binding of 13A7 nanobodies to glomerular cells, confirming their successful delivery to the target site. However, kidney resident T cells, the intended target cells in this study, did not display a detectable nanobody signal in the histological analysis.

Additionally, functional tests using P2X7-expressing HEK cells demonstrated that the 13A7 constructs effectively blocked P2X7, preventing large pore formation and DAPI uptake. In contrast, the control nanobody L-10 did not prevent those effects, resulting in DAPI uptake, showing an increased signal in flow cytometry analysis. These results confirm the functional integrity of the modified 13A7 nanobodies, refuting the suggestion that the nanobodies were unable to maintain their intended functions.

Despite the positive effect of P2X7 blockage in anti-podocyte nephritis of Danquah et al, the P2X7-blocking nanobodies did not prevent the progression of NTN, although it did significantly reduce glomerulosclerosis in the mNTN. Despite this reduction, there was no corresponding decrease in albuminuria. Additionally, immune cell infiltration and severe immune-mediated interstitial renal damage were not alleviated by the P2X7-blocking therapy. On the other side, P2X7 blockage tended to increase survival in the severe NTN.

A potential reason for the lack of effect of P2X7 blockade in the NTN model could be the loss of nanobodies through the damaged kidney filtration barrier, which allows molecules up to 100kDa to pass through (vs. up to 40 kDa in the healthy kidney) (D'Amico/Bazzi 2003, Tojo/Endou 1992). In addition, the nanobodies were constructed to include an anti-albumin domain to increase their half-life, although this could lead to their clearance along with albumin in severely proteinuric mice. Despite these assumptions, nanobody analysis showed its high concentration in the blood of all groups of animals (control, sNTN and mNTN) with its increased level in the urine in sNTN mice only on day 2, indicating that nanobodies were partially cleared (sNTN) or not cleared (mNTN) through the damaged filtrating barrier in the kidney.

A more significant reason for the failure to prevent or ameliorate NTN could be the rapid onset and progression of nephrotic syndrome in the mice. Previous studies of P2X7-blocking therapy in

anti-podocyte nephritis (Danquah et al. 2016) achieved success under conditions of gradual and mild disease development, which contrasts with our study. In the previous study, the ACR reached a maximum of around 20 mg/mg by day 15, whereas in our study, the ACR was already severely elevated by day 2, exceeding 200 mg/mg across all NTN groups. Similarly, in the accelerated NTN model, Taylor et al. demonstrated reduced disease progression in P2X7 KO mice, which showed minimal renal damage and significantly lower proteinuria (6 mg in WT). The administration of the P2X7 antagonist A-438079 in the NTN model resulted in a significant reduction of disease symptoms when administered at high doses, but not at lower doses. In this model, the disease was manifested mildly, with the ACR in the vehicle group reaching around 50 mg/mg (Taylor et al. 2009). These findings support the theory that the failure to observe protective effects in our study may be due to the severe and rapid development of nephrotic syndrome.

The rapid and severe disease progression in our study made it challenging to manage disease outcomes with nanobodies. The condition of NTN mice could be compared to AKI, which in patients requires a more aggressive treatment or renal replacement therapy (Lobo 2020). In this condition, despite increased P2X7 expression, 13A7 nanobodies alone were insufficient to manage disease development and progression.

Despite substantial evidence indicating a significant role of P2X7 in the autoimmune disease pathogenesis, its contribution to MN, as well as the pathophysiology of the disease itself remains unknown (Hoxha et al. 2022, Grassi/Salina 2023, Di Virgilio/Giuliani 2016, Cao et al. 2019). While NTN is induced by the administration of serum containing antibodies against the components of GBM (or podocytes in anti-podocyte nephritis), triggering complement activation and immune cell recruitment, MN mouse models involve the production of autoantibodies against PLA2R expressed on podocytes by the mice. The primary pathogenic mechanism in MN involves a breakdown of immunological tolerance, production and deposition of immune complexes in the glomeruli, resulting in GBM thickening and subsequent renal damage due to complement-mediated injury (Fogo et al 2015, Tomas et al. 2023a, Tomas et al. 2023b).

The P2X7-blocking trial conducted in acute MN also did not alleviate disease outcomes. In the spontaneously developing MN, proteinuria has been developing gradually but severely, also greatly exceeding ACR level in the anti-podocyte nephritis model of Danquah et al. study. Although the nanobody therapy was initiated before the onset of disease manifestations, P2X7 blocking was insufficient to prevent the development of anti-PLA2R IgG and the subsequent rapid glomerular damage. In this model, the nanobody levels in the blood remained high until the first signs

of proteinuria appeared: starting from week 5 of age, MN mice experienced an elevation in proteinuria, accompanied by a sharp drop in nanobody concentration in the blood. However, the first presence of nanobodies in the urine was observed only at 7 weeks of age (5 weeks after the initial 13A7 injection). By that time, most MN animals had reached the ethical endpoint and were therefore sacrificed.

Despite a sharp drop of nanobodies in the blood, immunofluorescent staining of MN kidneys discovered the uniform distribution of P2X7-blocking nanobodies to kidney glomerular and T cells, proving its presence and binding in the kidney and refuting the theory that nanobodies were lost through damaged filtration barrier.

The uniform distribution of 13A7 nanobodies in the kidneys in this model, compared to increased binding to glomerular cells in NTN, can be explained by the gradual MN development. In the NTN model, mice developed nephrotic syndrome and glomerulosclerosis within a few days after disease induction, as evidenced by severe proteinuria on day 2. Due to the rapid and severe glomerular damage, nanobodies from systemic circulation entered the kidney and could bind to cells in the glomeruli that overexpress P2X7. This rapid damage likely prevented nanobodies from effectively reaching or binding to interstitial immune renal cells.

In contrast, the nanobody therapy in the spontaneous MN model started much in advance of disease development, approximately two weeks before the first symptoms appeared. In this scenario, 13A7 nanobodies could be distributed to P2X7-expressing cells throughout the healthy kidney, without the increased binding to damaged and inflamed glomeruli.

In contrast to the acute GN models (NTN and spontaneous MN), the P2X7 blocking therapy in the slowly developing MN showed a positive result, showing increased survival, decreased proteinuria starting from week 12 and a significant reduction in allergic reactions related to immunization. Despite these positive effects of 13A7 therapy, the blocking of P2X7 did not affect anti-PLA2R antibody production, immune complex deposition in glomeruli and slit diaphragm disruption, resulting in continued severe proteinuria and health deterioration. However, two out of ten mice treated with 13A7 nanobody experienced remission after week 12 – 14 and a decrease in MN symptoms, despite having high mIgG levels in their blood. These mice survived an unusually long period (21 weeks) and were then sacrificed to adhere to the study's predefined guidelines. These contradictory effects suggest that while the P2X7-blocking approach could give promising results,

nanobody therapy alone is often insufficient to effectively modulate the entire inflammatory milieu in autoimmune MN.

In general, inflammatory processes often involve multiple redundant pathways and receptors. Regardless of whether P2X7 is successfully blocked, other receptors and pathways (such as TLRs, NLRs, or cytokine receptors) might still maintain inflammation. In addition, by blocking P2X7, the immune system might activate compensatory mechanisms that bypass the blocked P2X7 receptor, supporting the inflammatory response through alternative routes or upregulation of other purinergic receptors (e.g., P2X4, P2Y receptors). Especially it might be the case of P2X4, as its activation, similar to P2X7, leads to NLRP3 inflammasome assembly and the launch of inflammatory reactions, or the assembly of P2X2 and P2X5 that exhibit the P2X7-like properties (Chen et al. 2013, Compan et al. 2012).

Another important point is that P2X7 receptor expression can vary widely among different cell types and tissues. In diseases where inflammation is driven by cells with low or no P2X7 expression, blocking this receptor might not give significant therapeutic benefits. Immunofluorescent images of NTN kidneys in our study showed that P2X7 was expressed only in part of T cells, supporting the idea that a compensatory inflammatory mechanism may be led through infiltrated immune cells with no P2X7 expression.

In addition, the timing and duration of P2X7 blockade might be critical. Early or late intervention might not be effective, and prolonged inhibition might lead to adaptive changes in the immune system, which could be the case of the acute form of MN when the therapy was started 2 weeks before the first symptoms of the disease occurred.

4.2 Insights into P2X7 function

Bulk RNA sequencing of renal resident T cells revealed an unwanted effect of 13A7 therapy: blocking of pro-apoptotic P2X7 increased immune cell survival. T cells of NTN and healthy mice with blocked P2X7 receptor expressed genes associated with survival, proliferation, and cell spreading with a composition of several populations of T cells (Th1, Th2, Th17 and Treg). These effects are considered negative since the presence of T cells in the kidney during GN is usually associated with inflammation. Prolonged survival of these T cells can exacerbate the inflammatory response, leading to further tissue damage (Linke et al. 2022, Gao et al 2021). In addition, increased survival, proliferation and spreading of T cells can contribute to chronic inflammation, which may worsen the progression of GN, leading to more extensive kidney damage and fibrosis.

Additionally, blocking of P2X7 still resulted in upregulated expression of calcium ion channels CaV1-CaV3 and ROC, which could lead to Ca ions influx. In addition, calcium signalling analysis showed the upregulation of SERCA, STIM and ORAI, suggesting a coordinated response to regulate intracellular Ca^{2+} homeostasis, likely in response to increased cellular demand or stress. SERCA is responsible for actively pumping Ca^{2+} from the cytosol back to the storage in the sarcoplasmic or endoplasmic reticulum (SR/ER), its upregulation indicates an enhanced capacity to clear Ca^{2+} from the cytoplasm to maintain its low cytosolic level (Primeau et al. 2018). STIM acts as a sensor for Ca^{2+} levels within the ER, when its level is depleted STIM activates highly Ca^{2+} selective ORAI channels to facilitate Ca^{2+} entry from the extracellular space (Soboloff et al. 2012). These coordinated events suggest that the cells could experience an increased physiological demand to regulate Ca^{2+} homeostasis to support cellular functions. The increased activation of calcium channels and influx of Ca^{2+} resulted in the activation of NFAT, and as a result, cellular proliferation.

Contrary to our expectations, the activation of NFAT did not lead to increased *Il-2* expression in treated and untreated mice. This effect can be attributed to the genetic background of the C57BL/6 mice, which have a mutation in the *P2rx7* gene, which impairs its function, making these mice less responsive to eATP (Adriouch et al. 2002). This limitation poses a challenge when using C57BL/6 mice to study P2X7 blockage and its effects on immune regulation. In contrast, BALB/c mice express fully functional P2X7, making them more sensitive to eATP, whereas the nanobody therapy showed more promising P2X7-blocking results. Future research should take these genetic differences into account to achieve better evaluation and success of therapeutic strategies.

Taking this into consideration, genetic variations among humans might also affect the potential efficacy of P2X7 blockers. P2RX7 exhibits considerable polymorphism, including 11 splice variants and over 30 single nucleotide polymorphisms that may affect its activity. The functionality of the P2X7 receptor can differ between individuals, as some variants are functional while others are not. Variants linked to gain-of-function or loss-of-function can significantly influence the development of various pathophysiological conditions. These polymorphisms combine to create various haplotypes that can modify P2X7 receptor activity (Sluyter/Stokes 2011). Consequently, P2X7 blockage might be ineffective in certain individuals due to these genetic differences, highlighting the need for personalized approaches when considering P2X7-targeted therapies.

4.3 Future research directions

Taking together the previous positive results of P2X7-blocking therapy in anti-podocyte nephritis and the effect of P2X7 KO in accelerating NTN, with the partially successful results of 13A7 therapy in slowly developing MN, the P2X7 blocking remains a promising approach in GN. However, in the complex pathophysiological nature of different forms of GN, the blocking of P2X7 alone can be insufficient to manipulate numerous inflammatory reactions. For this reason, additional steps can be taken to improve P2X7-blocking therapy.

4.3.1 The possible advantages of double blocking of P2X4 and P2X7 receptors

In the presence of large amounts of eATP, the role of the P2X7 receptor can be overtaken by P2X4, leading to a similar effect in inflammasome activation and T cell activity (Chen et al. 2013). The P2X4 receptor is often co-expressed with P2X7 and can form heteromeric complexes, which modulate the function and signalling pathways of each other, thereby influencing the overall inflammatory response (Weinhold et al., 2010). In addition, the upregulation of P2X4 in the absence of P2X7 suggests a compensatory mechanism that maintains inflammation (Weinhold et al., 2010). Despite the fact that the role and functions of P2X4 in the inflammation is less studied, several data emerge to show its participation in CNS disorders (such as epilepsy, ischemia, chronic pain, anxiety, multiple sclerosis and neurodegenerative diseases), rheumatoid arthritis, airways inflammation of asthma and metabolic syndrome (Suurväli et al. 2017, Montilla et al. 2020). In the kidney, the activation of P2X4R is linked to diabetic nephropathy (DN), which was investigated using renal biopsies from patients with type-2 diabetes, showing increased expression of P2X4R in renal tubular epithelial cells and correlation in P2X4R expression with IL-1 and IL-18 presence in DN patients compared to non-DN patients (Chen et al. 2013, cited in Birch et al 2013:4). These data suggest that targeting of both P2X7 and P2X4 receptors can provide a comprehensive anti-inflammatory strategy in the treatment of inflammatory conditions.

However, the limitation of this approach in GN may be related to the complex role of P2X4 in renal physiology. Evidence suggests that blocking P2X4, which is important for sodium transport, could lead to hypertension by disrupting this process in the distal nephron. This underscores that although P2X receptors are considered attractive therapeutic targets for many inflammatory conditions, their widespread expression and diverse functions make their manipulation extremely complex (Birch et al. 2013).

4.3.2 Enhanced P2X7 levels on GEC and increased nanobody binding open new avenues for targeted gene therapy in the kidney

Analysis of P2X7 expression in the NTN mouse model showed its increased level in renal resident immune cells and to a greater degree in GEC, highlighting its role in the pathophysiology of inflammation. However, the KO of P2X7 on GEC in the mNTN did not improve the disease outcome despite the tendency to lower proteinuria. Despite the absence of a positive therapeutic effect in P2X7 blockage, the increased binding of 13A7 nanobody to GEC in NTN suggests a potential approach for targeted kidney gene therapy.

Adeno-associated virus (AAV) vectors are versatile tools in gene therapy, capable of delivering genetic material efficiently and safely to various tissues. However, despite the progress of using gene therapies in the clinic for other tissues, achieving renal-specific targeting with AAVs remains a significant challenge (Peek/Wilson 2023). AAV vectors engineered exclusively for renal targeting without off-target effects are still under development and refinement. The coupling of AAV and 13A7 nanobodies could facilitate specific targeting of the GEC. The nanobody would act as a guiding component, leading the AAV vectors to the inflamed glomeruli where P2X7 expression is elevated. Upon reaching the target cells within the glomeruli, the AAV vector would deliver the genetic sequence of interest to manipulate cellular function. If successful, AAV-mediated gene therapy targeting P2X7 with the 13A7 nanobody could offer a novel and precise treatment strategy for patients with glomerulonephritis and other renal inflammatory diseases, potentially improving therapeutic outcomes and patient quality of life.

Limitations of this approach may arise due to the widespread expression of P2X7 receptors across various organs and systems. As demonstrated in the spontaneous MN mouse model, 13A7 nanobodies were found distributed evenly throughout renal cells expressing P2X7, including immune cells, within the inflamed kidney. Targeted gene therapy might potentially have more successful outcomes in conditions with severely inflamed glomeruli, comparable with rapid and acute tissue damage shown in NTN.

Further analysis of human kidney biopsies on P2X7 expression in various renal diseases and stages is needed to investigate the possible potential of binding to glomerular cells by 13A7-coupled AAV vectors.

4.3.3 P2X7 blockade in allergic reactions

One of the most promising effects of P2X7 blockage observed in this study was the reduction in allergic reactions in mice with chronic MN. Two out of ten MN mice experienced allergies related to immunization, whereby the therapy with 13A7 nanobodies reduced those reactions within two weeks and in addition reduced mild proteinuria within one week. This suggests that P2X7 blocking could have a potential in the treatment of allergic reactions.

Weber et al. showed that Mice lacking P2X7 exhibited resistance to contact hypersensitivity due to the inability of dendritic cells to produce IL-1β in response to the contact allergen during the sensitization phase (Webet et al. 2010). P2X7 blocking therapy with 13A7 therapy was tested in a mouse model of allergic contact dermatitis in response to the contact allergen 1-fluoro-2,4-dinitrobenzene (DNFB) by Danquah et al. In this model, mice were sensitized by epicutaneous application of DNFB to the shaved abdominal skin on day 0. When challenged 6 days later with DNFB on the ear skin on day 6, mice respond with a characteristic local inflammatory response that can be monitored by the ear swelling reaction and the release of inflammatory cytokines 24 hours after the challenge (Danquah et al. 2016: 3 ff.).

Even though a single injection of 13A7-HLE before sensitization with DNFB on abdominal and ear skin did not significantly decrease inflammation, the application of nanobodies during the challenge phase, ameliorated local inflammation. Mice treated with 13A7 nanobodies had a significantly lower gain in ear weight than did control animals and significantly lower levels of the inflammatory cytokines IL-6 and IL-1β in ear tissue extracts (Danquah et al. 2016: 4).

These data, together with our findings on allergic reaction reductions indicate a promising approach of P2X7 blockage in treating mild, non-life-threatening inflammatory conditions such as dermatitis and similar disorders.

Conclusion

This study reinforces the established role of P2X7 in the pathogenesis of GN, demonstrating its upregulated expression under inflammatory conditions, as observed in the NTN model. Despite this, blocking of P2X7 with nanobodies did not prevent the progression of acute mouse models of GN (NTN and spontaneous MN). Despite the reduction of glomerulosclerosis in mice with mNTN, the treatment showed no significant impact on survival, albuminuria, immune cell infiltration, or interstitial renal damage. Functional assays and nanobody identification in the blood and tissue confirmed that the 13A7 nanobodies were successfully delivered to the target cells, effectively blocking P2X7 and maintaining their functional integrity. However, the observed increase in P2X7 expression by glomerular cells in the context of NTN, along with the enhanced binding of nanobodies to GEC, highlights a promising avenue for targeted kidney gene therapy, which is currently under exploration.

In the more slowly progressing form of MN, the application of 13A7 nanobodies yielded beneficial outcomes, including increased survival rates and reduced proteinuria. However, the treatment did not affect anti-PLA2R autoantibody production, deposition in the glomeruli, or the associated glomerular damage. Notably, this model also showed two cases of disease remission and the resolution of allergic reactions related to immunization, suggesting that P2X7 blocking could be a promising therapeutic approach in treating milder forms of GN and other milder inflammatory conditions, including allergic reactions.

Future studies are needed to further investigate the localization, expression levels, and splice variants of P2X7 in patients with various forms and stages of GN. This research could pave the way for more effective and personalized therapeutic strategies for GN and related inflammatory conditions.

Personal contributions

Publications

1. Wanner N*, Eden T, **Liaukouskaya N**, Koch-Nolte F*. Nanobodies: new avenue to treat kidney disease. Cell Tissue Res. 2021 Aug;385(2):445-456. doi: 10.1007/s00441-021-03479-8. Epub 2021 Jun 16.

2. Schreiber J*, **Liaukouskaya N***, Fuhrmann L, Hauser AT, Jung M, Huber TB, Wanner N*. BET Proteins Regulate Expression of Osr1 in Early Kidney Development. Biomedicines. 2021 Dec 10;9(12):1878. doi: 10.3390/biomedicines9121878.

3. Rudloff S*, Bileck A, Janker L, Wanner N, **Liaukouskaya N**, Lundby C, Huber TB, Gerner C, Huynh-Do U*. Dichotomous Responses to Chronic Fetal Hypoxia Lead to a Predetermined Aging Phenotype. Mol Cell Proteomics. 2022 Feb;21(2):100190. doi: 10.1016/j.mcpro.2021.100190. Epub 2021 Dec 24.

4. Pinto-Espinoza C*, Guillou C, Rissiek B, Wilmes M, Javidi E, Schwarz N, Junge M, Haag F, **Liaukouskaya N**, Wanner N, Nicke A, Stortelers C, Tan YV, Adriouch S, Magnus T, Koch-Nolte F*. Effective targeting of microglial P2X7 following intracerebroventricular delivery of nanobodies and nanobody-encoding AAVs. Front Pharmacol. 2022 Oct 10;13:1029236. doi: 10.3389/fphar.2022.1029236.

5. Junge M*, **Liaukouskaya N***, Schwarz N*, Pinto-Espinoza C, Schaffrath A Z, Rissiek B, Krebs C, Mittrücker H-W, Tomas N M, Nicke A, Haag F, Meyer-Schwesinger C, Koch-Nolte F*, Wanner N*. Nanobody-based in vivo blockade of the P2X7 ion channel uncovers a hitherto unknown large subpopulation of parenchymal kidney TRM and NKT cells. JASN – manuscript in revision.

6. Wanner N*, Keller J*, **Liaukouskaya N***, Andrieux G, Laufer S, Rogg M, Bork T, Liang W, Haas F, Wong M N, Puelles V G, Gies S, Meyer C, Börries M, Helmstädter M, Kretz O, Hild I, Schüle R, Bechtel-Walz W*, Huber T B*. LSD1 regulates nephron development and long-term transcriptional programming. Developmental cell – manuscript in submission.

Conference attendance as presenter

1. Poster presentation ‘Nanobody-based P2X7 blocking strategies in Glomerulonephritis’, 18th International Congress of Immunology (Cape Town, South Africa);

2. Poster presentation ‘The role and blocking of P2X7 in nephrotoxic nephritis’, SFP1192 Retreat (Imperia, Italy).

List of references

Adriouch S, Dox C, Welge V, Seman M, Koch-Nolte F, Haag F. Cutting edge: a natural P451L mutation in the cytoplasmic domain impairs the function of the mouse P2X7 receptor. J Immunol. 2002 Oct 15;169(8):4108-12.

Alinaghi F, Calov M, Kristensen LE, Gladman DD, Coates LC, Jullien D, Gottlieb AB, Gisondi P, Wu JJ, Thyssen JP, Egeberg A. Prevalence of psoriatic arthritis in patients with psoriasis: A systematic review and meta-analysis of observational and clinical studies. J Am Acad Dermatol. 2019 Jan;80(1):251-265.e19.

Alok A, Yadav A. Membranous Nephropathy. 2023 Jun 5. In: StatPearls [Internet]. Treasure Island (FL): StatPearls Publishing; 2024 Jan–. PMID: 32644595.
Anders HJ, Kitching AR, Leung N, Romagnani P. Glomerulonephritis: immunopathogenesis and immunotherapy. Nat Rev Immunol. 2023 Jul;23(7):453-471.

Anders, S.; Pyl, P. T.; Huber, W., HTSeq--a Python framework to work with high-throughput sequencing data. Bioinformatics 2015, 31, (2), 166-9.

Arbabi Ghahroudi M, Desmyter A, Wyns L, Hamers R, Muyldermans S. Selection and identification of single domain antibody fragments from camel heavy-chain antibodies. FEBS Lett. 1997 Sep 15;414(3):521-6.

Bannas P, Hambach J, Koch-Nolte F. Nanobodies and Nanobody-Based Human Heavy Chain Antibodies As Antitumor Therapeutics. Front Immunol. 2017 Nov 22;8:1603.

Ben-Sasson SZ, Hogg A, Hu-Li J, Wingfield P, Chen X, Crank M, Caucheteux S, Ratner-Hurevich M, Berzofsky JA, Nir-Paz R, Paul WE. IL-1 enhances expansion, effector function, tissue localization, and memory response of antigen-specific CD8 T cells. J Exp Med. 2013 Mar 11;210(3):491-502.

Bihlet AR, Balchen T, Goteti K, Sonne J, Ladel C, Karsdal MA, Ona V, Moreau F, Waterhouse R, Bay-Jensen AC, Guehring H. Safety, Tolerability, and Pharmacodynamics of the ADAMTS-5 Nanobody M6495: Two Phase 1, Single-Center, Double-Blind, Randomized, Placebo-Controlled Studies in Healthy Subjects and Patients With Osteoarthritis. ACR Open Rheumatol. 2024 Apr;6(4):205-213.

Birch RE, Schwiebert EM, Peppiatt-Wildman CM, Wildman SS. Emerging key roles for P2X receptors in the kidney. Front Physiol. 2013 Sep 27;4:262.

Burnstock G, Kennedy C. P2X receptors in health and disease. Adv Pharmacol. 2011;61:333-72.

Cao F, Hu LQ, Yao SR, Hu Y, Wang DG, Fan YG, Pan GX, Tao SS, Zhang Q, Pan HF, Wu GC. P2X7 receptor: A potential therapeutic target for autoimmune diseases. Autoimmun Rev. 2019 Aug;18(8):767-777.

Chen K, Zhang J, Zhang W, Zhang J, Yang J, Li K, He Y. ATP-P2X4 signaling mediates NLRP3 inflammasome activation: a novel pathway of diabetic nephropathy. Int J Biochem Cell Biol. 2013 May;45(5):932-43.

Clare M. Turner, Frederick W. K. Tam, Ping-Chin Lai, Ruth M. Tarzi, G. Burnstock, Charles D. Pusey, H. Terence Cook, Robert J. Unwin, Increased expression of the pro-apoptotic ATP-sensitive $P2X_7$ receptor in experimental and human glomerulonephritis, *Nephrology Dialysis Transplantation*, Volume 22, Issue 2, February 2007, Pages 386–395.

Collo G, Neidhart S, Kawashima E, Kosco-Vilbois M, North RA, Buell G. Tissue distribution of the P2X7 receptor. Neuropharmacology. 1997 Sep;36(9):1277-83.

Compan V, Ulmann L, Stelmashenko O, Chemin J, Chaumont S, Rassendren F. P2X2 and P2X5 subunits define a new heteromeric receptor with P2X7-like properties. J Neurosci. 2012 Mar 21;32(12):4284-96.

D'Amico G, Bazzi C. Pathophysiology of proteinuria. Kidney Int. 2003 Mar;63(3):809-25.

Danquah W, Meyer-Schwesinger C, Rissiek B, Pinto C, Serracant-Prat A, Amadi M, Iacenda D, Knop JH, Hammel A, Bergmann P, Schwarz N, Assunção J, Rotthier W, Haag F, Tolosa E, Bannas P, Boué-Grabot E, Magnus T, Laeremans T, Stortelers C, Koch-Nolte F. Nanobodies that block gating of the P2X7 ion channel ameliorate inflammation. Sci Transl Med. 2016 Nov 23;8(366):366ra162.

De Munter S, Ingels J, Goetgeluk G, Bonte S, Pille M, Weening K, Kerre T, Abken H, Vandekerckhove B. Nanobody Based Dual Specific CARs. Int J Mol Sci. 2018 Jan 30;19(2):403.

De Vos J, Devoogdt N, Lahoutte T, Muyldermans S. Camelid single-domain antibody-fragment engineering for (pre)clinical in vivo molecular imaging applications: adjusting the bullet to its target. Expert Opin Biol Ther. 2013 Aug;13(8):1149-60.

Di Virgilio F, Chiozzi P, Ferrari D, Falzoni S, Sanz JM, Morelli A, Torboli M, Bolognesi G, Baricordi OR. Nucleotide receptors: an emerging family of regulatory molecules in blood cells. Blood. 2001 Feb 1;97(3):587-600.

Di Virgilio F, Dal Ben D, Sarti AC, Giuliani AL, Falzoni S. The P2X7 Receptor in Infection and Inflammation. Immunity. 2017 Jul 18;47(1):15-31.

Di Virgilio F, Giuliani AL. Purinergic signalling in autoimmunity: A role for the P2X7R in systemic lupus erythematosus? Biomed J. 2016 Oct;39(5):326-338.

Duplantier AJ, Dombroski MA, Subramanyam C, Beaulieu AM, Chang SP, Gabel CA, Jordan C, Kalgutkar AS, Kraus KG, Labasi JM, Mussari C, Perregaux DG, Shepard R, Taylor TJ, Trevena KA, Whitney-Pickett C, Yoon K. Optimization of the physicochemical and pharmacokinetic attributes in a 6-azauracil series of P2X7 receptor antagonists leading to the discovery of the clinical candidate CE-224,535. Bioorg Med Chem Lett. 2011 Jun 15;21(12):3708-11.

Falzoni S, Munerati M, Ferrari D, Spisani S, Moretti S, Di Virgilio F. The purinergic P2Z receptor of human macrophage cells. Characterization and possible physiological role. J Clin Invest. 1995 Mar;95(3):1207-16.

Fogo AB, Lusco MA, Najafian B, Alpers CE. AJKD Atlas of Renal Pathology: Membranous Nephropathy. Am J Kidney Dis. 2015 Sep;66(3):e15-7.

Gabay C, Lamacchia C, Palmer G. IL-1 pathways in inflammation and human diseases. Nat Rev Rheumatol. 2010 Apr;6(4):232-41.

Gao M, Wang J, Zang J, An Y, Dong Y. The Mechanism of CD8+ T Cells for Reducing Myofibroblasts Accumulation during Renal Fibrosis. Biomolecules. 2021 Jul 5;11(7):990.

Ge SX, Jung D, Yao R. ShinyGO: a graphical gene-set enrichment tool for animals and plants. Bioinformatics. 2020 Apr 15;36(8):2628-2629.

Giuliani AL, Sarti AC, Falzoni S, Di Virgilio F. The P2X7 Receptor-Interleukin-1 Liaison. Front Pharmacol. 2017 Mar 16;8:123.

Giuliani AL, Sarti AC, Di Virgilio F. Extracellular nucleotides and nucleosides as signalling molecules. Immunol Lett. 2019 Jan;205:16-24.

Grassi F, Salina G. The P2X7 Receptor in Autoimmunity. Int J Mol Sci. 2023 Sep 14;24(18):14116.

Guile SD, Alcaraz L, Birkinshaw TN, Bowers KC, Ebden MR, Furber M, Stocks MJ. Antagonists of the P2X(7) receptor. From lead identification to drug development. J Med Chem. 2009 May 28;52(10):3123-41.

Harada H, Chan CM, Loesch A, Unwin R, Burnstock G. Induction of proliferation and apoptotic cell death via P2Y and P2X receptors, respectively, in rat glomerular mesangial cells. Kidney Int. 2000 Mar;57(3):949-58.

He WT, Wan H, Hu L, Chen P, Wang X, Huang Z, Yang ZH, Zhong CQ, Han J. Gasdermin D is an executor of pyroptosis and required for interleukin-1β secretion. Cell Res. 2015 Dec;25(12):1285-98.

Horai R, Asano M, Sudo K, Kanuka H, Suzuki M, Nishihara M, Takahashi M, Iwakura Y. Production of mice deficient in genes for interleukin (IL)-1alpha, IL-1beta, IL-1alpha/beta, and IL-1 receptor antagonist shows that IL-1beta is crucial in turpentine-induced fever development and glucocorticoid secretion. J Exp Med. 1998 May 4;187(9):1463-75.

Horde GW, Gupta V. Drug Clearance. 2023 Jun 20. In: StatPearls [Internet]. Treasure Island (FL): StatPearls Publishing; 2024 Jan–.

Hoxha, E., Reinhard, L. & Stahl, R.A.K. Membranous nephropathy: new pathogenic mechanisms and their clinical implications. *Nat Rev Nephrol* **18**, 466–478 (2022).

Hunt A, Qian V, Olds H, Daveluy S. The Current Clinical Trial Landscape for Hidradenitis Suppurativa: A Narrative Review. Dermatol Ther (Heidelb). 2023 Jul;13(7):1391-1407.

Iznardo H, Puig L. Dual inhibition of IL-17A and IL-17F in psoriatic disease. Ther Adv Chronic Dis. 2021 Aug 12;12:20406223211037846.

Jiang LH, Baldwin JM, Roger S, Baldwin SA. Insights into the Molecular Mechanisms Underlying Mammalian P2X7 Receptor Functions and Contributions in Diseases, Revealed by Structural Modeling and Single Nucleotide Polymorphisms. Front Pharmacol. 2013 May 7;4:55.

Kaczmarek-Hajek K, Zhang J, Kopp R, Grosche A, Rissiek B, Saul A, Bruzzone S, Engel T, Jooss T, Krautloher A, Schuster S, Magnus T, Stadelmann C, Sirko S, Koch-Nolte F, Eulenburg V, Nicke A. Re-evaluation of neuronal P2X7 expression using novel mouse models and a P2X7-specific nanobody. Elife. 2018 Aug 3;7:e36217.

Karasawa A, Michalski K, Mikhelzon P, Kawate T. The P2X7 receptor forms a dye-permeable pore independent of its intracellular domain but dependent on membrane lipid composition. Elife. 2017 Sep 18;6:e31186.

Kazi AM, Hashmi MF. Glomerulonephritis. 2023 Jun 26. In: StatPearls [Internet]. Treasure Island (FL): StatPearls Publishing; 2024 Jan–.

Keam SJ. Ozoralizumab: First Approval. Drugs. 2023 Jan;83(1):87-92.

Koch-Nolte F, Eichhoff A, Pinto-Espinoza C, Schwarz N, Schäfer T, Menzel S, Haag F, Demeules M, Gondé H, Adriouch S. Novel biologics targeting the P2X7 ion channel. Curr Opin Pharmacol. 2019 Aug;47:110-118.

Lan HY, Nikolic-Paterson DJ, Mu W, Vannice JL, Atkins RC. Interleukin-1 receptor antagonist halts the progression of established crescentic glomerulonephritis in the rat. Kidney Int. 1995 May;47(5):1303-9.

Lea-Henry TN, Carland JE, Stocker SL, Sevastos J, Roberts DM. Clinical Pharmacokinetics in Kidney Disease: Fundamental Principles. Clin J Am Soc Nephrol. 2018 Jul 6;13(7):1085-1095.

Linke A, Tiegs G, Neumann K. Pathogenic T-Cell Responses in Immune-Mediated Glomerulonephritis. Cells. 2022 May 12;11(10):1625.

Liu M, Li L, Jin D, Liu Y. Nanobody-A versatile tool for cancer diagnosis and therapeutics. Wiley Interdiscip Rev Nanomed Nanobiotechnol. 2021 Jul;13(4):e1697.

Liu S, Zhao Y, Lu S, Zhang T, Lindenmeyer MT, Nair V, Gies SE, Wu G, Nelson RG, Czogalla J, Aypek H, Zielinski S, Liao Z, Schaper M, Fermin D, Cohen CD, Delic D, Krebs CF, Grahammer F, Wiech T, Kretzler M, Meyer-Schwesinger C, Bonn S, Huber TB. Single-cell transcriptomics reveals a mechanosensitive injury signaling pathway in early diabetic nephropathy. Genome Med. 2023 Jan 10;15(1):2.

Liu W, Song H, Chen Q, Yu J, Xian M, Nian R, Feng D. Recent advances in the selection and identification of antigen-specific nanobodies. Mol Immunol. 2018 Apr;96:37-47.

Liu X, Zhang Z, Ruan J, Pan Y, Magupalli VG, Wu H, Lieberman J. Inflammasome-activated gasdermin D causes pyroptosis by forming membrane pores. Nature. 2016 Jul 7;535(7610):153-8.

Liu X, Tang Z, Duan Z, He Z, Shu M, Wang X, Gee SJ, Hammock BD, Xu Y. Nanobody-based enzyme immunoassay for ochratoxin A in cereal with high resistance to matrix interference. Talanta. 2017 Mar 1;164:154-158.

Lobo VA. Renal Replacement Therapy in Acute Kidney Injury: Which Mode and When? Indian J Crit Care Med. 2020 Apr;24(Suppl 3):S102-S106.

Lopez-Castejon G, Brough D. Understanding the mechanism of IL-1β secretion. Cytokine Growth Factor Rev. 2011 Aug;22(4):189-95.

Love, M. I.; Huber, W.; Anders, S., Moderated estimation of fold change and dispersion for RNA-seq data with DESeq2. Genome Biol 2014, 15, (12), 550.

Menon MC, Chuang PY, He CJ. The glomerular filtration barrier: components and crosstalk. Int J Nephrol. 2012;2012:749010.

Montilla A, Mata GP, Matute C, Domercq M. Contribution of P2X4 Receptors to CNS Function and Pathophysiology. Int J Mol Sci. 2020 Aug 3;21(15):5562.

Mortaz E, Adcock IM, Shafei H, Masjedi MR, Folkerts G. Role of P2X7 Receptors in Release of IL-1β: A Possible Mediator of Pulmonary Inflammation. Tanaffos. 2012;11(2):6-11.

Muyldermans S. Nanobodies: natural single-domain antibodies. Annu Rev Biochem. 2013;82:775-97.

Muzumdar MD, Tasic B, Miyamichi K, Li L, Luo L. A global double-fluorescent Cre reporter mouse. Genesis. 2007 Sep;45(9):593-605.

Oliveira-Giacomelli Á, Petiz LL, Andrejew R, Turrini N, Silva JB, Sack U, Ulrich H. Role of P2X7 Receptors in Immune Responses During Neurodegeneration. Front Cell Neurosci. 2021 May 26;15:662935.

Papp KA, Weinberg MA, Morris A, Reich K. IL17A/F nanobody sonelokimab in patients with plaque psoriasis: a multicentre, randomised, placebo-controlled, phase 2b study. Lancet. 2021 Apr 24;397(10284):1564-1575.

Pérez JM, Renisio JG, Prompers JJ, van Platerink CJ, Cambillau C, Darbon H, Frenken LG. Thermal unfolding of a llama antibody fragment: a two-state reversible process. Biochemistry. 2001 Jan 9;40(1):74-83.

Primeau JO, Armanious GP, Fisher ME, Young HS. The SarcoEndoplasmic Reticulum Calcium ATPase. Subcell Biochem. 2018;87:229-258.

Ronco P, Beck L, Debiec H, Fervenza FC, Hou FF, Jha V, Sethi S, Tong A, Vivarelli M, Wetzels J. Membranous nephropathy. Nat Rev Dis Primers. 2021 Sep 30;7(1):69.

Salvador JP, Vilaplana L, Marco MP. Nanobody: outstanding features for diagnostic and therapeutic applications. Anal Bioanal Chem. 2019 Mar;411(9):1703-1713.

Savio LEB, de Andrade Mello P, da Silva CG, Coutinho-Silva R. The P2X7 Receptor in Inflammatory Diseases: Angel or Demon? Front Pharmacol. 2018 Feb 6;9:52.

Scully M, Cataland SR, Peyvandi F, Coppo P, Knöbl P, Kremer Hovinga JA, Metjian A, de la Rubia J, Pavenski K, Callewaert F, Biswas D, De Winter H, Zeldin RK; HERCULES Investigators. Caplacizumab Treatment for Acquired Thrombotic Thrombocytopenic Purpura. N Engl J Med. 2019 Jan 24;380(4):335-346.

Sluyter R, Stokes L. Significance of P2X7 receptor variants to human health and disease. Recent Pat DNA Gene Seq. 2011 Apr;5(1):41-54.

Sluyter, R. (2017). The P2X7 Receptor. In: Atassi, M. (eds) Protein Reviews. Advances in Experimental Medicine and Biology(), vol 1051. Springer, Singapore.

Soboloff J, Rothberg BS, Madesh M, Gill DL. STIM proteins: dynamic calcium signal transducers. Nat Rev Mol Cell Biol. 2012 Sep;13(9):549-65.

Solini A, Menini S, Rossi C, Ricci C, Santini E, Blasetti Fantauzzi C, Iacobini C, Pugliese G. The purinergic 2X7 receptor participates in renal inflammation and injury induced by high-fat diet: possible role of NLRP3 inflammasome activation. J Pathol. 2013 Nov;231(3):342-53.

Solle M, Labasi J, Perregaux DG, Stam E, Petrushova N, Koller BH, Griffiths RJ, Gabel CA. Altered cytokine production in mice lacking P2X(7) receptors. J Biol Chem. 2001 Jan 5;276(1):125-32.

Sörensen I, Adams RH, Gossler A. DLL1-mediated Notch activation regulates endothelial identity in mouse fetal arteries. Blood. 2009 May 28;113(22):5680-8.

Stahl RA, Hoxha E. Glomerulonephritis [Glomerulonephritis]. Dtsch Med Wochenschr. 2016 Jul;141(13):960-8. German.

Sun S, Ding Z, Yang X, Zhao X, Zhao M, Gao L, Chen Q, Xie S, Liu A, Yin S, Xu Z, Lu X. Nanobody: A Small Antibody with Big Implications for Tumor Therapeutic Strategy. Int J Nanomedicine. 2021 Mar 22;16:2337-2356.

Surprenant A, Rassendren F, Kawashima E, North RA, Buell G. The cytolytic P2Z receptor for extracellular ATP identified as a P2X receptor (P2X7). Science. 1996 May 3;272(5262):735-8.

Suurväli J, Boudinot P, Kanellopoulos J, Rüütel Boudinot S. P2X4: A fast and sensitive purinergic receptor. Biomed J. 2017 Oct;40(5):245-256.

Swanson KV, Deng M, Ting JP. The NLRP3 inflammasome: molecular activation and regulation to therapeutics. Nat Rev Immunol. 2019 Aug;19(8):477-489.

Taylor SR, Turner CM, Elliott JI, McDaid J, Hewitt R, Smith J, Pickering MC, Whitehouse DL, Cook HT, Burnstock G, Pusey CD, Unwin RJ, Tam FW. P2X7 deficiency attenuates renal injury in experimental glomerulonephritis. J Am Soc Nephrol. 2009 Jun;20(6):1275-81.

Tesch GH, Yang N, Yu H, Lan HY, Foti R, Chadban SJ, Atkins RC, Nikolic-Paterson DJ. Intrinsic renal cells are the major source of interleukin-1 beta synthesis in normal and diseased rat kidney. Nephrol Dial Transplant. 1997 Jun;12(6):1109-15.

Tijink BM, Laeremans T, Budde M, Stigter-van Walsum M, Dreier T, de Haard HJ, Leemans CR, van Dongen GA. Improved tumor targeting of anti-epidermal growth factor receptor Nanobodies through albumin binding: taking advantage of modular Nanobody technology. Mol Cancer Ther. 2008 Aug;7(8):2288-97.

Timoshanko JR, Kitching AR, Iwakura Y, Holdsworth SR, Tipping PG. Contributions of IL-1beta and IL-1alpha to crescentic glomerulonephritis in mice. J Am Soc Nephrol. 2004 Apr;15(4):910-8.

Tojo A, Endou H. Intrarenal handling of proteins in rats using fractional micropuncture technique. Am J Physiol. 1992 Oct;263(4 Pt 2):F601-6.

Tomas NM, Dehde S, Meyer-Schwesinger C, Huang M, Hermans-Borgmeyer I, Maybaum J, Lucas R, von der Heide JL, Kretz O, Köllner SMS, Seifert L, Huber TB, Zahner G. Podocyte expression of human phospholipase A2 receptor 1 causes immune-mediated membranous nephropathy in mice. Kidney Int. 2023 a Feb;103(2):297-303.

Tomas NM, Schnarre A, Dehde S, Lucas R, Hermans-Borgmeyer I, Kretz O, Koellner SMS, Wiech T, Koch-Nolte F, Seifert L, Huber TB, Zahner G. Introduction of a novel chimeric active immunization mouse model of PLA2R1-associated membranous nephropathy. Kidney Int. 2023 b Nov;104(5):916-928.

Trautmann A. Extracellular ATP in the immune system: more than just a "danger signal". Sci Signal. 2009 Feb 3;2(56):pe6.

Turner CM, Tam FW, Lai PC, Tarzi RM, Burnstock G, Pusey CD, Cook HT, Unwin RJ. Increased expression of the pro-apoptotic ATP-sensitive P2X7 receptor in experimental and human glomerulonephritis. Nephrol Dial Transplant. 2007 Feb;22(2):386-95.

Van Roy M, Ververken C, Beirnaert E, Hoefman S, Kolkman J, Vierboom M, Breedveld E, 't Hart B, Poelmans S, Bontinck L, Hemeryck A, Jacobs S, Baumeister J, Ulrichts H. The preclinical pharmacology of the high affinity anti-IL-6R Nanobody® ALX-0061 supports its clinical development in rheumatoid arthritis. Arthritis Res Ther. 2015 May 20;17(1):135.

Vonend O, Turner CM, Chan CM, Loesch A, Dell'Anna GC, Srai KS, Burnstock G, Unwin RJ. Glomerular expression of the ATP-sensitive P2X receptor in diabetic and hypertensive rat models. Kidney Int. 2004 Jul;66(1):157-66.

Wang J, Bever CR, Majkova Z, Dechant JE, Yang J, Gee SJ, Xu T, Hammock BD. Heterologous antigen selection of camelid heavy chain single domain antibodies against tetrabromobisphenol A. Anal Chem. 2014 Aug 19;86(16):8296-302.

Wang Y, Fan Z, Shao L, Kong X, Hou X, Tian D, Sun Y, Xiao Y, Yu L. Nanobody-derived nanobiotechnology tool kits for diverse biomedical and biotechnology applications. Int J Nanomedicine. 2016 Jul 21;11:3287-303.

Wanner N, Eden T, Liaukouskaya N, Koch-Nolte F. Nanobodies: new avenue to treat kidney disease. Cell Tissue Res. 2021 Aug;385(2):445-456.

Weber FC, Esser PR, Müller T, Ganesan J, Pellegatti P, Simon MM, Zeiser R, Idzko M, Jakob T, Martin SF. Lack of the purinergic receptor P2X(7) results in resistance to contact hypersensitivity. J Exp Med. 2010 Nov 22;207(12):2609-19.

Weinhold K, Krause-Buchholz U, Rödel G, Kasper M, Barth K. Interaction and interrelation of P2X7 and P2X4 receptor complexes in mouse lung epithelial cells. Cell Mol Life Sci. 2010 Aug;67(15):2631-42.

Zhang X, Wang L, YangJ, Li J, Liu H, Li J, Lu P. High Efficacy and Safety of Nanobody Based Anti-BCMA CAR-T Cell Therapy in Treating Patients with Relapsed or Refractory Multiple Myeloma. *Blood* 2023; 142 (Supplement 1): 2107.

Yip L, Woehrle T, Corriden R, Hirsh M, Chen Y, Inoue Y, Ferrari V, Insel PA, Junger WG. Autocrine regulation of T-cell activation by ATP release and P2X7 receptors. FASEB J. 2009 Jun;23(6):1685-93.

Zhao J, Wang H, Dai C, Wang H, Zhang H, Huang Y, Wang S, Gaskin F, Yang N, Fu SM. P2X7 blockade attenuates murine lupus nephritis by inhibiting activation of the NLRP3/ASC/caspase 1 pathway. Arthritis Rheum. 2013 Dec;65(12):3176-85.

Zhu Y, Li Q, Chen Y, Tian M, Xun W, Sun S. P2X7 receptor inhibition attenuates podocyte injury by oxLDL through deregulating CXCL16. Cell Biol Int. 2022 Mar;46(3):454-461.

https://www.sanofi.com/en/our-science/our-pipeline - July 2024

https://www.sanofi.com/en/magazine/our-science/nanobody-technology-platform - July 2024